

Enclosure 9

PG&E Geosciences: "Technical Report TR-HBIP-2002-01

Seismic Hazard Assessment for the Humboldt Bay

ISFSI Project, Revision 0"

December 27, 2002

512 Pages



*Pacific Gas and
Electric Company*

**Humboldt Bay ISFSI Project
Technical Report TR-HBIP-2002-01**

**Seismic Hazard Assessment
for the Humboldt Bay ISFSI Project**

Revision 0 – 27 December 2002

Memorandum

Date: 31 December 2002
To: Roy Willis
HBIP Project Manager
From: Lloyd Cluff
Director, Geosciences Department
Subject: Transmittal of Technical Report TR-HBIP-2002-01, Seismic Hazard
Assessment for the Humboldt Bay ISFSI Project



***Pacific Gas and
Electric Company***

Dear Roy,

As part of our deliverables under Geosciences Work Plan GEO 2002-01, Completion of the Seismic Hazard Analysis Report for the Humboldt Bay ISFSI, please find enclosed nine copies of the following:

Technical Report TR-HBIP-2002-01, Seismic Hazard Assessment for the Humboldt Bay ISFSI Project, Revision 0.

The report has been reviewed in accordance with the Work Plan and all review comments have been addressed. If you have any questions or comments, please call me.


Lloyd Cluff

Enclosures

cc: MKMcLaren w/o
WDPAGE w/o
JISun w/o
RKWhite w/o

TITLE: Seismic Hazard Assessment for the Humboldt Bay ISFSI Project

PREPARED BY: Frank H. Swan DATE: 12/27/02
Frank H. (Bert) Swan Consultant
Printed Name Organization

VERIFIED BY: Robert K. White DATE: 12/31/02
Robert K. White Geosciences Department
Printed Name Organization

APPROVED BY: Lloyd Cluff DATE: 12/31/02
Lloyd Cluff Geosciences Department
Printed Name Organization

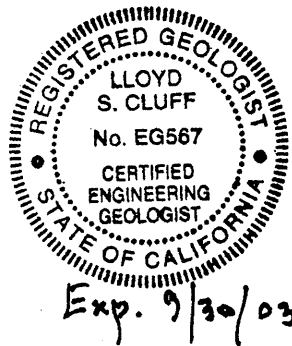


TABLE OF CONTENTS

		Page
1.0	INTRODUCTION	1-1
1.1	BACKGROUND.....	1-1
1.2	DEFINITION OF STUDY AREA	1-2
1.3	SCOPE OF SEISMIC HAZARD STUDIES.....	1-2
1.4	DEFINITION OF TERMS	1-3
1.5	ACKNOWLEDGEMENTS.....	1-4
2.0	TECTONIC FRAMEWORK.....	2-1
2.1	INTRODUCTION	2-1
2.2	NORTH AMERICAN PLATE BOUNDARY	2-3
2.3	PACIFIC/GORDA-JUAN DE FUCA PLATE BOUNDARY	2-5
2.4	CASCADIA SUBDUCTION ZONE	2-7
2.5	MENDOCINO TRIPLE JUNCTION REGION	2-14
2.6	ALEUTIAN SUBDUCTION ZONE ANALOG.....	2-17
2.7	SUMMARY OF TECTONIC FRAMEWORK	2-18
3.0	REGIONAL GEOLOGY AND SEISMICITY.....	3-1
3.1	INTRODUCTION	3-1
3.2	REGIONAL GEOLOGY	3-1
	3.2.1 Regional Stratigraphy	3-1
	3.2.2 Regional Geologic Structure.....	3-10
3.3	REGIONAL SEISMICITY.....	3-19
	3.3.1 Seismicity Catalog.....	3-19
	3.3.2 Magnitude 5 and Larger Earthquakes.....	3-22
	3.3.3 Association of Earthquakes with Tectonic and Geologic Structures	3-30
	3.3.4 Earthquake Ground Motions Recorded at Humboldt Bay Power Plant	3-33
3.4	SUMMARY OF REGIONAL GEOLOGY AND SEISMICITY	3-35
4.0	SITE GEOLOGY	4-1
4.1	INTRODUCTION	4-1
4.2	PHYSIOGRAPHIC SETTING	4-2
4.3	STRATIGRAPHY	4-4
	4.3.1 Rio Dell Formation (Late Pliocene to Early Pleistocene).....	4-4
	4.3.2 Scotia Bluffs(?) Formation (Early Pleistocene).....	4-5
	4.3.3 Hookton Formation (Middle to Late Pleistocene)	4-5
	4.3.4 Buhne Point Terrace and Paleosol (Late Pleistocene).....	4-7
	4.3.5 Surficial Deposits (Holocene).....	4-8
4.4	FAULTING IN THE SITE VICINITY ASSOCIATED WITH THE LITTLE SALMON FAULT ZONE	4-8
	4.4.1 Little Salmon Fault	4-8
	4.4.2 Bay Entrance Fault.....	4-9



TABLE OF CONTENTS
(Continued)

4.4.3	Buhne Point Fault	4-10
4.4.4	Discharge Canal Fault.....	4-11
4.4.5	Other Minor Faults.....	4-12
4.5	CONTINUITY OF STRATA BENEATH THE SITE	4-12
4.5.1	Unit F Clay (Upper Lower Hookton Formation).....	4-12
4.5.2	Upper Hookton Strata	4-14
4.6	SUMMARY OF SITE GEOLOGY	4-15
5.0	SEISMIC SOURCE CHARACTERIZATION.....	5-1
5.1	INTRODUCTION	5-1
5.2	DESIGN INPUTS	5-2
5.2.1	Width Approaches for Cascadia Interface	5-2
5.2.2	Dimensions of the Cascadia Interface.....	5-3
5.2.3	Little Salmon Fault Zone	5-3
5.3	METHOD AND EQUATION SUMMARY.....	5-4
5.3.1	Method.....	5-4
5.3.2	Equations.....	5-4
5.4	CALCULATION OF MAGNITUDE.....	5-6
5.4.1	Magnitude for the Cascadia Interface	5-6
5.4.2	Magnitude for the Little Salmon Fault System.....	5-8
5.5	RESULTS AND CONCLUSIONS	5-9
6.0	EARTHQUAKE GROUND MOTIONS	6-1
6.1	APPROACH	6-1
6.2	ATTENUATION RELATIONS	6-3
6.2.1	Shallow Crustal Earthquakes	6-4
6.2.2	Subduction Zone Earthquakes	6-5
6.2.3	Directivity	6-5
6.2.4	Synchronous Rupture.....	6-6
6.2.5	Outcrop Rock Site Condition.....	6-7
6.3	GROUND MOTIONS	6-7
7.0	LIQUEFACTION AND LANDSLIDE POTENTIAL	7-1
7.1	INTRODUCTION	7-1
7.2	FIELD EXPLORATION AND LABORATORY TESTING AT THE ISFSI SITE	7-1
7.3	SITE AND SUBSURFACE CONDITIONS AT THE ISFSI SITE	7-2
7.4	SLOPE STABILITY ANALYSES AT THE ISFSI SITE.....	7-3
7.5	SLOPE DISPLACEMENT ANALYSES AT THE ISFSI SITE.....	7-4
7.6	SITE AND SUBSURFACE CONDITIONS ALONG THE TRANSPORT ROUTE.....	7-5
7.7	SLOPE STABILITY ANALYSES AT THE TRANSPORT ROUTE CRITICAL CROSS SECTION	7-5
7.8	SLOPE DISPLACEMENT ANALYSES AT THE TRANSPORT ROUTE CRITICAL CROSS SECTION.....	7-6
7.9	SUMMARY OF LIQUEFACTION AND LANDSLIDE POTENTIAL	7-7
8.0	SURFACE-FAULTING POTENTIAL	8-1
8.1	INTRODUCTION	8-1
8.2	PROXIMITY OF SITE TO KNOWN ACTIVE FAULTS.....	8-2



TABLE OF CONTENTS

(Continued)

8.3	SURFACE DEFORMATION ASSOCIATED WITH THRUST FAULTS	8-2
8.3.1	Characteristics of Thrust Faults	8-3
8.3.2	Hanging-Wall Deformation on the Buhne Point Fault	8-6
8.4	AGE, CONTINUITY, AND STABILITY OF STRATA BENEATH THE SITE	8-7
8.5	RECURRENCE OF SURFACE FAULTING RELATIVE TO AGES OF STRATA BENEATH THE SITE	8-8
8.6	COMPARISON OF DEFORMATION AT BUHNE POINT WITH 1999 SURFACE FAULT RUPTURE ON THE CHELUNGPU FAULT, TAIWAN	8-10
8.7	SUMMARY OF SURFACE-FAULTING POTENTIAL AT THE SITE	8-11
9.0	TSUNAMI POTENTIAL	9-1
9.1	INTRODUCTION	9-1
9.2	DEFINITION OF TSUNAMIS	9-2
9.3	HISTORICAL TSUNAMIS IN THE HUMBOLDT BAY AREA	9-4
9.4	GEOLOGIC STUDY OF PAST TSUNAMIS ALONG THE NORTHERN CALIFORNIA COAST	9-7
9.4.1	Characteristics of Tsunami Deposits	9-8
9.4.2	Methods Used for Tsunami Investigation	9-11
9.4.3	Evidence for Past Tsunamis in Northern California	9-13
9.4.4	Humboldt Bay Sites Having No Evidence of past Tsunamis	9-21
9.4.5	Correlation on Tsunami Deposits	9-22
9.4.6	Runup Estimates for Past Tsunamis	9-28
9.4.7	Potential for Local Landslide-Generated Tsunamis	9-33
9.4.8	Summary of Results of the Paleotsunami Study	9-35
9.5	ADDITIONAL ASSESSMENTS OF TSUNAMIS HAZARD	9-36
9.5.1	Empirical Comparisons of Worldwide Tsunami Runup Heights	9-36
9.5.2	Analytical Models of Potential Tsunami Inundation	9-38
9.6	ADDITIONAL FACTORS INFLUENCING THE TSUNAMI HAZARD AT THE ISFSI SITE	9-46
9.6.1	Estimated Runup at the Open Coast at Humboldt Bay	9-46
9.6.2	Runup Heights at the ISFSI Site	9-50
9.7	SUMMARY OF TSUNAMI HAZARD AT THE HUMBOLDT BAY ISFSI SITE	9-54
10.0	REFERENCES	10-1

TABLES

Table 1-1	Geologic Time Scale and Subdivisions of the Mesozoic and Cenozoic Eras
Table 2-1	Comparison of the Timing of Events on the Main Segment of the Cascadia Subduction Zone with Events on the Eel River Segment
Table 3-1	Geologic History of the Humboldt Bay ISFSI Site
Table 3-2	Magnitude 5 and Larger Earthquakes within 160 Kilometers (100 Miles) of the HB-ISFSI Site, 1850 through April 2002



TABLE OF CONTENTS

(Continued)

Table 3-3	Earthquakes that Produced Ground Motions Greater than 10%g at Humboldt Bay Power Plant, 1975 through 1994
Table 4-1	Descriptions of Soil Profiles
Table 5-1	Alternative Segment Lengths and Weights for the Cascadia Interface Using the Carver Model (Carver, 2002c, Page 5A-3)
Table 5-2	Distance (km) from U. S. Coastline to 4 Updip Reference Boundaries of the Cascadia Subduction Zone
Table 5-3	Horizontal Extent (km) of the Cascadia Interface Using the Change in Fold Trends (Figure 2-16) as the Updip Interface Boundary
Table 5-4	Downdip Width (km) of the Cascadia Interface
Table 5-5	Maximum Rupture Downdip Width (km) of the Cascadia Interface Averaged along the Rupture Length
Table 5-6	Mean Characteristic Magnitudes for the Cascadia Interface Using the Carver Segmentation Model
Table 5-7	Mean Characteristic Magnitudes for the Little Salmon Fault System
Table 5-8	MCE for Cascadia Interface and Little Salmon Fault
Table 6-1	84th Percentile MCE Design Spectra for the Fault Normal Component
Table 6-2	84th Percentile MCE Design Spectra for the Fault Parallel Component
Table 6-3	84th Percentile MCE Design Spectra for the Vertical Component
Table 8-1	Well-Studied Historical Thrust Earthquakes Associated with Surface Fault Ruptures
Table 9-1	Observations of Runup Elevations at Humboldt Bay and Other Locations in Northern California from the 27-28 March 1964 Alaska Earthquake (PG&E, 1966)
Table 9-2	Evidence of Past Tsunamis at Marsh Sites in Northern California
Table 9-3	Cascadia Subduction Zone Events



TABLE OF CONTENTS

(Continued)

- Table 9-4 Open Coast Runup Estimates from Paleoseismic Sites along the Northern California Coast and World Wide Data
- Table 9-5 Estimated Runup Heights at Lagoon Creek from the Sediment Transport Model
- Table 9-6 Wiegel's (in PG&E, 1966) Estimates of Tsunami Runups and their Probability at Humboldt Bay Power Plant

FIGURES

- Figure 1-1 Topographic map of Humboldt Bay showing the location of the Humboldt Bay ISFSI site.
- Figure 1-2 Color shaded-relief map (oblique Mercator projection) of the Cascadia subduction zone along the northwest coast of the United States and Canada.
- Figure 2-1 General plate tectonic setting of the western United States.
- Figure 2-2 Tectonic evolution of the west coast of the United States during the past 50 million years (from National Geographic Society, 1995).
- Figure 2-3 Map of subplates in the North American plate and major faults in northwestern California.
- Figure 2-4 Tectonics of the Gorda plate (Modified from Wilson, 1989, Figure 3).
- Figure 2-5 Schematic maps showing the components of the Little Salmon fault system.
- Figure 2-6 Major active faults and known or inferred earthquake rupture areas (line pattern) in the Mendocino triple junction region (stippled area).
- Figure 2-7 Schematic cross section showing the suggested mechanisms for the 1964 Alaska earthquake (Plafker, 1972), and postulated Cascadia subduction zone earthquake sources.
- Figure 3-1 Generalized regional geologic map showing principal faults and folds, area of active Mendocino uplift (stippled pattern), and major plates (after McLaughlin and others, 2000).
- Figure 3-2 Generalized regional structure section A-A' showing depth distribution of epicenters (open circles) and selected focal mechanisms (beach balls) of earthquakes from M. Magee (Stanford University and USGS), 1994 (after McLaughlin and others, 2000).
- Figure 3-3 Geologic map of the Humboldt Bay region.



TABLE OF CONTENTS
(Continued)

- Figure 3-4 Geologic cross section of the Humboldt Bay region.
- Figure 3-5 Composite stratigraphic column, onshore Eel River basin (after Clarke, 1992).
- Figure 3-6 Marine terrace map of the Humboldt Bay region.
- Figure 3-7 Surface traces of the Little Salmon fault zone south of the ISFSI site.
- Figure 3-8 Cross section A-A' across the Little Salmon fault zone at Humboldt Hill (after Woodward-Clyde Consultants, 1980, Figure C-15).
- Figure 3-9 Geologic cross-section A-A' across a trace of the Little Salmon fault zone at College of the Redwoods, 5 kilometers south of Humboldt Bay ISFSI site (after LACO Associates, 1999, Figure 5).
- Figure 3-10 Geologic cross section B-B' across a trace of the Little Salmon fault zone at College of the Redwoods, 5 kilometers south of Humboldt Bay ISFSI site (after LACO Associates, 1999, Figure 6).
- Figure 3-11 Geologic cross section C-C' across a trace of the Little Salmon fault zone at College of the Redwoods, 5 kilometers south of Humboldt Bay ISFSI site (after LACO Associates, 1999, Figure 7).
- Figure 3-12 Geologic cross section D-D' across a trace of the Little Salmon fault zone at College of the Redwoods, 5 kilometers south of Humboldt Bay ISFSI site (after LACO Associates, 1999, Figure 8).
- Figure 3-13 Magnitude 5 and larger earthquakes for the period 1850 through April 2002 within 160 kilometers (100 miles) of the site.
- Figure 3-14 Magnitude 3 and larger earthquakes from the period 1974 through April 2002 within 160 kilometers (100 miles) of the site.
- Figure 3-15 Seismic cross sections of magnitude 3 and larger earthquakes from the period 1974 through April 2002.
- Figure 3-16 Magnitude 2 and larger earthquakes from the period 1974 through April 2002, within 40 kilometers (25 miles) of the site, and earthquakes of magnitude 5 and larger from 1850 through 1973 within the map boundary.
- Figure 3-17 Seismic cross section of magnitude 2 and larger earthquakes from the period 1974 through April 2002.



TABLE OF CONTENTS

(Continued)

- Figure 4-1 Locations of borings, cross-sections, and seismic reflection lines used in the 1980 Woodward-Clyde Consultants report.
- Figure 4-2 Geologic map of the ISFSI site.
- Figure 4-3 Locations of geologic trenches and borings near the ISFSI site.
- Figure 4-4 Comparison of the shoreline shown on 1858 and 1959 surveys.
- Figure 4-5 Geologic cross-section of X-X⁵.
- Figure 4-6 Generalized stratigraphic section at the ISFSI site.
- Figure 4-7 Stratigraphic section of the uppermost lower Hookton and upper Hookton Formation exposed in Woodward-Clyde Consultants' trenches 11-T6a, 11-T6b, and 11-T6c (after Woodward-Clyde Consultants, 1980, Figure C-28).
- Figure 4-8 Composite log of trenches WCC-11T6a and GMX-T1.
- Figure 4-9 Log of Trench GMX-T2.
- Figure 4-10 Geologic cross section Y-Y¹.
- Figure 4-11 Relict soil and upper Hookton Formation deposits exposed in trench GMX-T2 (NW wall at station 180 ft.).
- Figure 4-12 Structure contour map of the Little Salmon fault north of Humboldt Hill (after Woodward-Clyde Consultants, 1980, Figure C-14).
- Figure 4-13 Structure contour map of the Bay Entrance fault (modified from Woodward-Clyde Consultants, 1980, Figure C-18).
- Figure 4-14 Structure contour map of the Buhne Point fault (reinterpretation of data presented on Woodward-Clyde Consultants, 1980, Figure C-25).
- Figure 4-15 Cross section A-A' across the Little Salmon fault zone at Humboldt Hill (modified from Woodward-Clyde Consultants, 1980, Figure C-15).
- Figure 4-16 Cross section B-B' across the Bay Entrance and Buhne Point faults.
- Figure 4-17 Structure contour map of top of Unit F.
- Figure 4-18 Log of WCC trench 11-T6b.
- Figure 4-19 Log of WCC trench 11-T6c.



TABLE OF CONTENTS
(Continued)

- Figure 4-20 Log of WCC (1980) trench at McKinleyville.
- Figure 4-21 Geologic cross section W-W'.
- Figure 4-22 Exposure of Discharge Canal fault.
- Figure 4-23 Log of ESA (1977) trench BP-2.
- Figure 4-24 Log of ESA (1977) trench BP-3.
- Figure 4-25 Alternative interpretations of the irregularities in the top of the Unit F clay between boreholes WCC80-CH4 and WCC80-CH5.
- Figure 6-1 Fault normal design spectrum for damping values of 2%, 4%, 5%, and 7%
- Figure 6-2 Fault parallel design spectrum for damping values of 2%, 4%, 5%, and 7%
- Figure 6-3 Vertical spectrum for damping values of 2%, 4%, 5%, and 7%
- Figure 8-1 Typical types of surface deformation associated with thrust faulting.
- Figure 8-2 Log of north wall of trench WCC-11-T2a across the Trinidad fault (Mad River fault zone).
- Figure 8-3 Comparison of faulting near the Humboldt Bay ISFSI site with deformation mapped in the hanging wall of the Little Salmon fault zone at College of the Redwoods, about 5 kilometers south of the site.
- Figure 8-4 Complex zones of deformation where crustal shortening is accommodated by numerous small-displacement conjugate faults.
- Figure 8-5 Schematic progressive development of fault bend and fault propagation folds (*from Suppe, 1983*).
- Figure 8-6 Log of trench across a trace of the Mad River fault zone.
- Figure 8-7 Comparison of faulting near the Humboldt Bay ISFSI site with 1999 surface rupture along the Chelungpu fault, Taiwan.
- Figure 9-1 Schematic diagrams of major tsunami sources
- Figure 9-2 Illustration of tsunami terms



TABLE OF CONTENTS

(Continued)

- Figure 9-3 Diagrams illustrating progression of tsunamis at the coast, and stratigraphic columns in the quiet water of bays and ponds
- Figure 9-4 Coastal sites investigated for evidence of paleotsunamis in northwestern California
- Figure 9-5 Cross section of a typical intertidal marsh
- Figure 9-6 Cross section of a typical coastal freshwater marsh
- Figure 9-7 Comparison of ages for Cascadia earthquakes from tsunami data between northern California and Washington
- Figure 9-8 Location of cores in Crescent City marsh
- Figure 9-9 Correlation of tsunami sands in selected cores across Crescent City marsh
- Figure 9-10 Idealized detailed section showing multiple graded sands in a tsunami deposit
- Figure 9-11 Location of cores in the Lagoon Creek marsh
- Figure 9-12 Correlation of tsunami sands in selected cores across the Lagoon Creek marsh
- Figure 9-13 Detailed stratigraphy of core LC-16 from the Lagoon Creek marsh
- Figure 9-14 Detailed stratigraphy of core LC-2 from the Lagoon Creek marsh
- Figure 9-15 Townsite of Orekw (Oreck) and location of cores in Orick marsh
- Figure 9-16 Geomorphology of the North and South spits of Humboldt Bay
- Figure 9-17 Map of the South Bay sites and other Humboldt Bay marsh sites
- Figure 9-18 Correlation of tsunami sands in selected cores across the South Bay marsh
- Figure 9-19 Plot of moment magnitude versus average maximum tsunami runup for the better-documented tsunamigenic earthquakes
- Figure 9-20 Schematic diagram showing estimated tsunami runup heights at the Humboldt Bay ISFSI site
- Figure 9-21 Present coastline superimposed on the 1858 map of mouth of Humboldt Bay
- Figure 9-22 The 1806 map of Humboldt Bay (Bay of Rezanov) made by Russian explorers

TABLE OF CONTENTS

(Continued)

PHOTOS

- Photo 1-1 South Humboldt Bay. View is southeast.
- Photo 3-1 Oblique aerial views looking north along the Humboldt Hill anticline and the Little Salmon fault zone.
- Photo 4-1 Oblique aerial view of the Humboldt Bay ISFSI site.
- Photo 4-2 Oblique aerial view looking northwest from above Humboldt Hill toward the entrance of Humboldt Bay.
- Photo 4-3 View looking west from Buhne Point showing the escarpment along the north side of the Buhne Point terrace and riprap along the shoreline of Humboldt Bay.
- Photo 4-4 View to east of Buhne Point terrace surface and ISFSI site.
- Photo 4-5 Oblique aerial photographs showing disturbance of Buhne Point terrace during trenching activities by Earth Sciences Associates (circa 1975).
- Photo 4-6 Outcrop of sand with interbedded silt (light layers) in sea cliff north of ISFSI site.
- Photo 4-7 Trench GMX-T1, view east-southeast.
- Photo 4-8 Surveying geologic contacts in trench GMX-T2.
- Photo 4-9 Artificial fill overlying sand and silt layers of the upper Hookton Formation in northwest wall of trench GMX-T2 between station 36 ft. and station 44 ft.
- Photo 4-10 Clay fractures in upper Hookton Formation in trench GMX-T2.
- Photo 4-11 Fracture lined with black compressed rootlets in clayey-silt bed in trench GMX-T2.
- Photo 4-12 Continuous bedding across bleached fracture in silty clay in trench GMX-T2.
- Photo 8-1 Collapsed fault scarp in alluvium on the Hanning Bay fault, Montague Island, Alaska.
- Photo 8-2 Fault scarp on the Chelungpu fault at the Kuang Fu Middle School, Taiwan.



TABLE OF CONTENTS
(Continued)

- Photo 8-3 Fault bend fold and associated shears and fractures of the Chelungpu fault, Fengyuan, Taiwan.
- Photo 8-4 Fractures and faults in the hanging wall of the Qued Fodda fault, Algeria.
- Photo 9-1 North Spit, Humboldt Bay (foreground), and Arcata Bay (background).
- Photo 9-2 Gouge coring at Crescent City marsh.
- Photo 9-3 Typical gouge core.
- Photo 9-4 Drilling using the Vibracore at Lagoon Creek.
- Photo 9-5 Typical drive cores.
- Photo 9-6 Crescent City, view to west.
- Photo 9-7 Crescent City marsh.
- Photo 9-8 Lagoon Creek pond and marsh.
- Photo 9-9 Wilson Creek and Lagoon Creek.
- Photo 9-10 Beach berm at Lagoon Creek 23 feet above MLLW.
- Photo 9-11 Townsite of Orick and the Orick marsh at the mouth of Redwood Creek.
- Photo 9-12 South Spit.
- Photo 9-13 Mouth of Humboldt Bay, and the South Bay Hookton Slough sites.
- Photo 9-14 Lag pebbles at elevation 27 feet (MLLW) on the sand dunes on the North Spit believed to be deposited by a tsunami that inundated the dunes.
- Photo 9-15 South Bay Site.

APPENDIXES

- Appendix 2A Comparison of the Southern Cascadia Subduction Zone with the Tectonic Setting of the 1964 Alaska Earthquake
- Appendix 4A Logs of Earth Sciences and Associates (1977) and Woodward-Clyde Consultants (1980) Site Trenches
- Appendix 5A Seismic Source Characterization of the Cascadia Subduction Zone



TABLE OF CONTENTS
(Continued)

Appendix 9A A Review of Empirical Data on Tsunami Runup versus Earthquake Source
Parameters



Section 1.0

Introduction

These studies were conducted and this report prepared to update the tectonic setting of the Humboldt Bay region, and reevaluate the seismic hazards that could affect the proposed site for an Independent Spent Fuel Storage Installation (ISFSI) on the Humboldt Bay Power Plant property. This report also provides earth sciences data, earthquake hazards assessments, and geotechnical foundation data and analyses in support of the licensing application for construction and operation of the Humboldt Bay Power ISFSI project.

1.1 BACKGROUND

The Humboldt Bay Power Plant is located in coastal northern California, on the east side of Humboldt Bay, south of Eureka (Figures 1-1, 1-2). The plant is sited near Buhne Point, on the southern slope of a hill (herein called Buhne Point hill) that dips gently to the southeast. Units 1 and 2 are fossil-fueled generating plants built in 1954 and 1956, respectively, and operate today.

Unit 3, a small (62 MW) nuclear power plant, was constructed in 1962. It was initially designed for a peak ground acceleration of 0.2 g. On June 7, 1975, the local magnitude 5.3 Ferndale earthquake, 14 miles (22 km) distant (at a depth of 23.6 km) resulted in a free-field peak ground acceleration of 0.3 g at the plant site. In 1976, when Unit 3 was shut down for refueling, the seismic criteria were reevaluated. A preliminary analysis indicated that a free-field peak ground acceleration of 0.5 g would be appropriate, and consequently some of the plant facilities were retrofitted to withstand this larger ground motion. Concurrently, a detailed reevaluation of seismic sources was conducted (Woodward-Clyde Consultants, 1980). This reevaluation led to the discovery of the Little Salmon fault zone within a mile (kilometer) of the ISFSI site.

Because of the potential for a large-magnitude earthquake on the Little Salmon fault zone, the



application to restart the plant was withdrawn, and, in 1985, Unit 3 was put into a SAFSTOR mode. Seismic strong-motion monitoring has continued to the present.

On December 26, 1994, a moment magnitude 5.4 earthquake occurred 9 miles (14 km) west of the Humboldt Bay Power Plant site at a depth of 23.5 kilometers. The earthquake resulted in a free-field peak ground acceleration of 0.55 g at the plant site, slightly higher than the 0.5 g used during evaluations of Unit 3 from 1976 to 1982. The event prompted NRC staff to inspect the site in February 1995. During the site visit, the NRC requested PG&E to reevaluate the seismic hazards at the plant site. The reevaluations were to include an analysis of potential ground motions, incorporating new near-source data from recent earthquakes in Northridge (1994) and in Kobe (1995).

In 1998, PG&E began studies for dry cask storage at the plant, and the reevaluation requested by the NRC was expanded to include assessment of seismic hazards at the proposed ISFSI site. The reevaluation was also expanded to include data and relevant research from the 1999 earthquakes in Turkey and Taiwan, which have provided valuable new data that contribute to our understanding of the tectonics in the Humboldt Bay region.

1.2 DEFINITION OF THE STUDY AREA

This review considered the seismic hazards to the Humboldt Bay ISFSI site, which is located within the Humboldt Bay Power Plant site area (called “plant site”), enclosed by the outer farm fence that also envelops Units 1, 2, and 3, and associated structures (Figure 1-1). Because of the extensive previous studies for the nuclear power plant, Unit 3 occasionally is mentioned in this report as a geographic reference point.

1.3 SCOPE OF SEISMIC HAZARD STUDIES

The Humboldt Bay ISFSI site is on the western edge of the North American plate, near the southern end of the Cascadia subduction zone (Figure 1-3). Since the evaluation of seismic



sources conducted for the plant site in 1980, knowledge about the Cascadia subduction zone has changed significantly. In the early 1980s, it was widely thought that the interface part of the Cascadia subduction zone was aseismic. During the past 10 years, studies of tectonic subsidence, paleotsunamis, and paleoliquefaction along the Pacific Northwest coast have shown that the Cascadia interface has generated several large earthquakes during the past few thousand years.

We have developed a comprehensive model of the tectonic framework of the region to better understand the seismic potential of the Cascadia subduction zone. Section 2.0 of this report summarizes the latest thinking on the tectonic framework of the ISFSI site region. In Section 3.0, we update earlier studies of the regional geology and seismicity, including recent evaluations of the Little Salmon fault zone. The geology of the ISFSI site is presented in Section 4.0. The seismic potential of the Cascadia interface and the characterization of other seismic sources in the Humboldt Bay region that could affect the site are discussed in Section 5.0. There have been major improvements in the evaluation of ground motions caused by large earthquakes since the 1980 evaluations. Due to the large increase in strong-motion recordings, for both shallow crustal earthquakes in active tectonic regions and subduction zone earthquakes, ground motion attenuation relations have been revised significantly (for example, Idriss, 1991; 1994; 1995; Abrahamson and Silva, 1997; Boore and others, 1997; Campbell, 1997; Sadigh and others, 1997; Youngs and others, 1997). Attenuation relations and the ground motions for the ISFSI site are discussed in Section 6.0.

Based on recent drilling and trenching investigations, the hazards of liquefaction and landsliding, and surface faulting were evaluated and are discussed in Section 7.0 and Section 8.0, respectively. In Section 9.0, we present new data, based on an active Cascadia subduction zone, that are used to evaluate the hazard of tsunamis at the Humboldt Bay ISFSI site.



1.4 DEFINITION OF TERMS

Units of measure - These studies use both English and metric measurements. Metric measurements were used because they are the professional standard in seismicity and seismic geology evaluations. However, site geotechnical investigations typically use English measurements. Both measurements may be given, as necessary.

Reference elevation - Mean lower low water is the reference elevation for bathymetry and topography at the site. Hence, all elevation measurements at the site are referenced to mean lower low water, which is set at 0. The tidal range is 6.9 feet to mean higher high water (MHHW), and mean sea level is 3.7 feet. The top of the ISFSI site is about elevation 44 feet above mean lower low water.

Magnitude scale - All earthquake magnitudes are moment magnitudes, **M**, (Hanks and Kanamori, 1979) unless stated otherwise.

Geologic time scale - A geologic time chart that shows the subdivisions of the Mesozoic and Cenozoic Eras as used in these studies is presented in Table 1-1.

1.4 ACKNOWLEDGEMENTS

The seismic hazards analyses for the Humboldt Bay ISFSI project were conducted under the direction of PG&E's Geosciences Department. The individuals responsible for preparing the various parts of the report and for providing technical peer review are listed below. Dr. William Savage (formerly of the PG&E Geoscience Department and now at the U. S. Geological Survey) and Ms. Janet Cluff (Word Engineering) helped prepare the initial draft of the report.

Section 1.0: Introduction

Prepared by: Ms. Janet Cluff⁸
Reviewed by: Dr. William D. Page¹



Section 2.0: Tectonic Framework

Prepared by: Dr. Frank H. Swan²
Dr. Gary A. Carver⁴
Dr. William D. Page¹

Reviewed by: Dr. Harvey M. Kelsey³

Section 3.0: Regional Geology and Seismology

Prepared by: Dr. Frank H. Swan (Regional Geology)²
Dr. Gary A. Carver (Regional Geology)⁴
Ms. Marcia McLaren (Seismology)¹
Dr. William D. Page¹

Reviewed by: Dr. Harvey M. Kelsey (Geology)³
Dr. Stuart Nishenko (Seismology)¹

Section 4.0: Site Geology

Prepared by: Dr. Frank H. Swan²
Mr. John Wessling⁵
Dr. William D. Page¹

Reviewed by: Dr. Robert Witter⁶

Section 5.0: Seismic Source Characterization

Prepared by: Dr. Norm Abrahamson¹
Dr. Gary A. Carver⁴

Reviewed by: Dr. Stuart Nishenko¹

Section 6.0: Earthquake Ground Motions

Prepared by: Dr. Norm Abrahamson¹

Reviewed by: Dr. Joseph Sun¹

Section 7.0: Liquefaction and Landslide Potential

Prepared by: Mr. Karthik Narayanan⁵
Dr. Dante Legaspi⁵
Dr. Chih-Cheng Chin⁵

Reviewed by: Mr. Robert K White¹

Section 8.0: Surface-Faulting Potential

Prepared by: Dr. William D. Page¹
Dr. Frank H. Swan²

Reviewed by: Dr. Gary A. Carver⁴



Section 9.0: Tsunami Potential

Prepared by: Dr. Gary A. Carver⁴
Dr. William D. Page¹

Reviewed by: Dr. George Plafker⁷
Dr. Robert Witter⁶

Appendix 2A: Comparison of the southern Cascadia subduction zone with the tectonic setting of the 1964 Alaska Earthquake

Prepared by: Dr. George Plafker⁷

Reviewed by: Dr. William D. Page¹

Appendix 4A: Logs of Earth Sciences Associates (1977) and Woodward-Clyde Consultants (1980) site trenches

Compiled by: Dr. Frank H. Swan²
Dr. William D. Page¹

Reviewed by: Mr. Robert K White¹

Appendix 5A Seismic Source Characterization of Cascadia Subduction Zone

Prepared by: Dr. Norm Abrahamson¹
Dr. Gary A. Carver⁴

Reviewed by: Dr. Joseph Sun¹

Appendix 9A: A Review of Empirical Data on Tsunami Runup versus Earthquake Source Parameters

Prepared by: Dr. George Plafker⁷

Reviewed by: Dr. William D. Page¹

¹ PG&E Geosciences Department, San Francisco, CA

² Frank H. (Bert) Swan, Consulting Geologist, San Francisco, CA

³ Harvey Kelsey, Consulting Geologist, Arcada, CA

⁴ Carver Geologic, Kodiak, AK

⁵ Geomatrix Consultants, Inc, Oakland, CA

⁶ William Lettis and Associates, Walnut Creek, CA

⁷ Plafker Geohazard Consultants, Woodside, CA

⁸ Word Engineering, San Francisco, CA



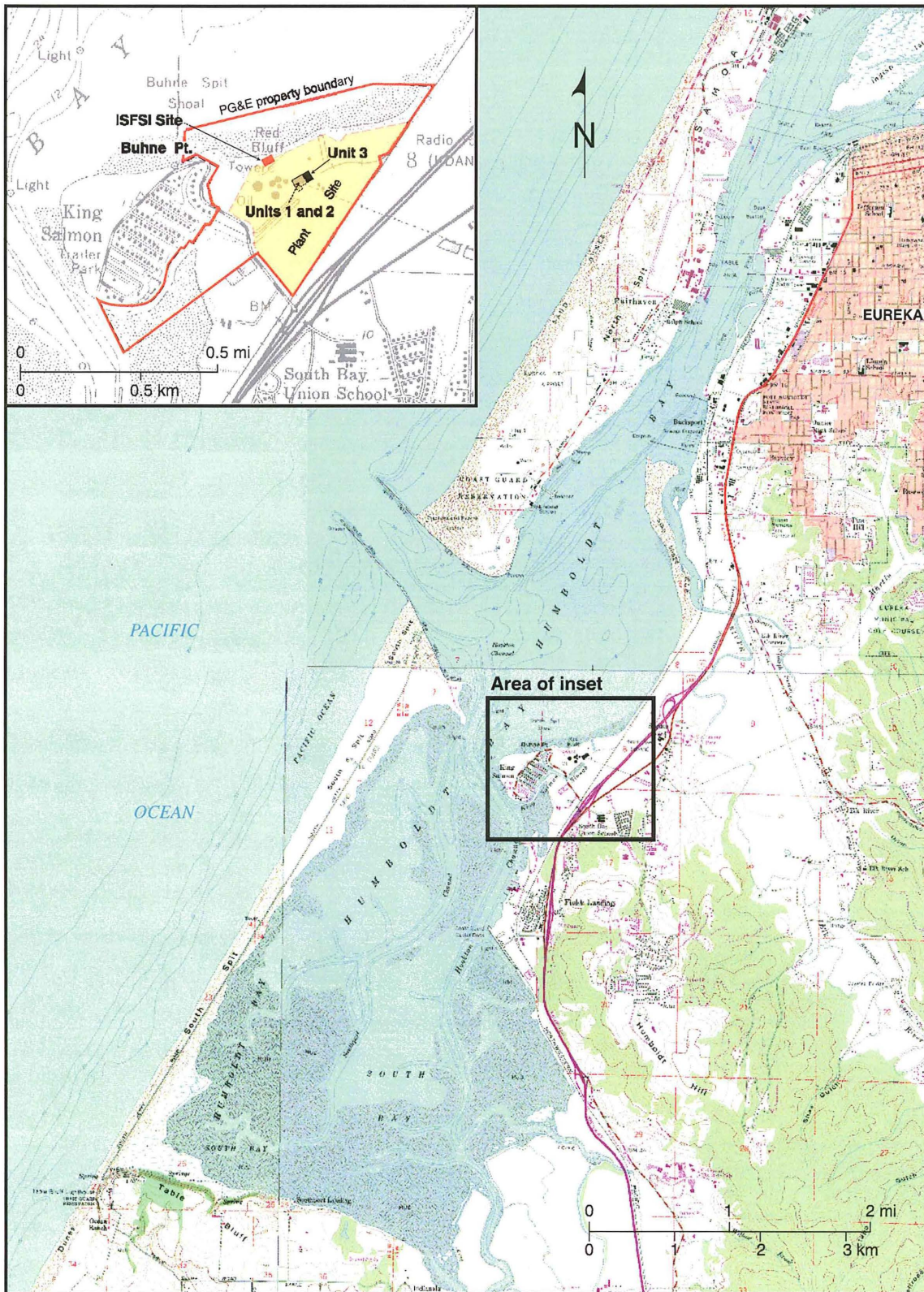


Figure 1-1 Topographic map of Humboldt Bay showing the location of the Humboldt Bay ISFSI site.

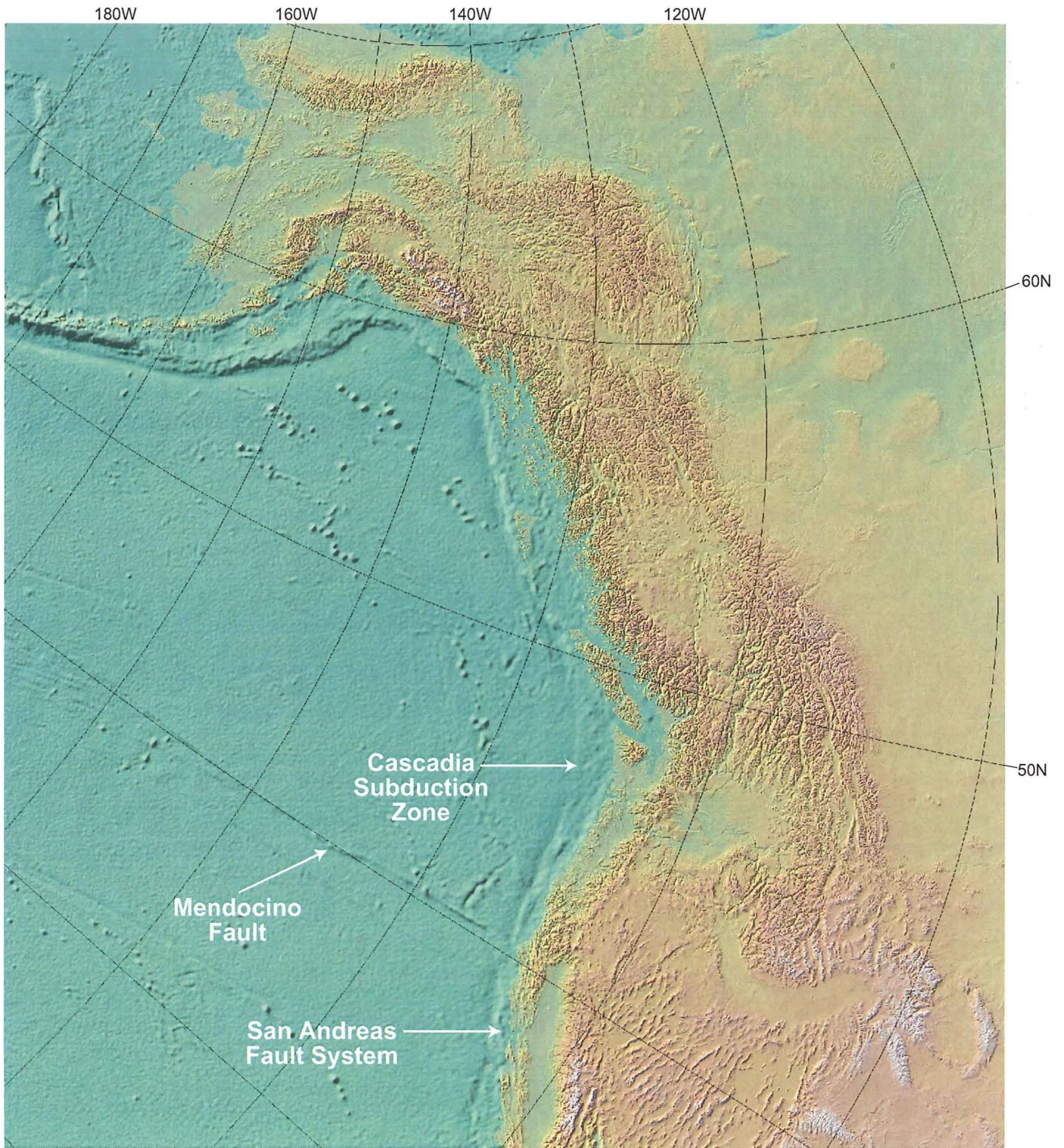


Figure 1-2 Color shaded-relief map (oblique Mercator projection) of the Cascadia subduction zone along the northwest coast of the United States and Canada (from R.A. Haugerud, 1998, USGS Open-File Report 98-140).

S:\5100s\5117\5117.009\task_13\02_1230_s1\fig_01-02(87,88).ai





Photo 1-1 South Humboldt Bay. View is southeast.

S:\5100s\5117\5117.009\task_13102_1230_s1\photo_01-01(86).ai



Section 2.0

Tectonic Framework

2.1 INTRODUCTION

The Humboldt Bay ISFSI site is on the western edge of the North American plate, near the southern end of the Cascadia subduction zone, and a short distance north of the Mendocino triple junction region (Figure 2-1). The region is traversed by many active faults, which form the complex structural and tectonic architecture of the southern part of the subduction zone and the triple junction. Although the region is among the most seismically active of any in western North America, the seismicity observed over the relatively short historical period (the past 150 years or so) undoubtedly does not reflect the full seismic potential of the region. The largest earthquakes include very large subduction-zone earthquakes that are not represented by the historically observed seismicity, but evidence of these earthquakes is preserved in the paleoseismic record.

We have studied this record along the coast of northern California, Oregon, and Washington, especially in the Humboldt Bay region, to better understand the tectonic framework and, thus, the seismic potential of the Cascadia subduction zone. This data base, which has undergone dramatic changes during the past two decades, is crucial to assessing the seismic hazards at the ISFSI site. Our tectonic model is based on today's knowledge, and is consistent with worldwide observations of subduction zones and their earthquake potential. We believe our comprehensive model of the tectonic framework results in a reasonable but conservative seismic hazard assessment for the Humboldt Bay ISFSI site.

The tectonics of coastal northwestern California are dominated by plate boundary interactions among the North American plate, the Pacific plate, and the combined Gorda-Juan de Fuca plates (Figure 2-1). North of the triple junction, the Gorda-Juan de Fuca plates are being subducted beneath the North American plate along the Cascadia subduction zone, whereas south of this junction, the Pacific plate moves northward relative to the North American plate along the



San Andreas fault zone. The Mendocino fault marks the right lateral transform boundary between the Pacific plate and the Gorda-Juan de Fuca plates. On a global-plate-tectonics scale, these three plates meet at the Mendocino triple junction: the intersection of the San Andreas and Mendocino transform fault zones with the Cascadia subduction zone. Although it is commonly depicted as a point slightly offshore and south of Cape Mendocino, the junction is actually a broad region of complex structure.

Both transform faults have been seismically active historically. The San Andreas fault slipped as much as 6 meters in northern California in the magnitude 7.8¹ San Francisco earthquake in 1906; the fault rupture extended at least as far north as Point Arena, and possibly north to Point Delgada, a short distance south of the triple junction (Lawson, 1908; Brown and Wolf, 1972; Prentice, 1989). The Mendocino fault zone has produced earthquakes up to magnitude 7.25, which have occurred at different locations along much of its length. In contrast, the Cascadia subduction zone leg of the triple junction has been nearly aseismic historically. The April 25, 1992, magnitude 7.1 Petrolia earthquake is the only recorded large seismic event associated with the subduction zone (Oppenheimer and others, 1993).

Field studies in the triple junction region show that the transform and subduction zone boundaries of the three principal plates are broad zones containing elaborate systems of individual faults and fault-bounded crustal blocks tens of kilometers wide. Thus, on a more detailed scale, the Mendocino triple junction is a large, structurally complex region encompassing the intersection of these wide plate boundaries and, we believe, is best characterized by distinct subplates. To provide a better understanding of this complicated region, we first present a brief discussion of the three plate-boundary elements of the triple junction, and then describe the triple junction region itself. Details of the geology of the Humboldt Bay ISFSI region are presented in Section 3.0.

¹ Earthquake magnitudes are moment magnitudes (**M**), unless stated otherwise.

2.2 NORTH AMERICAN PLATE BOUNDARY

The present plate configuration in northern California was initiated during the early Miocene, about 20 million years ago, when the former Farallon and Kula plates (Figure 2-2) were consumed by subduction beneath the western edge of North America, and contact was made between the Pacific plate and the North American plate (Atwater, 1970). The first Pacific/North American plate contact occurred in southwestern California, and produced the Mendocino triple junction and proto San Andreas fault system. The unsubducted remnant of the former Farallon plate became the predecessor to the modern Juan de Fuca plate. Throughout the late Cenozoic, (past 5 million years) the Juan de Fuca plate continued to subduct obliquely to the northeast beneath the western edge of North America, as the Mendocino triple junction migrated northward through central and into northwestern California, extending the San Andreas fault system into northern California. Thus, the San Andreas fault system decreases in age and total net slip from south to north. In the northernmost part of California, near the triple junction region, the fault system has experienced relatively little net displacement, and is no older than Quaternary (1.6 million years).

As the Mendocino triple junction migrated northward through western California, and the San Andreas transform system increased its length, large crustal slivers were broken off from the North American plate (Dickinson and Snyder, 1979). Several of these detached blocks of continental crust, including the continental Salinian block in central and northern California and the oceanic Vizcaino block at the northern end of the San Andreas fault system (Leitner and others, 1998), were attached to the eastern edge of the Pacific plate as the San Andreas fault motions were transferred eastward (Griscom and Jachens, 1989).

Other detached pieces of the North American plate were entrained between east-stepping branches of the San Andreas fault zone. Two of these fault-bounded crustal slivers in northwestern California are interpreted by Kelsey and Carver (1988) to have persisted through the latest Cenozoic to the present. According to these authors, the western crustal sliver, herein designated the Petrolia subplate, is in contact with the Pacific plate on its western side along the San Andreas fault zone. The Petrolia subplate is bordered on the east by the Bear River shear zone and a zone of right-slip faults including, from northwest to southeast, the Garberville fault,



the Maacama fault, the Rogers Creek fault, and the Hayward fault (Figure 2-3). The second fault-bounded crustal block, the Eel River subplate, is interpreted to lie between the Petrolia subplate and the North American plate (Figure 2-3). This sliver of North American plate crust is bounded on the west by the Bear River shear zone and the Garberville/Maacama/Rogers Creek/Hayward fault zone, and on the east by a similar system of predominately right-slip faults, including, from northwest to southeast, the Lake Mountain fault, the Bartlett Springs fault, the Green Valley fault, and the Calaveras fault. These right-slip fault zones are part of the San Andreas fault system, which separates the Pacific and North American plates south of the Mendocino fault zone.

North of the Mendocino fault zone, the western side of the North American plate is bounded by the Cascadia subduction zone, which includes the plate boundary megathrust and a broad west-vergent, overlapping system of thrust faults along the plate margin. In northwestern California, this imbricate system includes two major fault zones: the Mad River fault zone, and the Little Salmon fault zone, which we interpret to accommodate a large part of the convergence between the North American plate and subducting Gorda plate. Where the southern part of the Gorda plate is subducting beneath the Eel River and Petrolia subplates, there are two subduction zone segments, called the Eel River and Petrolia segments. Historical seismicity and paleoseismic evidence indicate these segments have slip histories that are independent of the main Cascadia subduction zone, as discussed in Section 2.4.

In contrast to the San Andreas fault zone in northern California, which has been nearly aseismic since the 1906 earthquake, both the Garberville/Maacama/Rogers Creek/Hayward and the Lake Mountain/Bartlett Springs/Green Valley/Calaveras fault zones are well-defined seismically, and have been the source of many predominately right-slip to right-oblique or reverse-slip earthquakes² (Castillo and Ellsworth, 1993). The seismicity reflects right-slip transform motion, resulting from northwest movement of the Pacific plate relative to the western North American plate margin. Focal mechanisms show these faults to have steep northeasterly dips. Focal depths

² Regional faults are shown on Figure 2-3 (except for the Rogers Creek, Hayward, Green Valley and Calaveras faults, which are south of the mapped area).

range from a few kilometers to the base of the crust in this region, which is about 20 kilometers (Castillo and Ellsworth, 1993; Trehu and others, 1995). The depth distribution of seismicity associated with the Garberville/Maacama/ Rogers Creek/ Hayward and the Lake Mountain/Bartlett Springs/Green Valley/Calaveras fault zones shows the crustal blocks bounded by these fault zones are detached from the North American plate and are moving within the San Andreas transform system as small subplates.

This interpretation of the interplate structure of the Garberville/ Maacama/Rogers Creek/ Hayward fault zone and the Lake Mountain/Bartlett Springs/Green Valley/Calaveras fault zone is supported by the results of deep-crustal and upper-mantle seismic imaging studies that show apparent offset of prominent lower-crustal and upper-mantle reflectors across these faults (Trehu and others, 1995). Trilateration, triangulation, and Global Positioning Satellite geodetic measurements of strain across northwestern California south of the Mendocino triple junction show that much of the right-slip motion between the Pacific plate and the North American plate currently is localized along these two fault zones (Freymueller and others, 1999; Lisowski and Prescott, 1989).

2.3 PACIFIC/GORDA-JUAN DE FUCA PLATE BOUNDARY

The plate boundary between the Pacific and Gorda-Juan de Fuca plates has traditionally been defined as the Mendocino transform fault zone, a nearly west trending, right-slip fault zone that extends about 1,400 kilometers across the sea floor from Punta Gorda, 15 to 25 kilometers south of Cape Mendocino, to the southern end of the Gorda rise. The landward end of the fault zone is well expressed topographically and bathymetrically by the Mendocino escarpment, a prominent sea floor escarpment having more than 900 meters of relief. The escarpment separates the anomalously shallow continental marine margin underlain by the Vizcaino block of the Pacific plate south of the Mendocino fault zone (Figure 2-1) from the deep Gorda basin to the north (Leitner and others, 1998). The Mendocino fault zone is highly seismic, and has produced many moderate to large earthquakes during the historical period, including several in the magnitude range of 7 to 7.25 (Bolt and Miller; 1975, Dengler and others, 1992a).

There is considerable evidence of north/south compression across the eastern part of the Mendocino fault zone. Many of the earthquakes along this part of the zone have oblique



compressional focal mechanisms. Additionally, the topographic relief of the Mendocino escarpment is attributed to compression-driven uplift of the northern edge of the Vizcaino block. Rounded cobbles dredged from the crest of the Mendocino ridge, a prominent fault-parallel ridge on the sea floor along the northern edge of the Vizcaino block, suggest the ridge was emergent during the late Cenozoic, and has since subsided below sea level (Krause and others, 1964; Duncan and others, 1994; Leitner and others, 1998). The elevation of the thicker and older crust of the Vizcaino block above the thinner and younger Gorda plate oceanic crust north of the transform fault zone is the opposite of what would be predicted from isostatic effects. The elevation of the northern edge of the Vizcaino block has been attributed to dynamically supported uplift driven by the north/south compression between the Pacific and Gorda plates (Leitner and others, 1998).

The southern half of the Gorda plate, north of the Mendocino fault zone and west of the Cascadia subduction zone, is strongly deformed and highly seismic. Northeast-trending, high-angle, left-slip faults distributed across this part of the plate have produced many historical earthquakes having magnitudes as large as 7.2 (Bolt and Miller, 1975; Dengler and others, 1992a) (Figure 2-4). Near the triple junction, some of the seismicity also yields north/south compressional focal mechanisms (McPherson, 1989; 1992). Magnetic anomalies in the southern part of the Gorda plate have been rotated clockwise relative to the Gorda rise; older anomalies have progressively greater rotation. In the triple junction region, this apparent rotation approaches 60 degrees for anomaly 3 (isochrons 3.86 to 4.79 million years old, Figure 2-4). Additionally, the length of the deformed anomalies is less than the length of the parent Gorda rise; older anomalies have progressively more shortening. Wilson (1989) called the deforming southern part of the plate the “Gorda deformation zone,” and questioned whether it could be considered part of an internally rigid crustal plate.

The northern boundary of the Gorda deformation zone is a relatively sharp transition from rotated oceanic crust on the south to rigid crust having sparse seismicity and magnetic anomalies that are generally parallel to the Gorda rise to the north. This transition strikes N60°W, and intersects the subduction zone offshore of the coast a short distance north of the latitude of Humboldt Bay. Although no discernible offset of magnetic anomalies or rise-generated structural fabric in the Gorda plate is evident along this transition, Wilson (1989) attributes the

boundary to right shear at depth, possibly localized along faults in a narrow zone in the lower part of the oceanic plate. The transition is generally coincident with the northern limit of concentrated Gorda plate seismicity (Smith and Knapp, 1980).

Two kinematic models have been proposed to explain the deformation within the Gorda deformation zone. Riddihough (1984) postulated the southern part of the Gorda plate has behaved as an internally rigid block that has undergone clockwise rotation around a nearby pole. He postulated shortening along the southern margin of the block by obduction of the Pacific plate along the eastern end of the Mendocino transform fault zone. However, the lack of evidence of thrusting of the Vizcaino block over the southern margin of the Gorda plate, and the evidence of widely distributed faulting within the plate do not support this interpretation.

A preferred alternative explanation for the deformation of the southern part of the Gorda plate includes asymmetrical spreading at the Gorda rise, and pervasive left shear distributed on many vertical faults aligned along the original structural fabric of the Gorda crust (Smith and Knapp, 1980; Wilson, 1989). More rapid spreading to the north along the rise is apparent in the rotation of the magnetic anomalies. Left shear along zones of structural weakness inherited from the rise results from the plate rotation, as long, narrow, fault-bounded blocks slide past one another, analogous to a toppling stack of books.

2.4 CASCADIA SUBDUCTION ZONE

The Cascadia subduction zone extends from northern California 1,100 kilometers north to southern British Columbia. The oblique convergence of the Gorda-Juan de Fuca plate with the North American plate is accommodated by subduction along this zone. The zone is characterized by the very young age of the subducting Gorda-Juan de Fuca plate (less than 10 million years at the trench), a shallow angle of subduction of the down-going oceanic plate (dip less than 10 degrees), a moderate rate of convergence (3 to 4 cm/yr), a moderate rate of the oblique component of the convergence (1 to 2 cm/yr), and a relatively shallow trench. Based on these properties, when compared to other subduction zones worldwide, Cascadia belongs to a class of strongly coupled (Chilean-type) subduction zones, compared with subduction zones where the plates are weakly coupled (Mariana-type) (Heaton and Kanamori, 1984). Examples of other



Chilean-type subduction zones include those in Alaska, the eastern and central Aleutians, southern Chile, northwestern South America, southeastern Russia, and southwestern Japan (Heaton and Kanamori, 1984). Chilean-type subduction zones have produced the largest earthquakes (magnitude 7.7 to 9.5; average magnitude, 8.7) and longest rupture lengths (150 to 1,000 km; average rupture length, 540 km), compared with weakly coupled subduction zones (average magnitude, 7.7; average rupture length, 110 km).³

Within the Mendocino triple junction region, three Cascadia subduction zone segments can be defined (Figure 2-3). The main segment is the 1,000-kilometer-long Cascadia subduction zone segment that extends north from Humboldt Bay. South of Humboldt Bay, we interpret the Eel River segment, an approximately 80-kilometer-long segment along which the northern part of the Gorda deformation zone is obliquely subducting beneath the Eel River subplate. The southern segment, designated the Petrolia segment, reflects convergence of the southern part of the Gorda deformation zone and the Petrolia subplate. The Petrolia segment has a mapped length of 25 to 30 kilometers. These three segments have different seismic histories.

Although the main Cascadia subduction zone segment has been seismically quiet during recorded history, paleoseismic and tsunami evidence has led to wide acceptance that the zone has produced great earthquakes in the past, most recently about 300 years ago, and has the potential to generate great earthquakes in the future (Atwater and others, 1995). High-precision radiocarbon ages have been obtained from tree ring series from trees interpreted to have been killed by saltwater incursion due to coseismic subsidence along the Washington (Atwater and Yamaguchi, 1991) and Oregon coasts (Atwater and others, 1991) and in the Mad River Slough at Humboldt Bay (Carver and others, 1992; Jacoby and others, 1995). These ages indicate the most recent great Cascadia earthquake occurred during a 10- to 20-year interval around AD 1700. Additionally, high-precision radiocarbon ages for herbaceous salt marsh plants, also interpreted as having been killed by flood water due to earthquake-generated coastal subsidence, were derived from nine coastal locations along the main Cascadia subduction zone segment in northern California, Oregon, and Washington (Nelson and others, 1995). These ages also

³ Based on a summary of 53 worldwide subduction zone events between 1938 and 1991 (Geomatrix Consultants, 1995, Table 2-2).

indicate the most recent great earthquake on the main Cascadia subduction zone segment occurred during a 10- to 20-year interval around AD 1700.

The date of this earthquake can be further pinpointed by observations of a trans-Pacific tsunami that destroyed houses in Kuwagasaki and was recorded at four other locations in Japan on January 27, 1700. This wave is interpreted to have been caused by the most recent large slip event on the Cascadia subduction zone (Satake and others, 1996). Satake and his colleagues (1996) modeled both segmented (magnitude ~8) and long (magnitude ~9) rupture lengths on the Cascadia subduction zone. They found the long rupture was necessary to produce a tsunami large enough to cause the damage reported in the Japanese literature. Additionally, because the stratigraphy in many of the coastal marshes in North America (from California to British Columbia) shows only one sand deposit from the 1700 tsunami, not several, the paleoseismic evidence also suggests the most recent Cascadia earthquake resulted from a long, single rupture of the subduction zone, causing an earthquake near magnitude 9.

The April 25, 1992, magnitude 7.1 Petrolia earthquake was a thrust event that broke along the southernmost segment of the Cascadia subduction zone (Oppenheimer and others, 1993). The earthquake resulted from rupture of the plate interface along the northwestern end of the Petrolia subplate (Humboldt plate of Tanioka and others, 1995). This earthquake demonstrated the seismic potential of the southernmost part of the subduction zone, and the segmentation associated with the subplates, defined by the branches of the San Andreas fault system (Figures 2-1 and 2-3). As discussed in Section 5.0, although the Petrolia segment has a mapped length of 25 to 30 kilometers, only the eastern part of the subplate, which has a north to south width of 18 kilometers, is considered to be seismogenic.

The third segment of the Cascadia subduction zone in the triple junction region is between the 1992 rupture and the main Cascadia subduction zone segment north of Humboldt Bay. This segment is the convergent margin between the deforming Gorda plate (Gorda deformation zone) and the Eel River subplate. It has not generated a notable earthquake in more than 150 years, but the paleoseismic record for this part of the subduction zone demonstrates the segment is tectonically active. Fossil tree stumps in the lower Eel River Valley are presently below sea level, and tree ring analyses show these trees died suddenly (Li, 1992; Jacoby, personal



communication, 1998). The submergence was associated with subsidence in the Eel River Valley, presumably during a prehistoric earthquake.

The Eel River Valley is located in the core of a syncline filled with a thick sequence of late Cenozoic sediments. The syncline is interpreted to represent the structural depression formed in the backstop region of elastic relaxation behind a large northwest-striking, northeast-dipping thrust fault, possibly the Russ fault (Aalto and others, 1995), which reaches the surface to the southwest near the southern edge of the Eel River subplate.

The timing of the late Holocene paleoseismic events in northwestern California cannot be differentiated on the basis of conventional radiocarbon ages from the Cascadia events farther north, suggesting most of the subduction zone may have been unsegmented during most seismic cycles (Carver, 2000). Li (1992) used conventional radiocarbon dating to estimate the ages of a series of subsidence events in the Eel River syncline based on detailed analysis of the marsh stratigraphy (Table 2-1). Several of the subsidence events, which are interpreted to have been caused by coseismic subsidence associated with earthquakes on the Cascadia subduction zone, have ages similar to events on the Little Salmon fault zone and to events on the main segment of the Cascadia subduction zone farther north (Table 2-1; Figure 9-7). However, high-precision carbon-14 ages for tree ring series from submerged trees in the lower Eel River Valley indicate the most recent large earthquake on the Eel River segment of the Cascadia subduction zone occurred during the early 1800s (Carver, 2002, written communication⁴). This is significantly younger than the most recent event on the main segment of the subduction zone to the north, which occurred in 1700 AD. Therefore, we conclude the Eel River and main segments of the Cascadia subduction zone ruptured independently during the most recent event on each of these segments.

Nelson and others (2000) correlate turbidite deposits in the offshore channels from Vancouver Island to the Noyo Channel, south of Cape Mendocino, to regional earthquakes. They postulate that the 13 turbidites since about 7,200 years ago in the Cascadia, Astoria, and Rogue channel

⁴ Copies of the original data records for these carbon-14 ages are in the PG&E files.

systems were caused by earthquakes on the Cascadia subduction zone (average recurrence of 600 years). South of the Rogue River, the number of turbidites progressively increases; there are 50 Holocene turbidites in the Eel River channel. They ascribe 20 of these to Cascadia events, and 30 to San Andreas events. We believe some of these may have been triggered by events on the Petrolia and Eel River subplates at the southern end of the Cascadia subduction zone.

The structure of the main Cascadia subduction zone segment in the study region is interpreted to include a 65- to 100-km-wide active fold and thrust belt in the North American plate margin that extends onshore in northern California (Figure 2-5). The fold and thrust belt is composed mainly of two distinct groups of thrust faults: the Mad River fault zone, and the Little Salmon fault system (Clarke and Carver, 1992). Both groups are composed of right-stepping, en echelon, seaward-vergent imbricate thrust faults. Although the groups are subparallel to the trench, their component faults are oriented normal to the direction of oblique convergence between the Gorda-Juan de Fuca and North American plates.

The Mad River fault zone and Little Salmon fault system are separated by the Freshwater syncline (Figures 2-5 and 2-6), a long flat-floored synclinal structure filled with young sediment that extends onshore through the northern part of Humboldt Bay. This structure is adjacent and parallel to the Little Salmon fault system offshore for more than 200 kilometers. It is interpreted to represent the zone of elastic extension and subsidence associated with the Little Salmon fault zone and other faults within the Little Salmon fault system. The high-precision radiocarbon ages from trees at Mad River Slough, which indicate coseismic subsidence of this syncline in 1700 (Carver and others, 1992; Jacoby and others, 1995), supports an interpretation that the Little Salmon fault zone and the main Cascadia subduction zone experience coseismic slip during great Cascadia subduction zone earthquakes. It is possible that the subsidence in Mad River Slough in 1700 is primarily the result of slip on the underlying subduction zone and that vertical deformation caused by the Little Salmon fault in northern Humboldt Bay is secondary deformation and superimposed on top of the subduction zone (megathrust) related deformation.

The interpretation of coseismic slip on the Little Salmon fault zone and the main Cascadia subduction zone, however, is supported by two types of evidence. First, most of the coast from Big Lagoon south to the triple junction (Figure 2-6), a distance of 50 kilometers, exhibits

evidence of late Holocene uplift. This area is underlain by the plate interface at a typically shallow depth of 10 to 20 kilometers (about 12 ± 1 km below Eureka). Second, in the Humboldt Bay region, field evidence of coseismic subsidence is localized in the Freshwater, South Bay, and Eel River synclines. Each of these synclines trends parallel to and is in the hanging wall of a major fault: the Russ and Table Bluff faults with the Eel River and South Bay synclines, respectively, and the Little Salmon fault which is bordered by the Freshwater syncline from Humboldt Bay north into southern Oregon (Clarke, 1990, 1992). Each of these three faults has a high slip rate and large amount of net vertical displacement. Dislocation modeling for this region was conducted as part of the NOAA Cascadia tsunami inundation study (Bernard and others, 1994) and the CDMG Northern California Cascadia Earthquake Scenario (Topozada and others, 1995). The modeling suggests slip on the Little Salmon fault during a megathrust event would result in regional uplift along the coast and subsidence of the axis of the Freshwater syncline. Results of the dislocation modeling presented in the NOAA publication (Bernard and others, 1994, p. 54) illustrate the form of the surface elevation changes along the coast.

The close proximity of the syncline axis to the surface trace of the Little Salmon fault zone (~10 kilometers) places constraints on the dip of the Little Salmon fault zone. Assuming the fault joins the subduction zone megathrust at the base of the accretionary wedge, about 14 ± 1 kilometers below the surface at the coast at Humboldt Bay (Beaudoin and others, 1996), the dip of thrusts in the Little Salmon fault zone must be greater than 40 degrees. Much shallower dips have been observed on the near-surface traces of the fault zone at the coast (Clarke and Carver, 1992). Isopach maps of the Little Salmon fault based on measured depths of intercepts of the fault in gas wells at the Tompkins Hill gas field, about 16 kilometers southeast of the plant site, show the fault steepens from less than 12 degrees at the surface to more than 28 degrees at a depth of about 1,800 meters. Large anticlines on the hanging wall of the fault, including the Humboldt Hill anticline, also indicate the dip of the fault increases with depth.

The outer 15 to 25 kilometers of the accretionary margin is cut by thrusts that are parallel to the subduction front and are both seaward- and landward-vergent (Gulick and others, 1998). The part of the accretionary margin containing the subduction-front-parallel thrusts and the landward part cut by the en echelon thrust zones are separated by a structural discontinuity (Figure 2-6) (Humboldt discontinuity of Clarke and Carver, 1992; Clarke, 1992). Seismic reflection profiles



across the structural discontinuity show the eastern part of the accretionary margin, the part cut by the en echelon faults, is floored with older basement rocks (Franciscan Formation), whereas seaward of the structural discontinuity, the accretionary prism is composed of recently scraped-off Gorda plate sediments (Clarke, 1992; Gulick and others, 1998). We interpret the difference in orientation of thrusts on either side of the structural discontinuity as reflecting the limit of strong interseismic coupling between the subducting oceanic plate and the accretionary margin.

Active thrusting on the Little Salmon fault system also is inferred from the evidence of large, locally generated tsunamis that has been found along the Cascadia subduction zone from Vancouver Island to northern California (Atwater and others, 1995; Section 9.0). Radiocarbon ages for the seven most recent tsunamis along the northern California coast are indistinguishable from the ages for subduction earthquakes from coastal subsidence data in Washington State (Atwater and Hemphill-Haley, 1997; Section 9.0). Both the Japanese records of the trans-Pacific Cascadia tsunami (Satake and others, 1996) and runup-height estimates from paleotsunami evidence in northern California (see Section 9.0) indicate the tsunamis were too large to be generated by slip on the shallowly dipping megathrust only. This assessment is supported by the results of attempts to model tsunami generation on the southern part of the Cascadia subduction zone (Bernard and others, 1994). However, if a large part of the slip on the plate boundary were taken up on thrusts in the Little Salmon fault system, the resulting large vertical sea-floor deformations would be capable of producing tsunamis large enough to produce the evidence found in the paleotsunami record along the northern California coast and reported in early 18th century Japanese literature. The paleotsunami evidence of large tsunami runup heights for previous tsunamis along the northern California coast (Section 9.0) also implies that intraplate slip during the most recent seven subduction earthquakes largely has been transferred to the Little Salmon fault system, and the outer 15 to 25 kilometers of the megathrust has experienced relatively less displacement.

A steep, strike-slip fault with flower-structure-like splays can be inferred approximately 10 kilometers offshore along the projected seaward trend of the Little Salmon fault (Gulick and others, 2002, Figure 10A). As shown on a multichannel seismic reflection profile, this offshore fault is associated with little vertical separation of the basement offshore and little evidence of offset of the Pliocene through Holocene strata (unit A of Gulick and others, 2002). A strike-slip



interpretation for offshore faults would not support the interpretation, proposed in the discussion directly above, that a large part of the slip on the plate boundary is taken up on thrusts in the Little Salmon fault system. The offshore profile of Gulick and others (2002), however, is not consistent with cross sections of the Little Salmon fault onshore. Specifically, onshore cross sections show that the Little Salmon fault is associated with large near-surface displacements on moderate to low angle imbricate thrusts and large vertical separation of the basement/Wildcat contact. Abundant evidence for reverse/thrust displacement on the Little Salmon and Mad River fault zones onshore is found in exposures, trenches, gas wells, and borings. Additionally, the large-scale morphology of the Little Salmon fault includes prominent upper plate anticlines, providing clear evidence of predominantly dip-slip movement.

2.5 MENDOCINO TRIPLE JUNCTION REGION

As stated previously, the Mendocino triple junction is the intersection of three plate boundaries, each of which is a wide zone of deformation composed of multiple faults. Several previous investigators have recognized this complex and broad architecture (Tanioka and others, 1995; Gulick and others, 1998). However, most previous analyses of tectonics and seismic sources in the northwestern California region have generalized the intersecting plate boundaries into discrete narrow zones, and have treated the triple junction as a point, or they have avoided detailed treatment of the triple junction region altogether, considering only the major plate-bounding faults and seismically active areas outside the triple junction region.

New information useful for developing a detailed tectonic model for the Mendocino triple junction region comes from offshore and onshore geologic mapping, identification and characterization of active tectonic structures, seismic refraction and reflection studies of shallow and deep crustal structure, seismicity and seismological investigations, and paleoseismic studies conducted during the past decade. The updated tectonic framework we use for assessing seismic sources in the northwestern California region considers the seismotectonic interactions of the subplates and the individual faults within the triple junction region. We treat the triple junction as a broad region at the intersection of the three, wide, plate-boundary deformation zones.



The northwestern extent of the triple junction region is marked by the deformation front of the subduction zone south of the intersection with the transition between the Gorda deformation zone and the undeformed Gorda plate. This point coincides in general with a change in the architecture of the accretionary margin of the Cascadia subduction zone. Along this part of the convergent margin, the internally deforming Gorda deformation zone is subducting at a highly oblique angle beneath the northwestern ends of the Eel River and Petrolia subplates. North of the intersection of the Gorda plate/Gorda deformation zone transition and the subduction zone, the rigid Gorda-Juan de Fuca plate is subducting beneath the North American plate along the main Cascadia subduction zone segment.

The southern part of the accretionary margin, south of the intersection of the subduction front and the transition in the Gorda plate, has a distinctly different architecture than the margin to the north of this intersection (Figure 2-6). The structural discontinuity that is prominent northeast of the rigid Gorda plate/Gorda deformation zone transition is absent to the south; instead, west-northwest-trending thrust faults extend from the coast to near the deformation front (Clarke, 1990). These faults and associated folds are generally parallel to large, young, onshore structures, including the Eel River syncline, the Russ fault, and the Bear River shear zone, and appear to reflect tectonics driven by the northward movement of the Pacific plate in the triple junction region (Wang and others, 1997).

We place the northeastern limit of the triple junction region along the landward projection of the transition zone in the subducted Gorda plate. It is interpreted to be along the southern part of the Little Salmon and Table Bluff fault zones in the overlying continental crust. Within this triple junction region, the subplates within the San Andreas transform zone and the fault-bounded blocks of the Gorda deformation zone converge. Their rates and directions of convergence differ from those along the main Cascadia subduction zone segment to the north, where the internally rigid oceanic plate is subducting beneath the North American plate.

The eastern extent of the triple junction region is interpreted to be along the Lake Mountain fault along the eastern edge of the Eel River subplate (Figures 2-3 and 2-6), and conforms to the eastern limit of the San Andreas transform fault zone. At depth, west of this eastern boundary of the triple junction, the Mendocino transform is represented by the southern edge of the

seismically active subducted Gorda plate (Figure 2-4) (Jachens and Griscom, 1983, Beaudoin and others, 1996). Both the Eel River subplate and the Petrolia subplate overlie the subducted southern Gorda plate edge.

The southern extent of the triple junction region is interpreted to be at the extreme eastern end of the Mendocino fault zone, near Punta Gorda (Figure 2-6), and is defined by the northern edge of the rigid Pacific plate. The Mendocino fault zone is very well expressed offshore and to the west of the subduction zone deformation front; however, the location of the fault zone near the coast is not well known. A linear projection of the fault zone from its well-defined trace offshore to the shoreline places the plate boundary in the Mendocino Canyon as it crosses the continental shelf, and under the coastline near Mussel Rocks and McNutt Gulch, west of Petrolia (Clarke, 1992). However, aftershocks following the 1992 Petrolia earthquake defined a strike-slip fault trending beneath the Mattole submarine canyon and extending under the coast near the mouth of the Mattole River (Oppenheimer and others, 1993), implying a slight southward bend in the fault around the northeast corner of the Pacific plate (Figure 2-6). Coastal uplift during the 1992 Petrolia earthquake extended several kilometers farther south to Punta Gorda (Carver and others, 1994), and may represent obduction of the southwestern edge of the Petrolia subplate over the Mendocino fault zone during the Petrolia earthquake.



2.6 ALEUTIAN SUBDUCTION ZONE ANALOG

The eastern Aleutian subduction zone has many characteristics similar to those of the Cascadia subduction zone. Analysis of the 1964 Alaska earthquake provides a useful analog to better understand the potential earthquake and tsunami hazards associated with the Cascadia subduction zone.

The 1964 magnitude 9.2 Alaska earthquake was caused by rupture on the eastern part of the Aleutian subduction zone, and by displacements on intraplate faults. These combined displacements uplifted part of the accretionary continental margin, creating the large tsunami associated with this earthquake. This Alaskan structural setting is comparable to the Cascadia subduction zone, with the Little Salmon fault system cutting through the accretionary prism, and provides an analog for northern California (Figure 2-7). The details of this earthquake are presented in Appendix 2A; the important points are summarized below.

The 1964 Alaska earthquake deformation involved a segment of the eastern Aleutian arc 800 kilometers long and 275 to 400 kilometers wide. This major tectonic event was characterized by seismicity less than 30 kilometers deep, regional vertical displacements in a broad asymmetric downwarp to 2 meters, and flanking zones of marked uplift to 11.3 meters on the seaward side (Plafker, 1969; 1972).

Subordinate northwest-dipping reverse faults, the Patton Bay and Hanning Bay faults, displaced the surface on Montague Island. The Patton Bay fault, which experienced at least 7.9 meters of dip-slip, extends offshore to the southwest onto the continental shelf, and intraplate fault displacement seaward of Middleton Island near the continental shelf edge is suggested by 3.5-meter coseismic uplift and northeastward tilting of the island. The intraplate thrust faults at Montague and Middleton Islands alone accommodated at least 23 meters of the total slip on the Aleutian megathrust, assuming average fault dips of about 30 degrees (Figure 2-7).

Arrival times on the Alaskan coast show the source area for a major train of destructive sea waves (tsunamis) generated on the continental shelf corresponds closely to the zone of major uplift on the Patton Bay fault and subsidiary faults on the continental shelf and slope. The waves



clearly resulted from sudden coseismic upheaval of the sea floor (Plafker and Rubin, 1967; Plafker, 1969).

These data show that a major fraction of the slip may be partitioned among intraplate thrust faults that break relatively steeply to the surface and consequently can result in greater seafloor uplift than an equivalent displacement entirely on the megathrust. In Cascadia, the zones of active faults and related folds of the Little Salmon fault zone appear analogous in tectonic behavior to the intraplate faults observed or inferred within the focal regions of the 1964 Alaska earthquake, which generated a major tsunami.

2.7 SUMMARY OF TECTONIC FRAMEWORK

- The Humboldt Bay ISFSI site is situated near the southern end of the Cascadia subduction zone, at the northern margin of the complex and highly seismic Mendocino triple junction region.
- Within the Mendocino triple junction region, we have delineated three distinct Cascadia subduction zone segments. The southernmost, about 25 to 30 kilometers long, represents the part of the subduction zone where the deforming southern margin of the Gorda plate is converging with the Petrolia subplate at the northern end of the San Andreas transform fault zone. The April 25, 1992, magnitude 7.1 Petrolia earthquake demonstrated the seismic potential of this segment. The second segment of the subduction zone, about 80 kilometers long, is defined by convergence of the deforming southern part of the Gorda plate with the Eel River subplate at the northern end of the San Andreas transform zone. It has not produced an historical earthquake, but paleoseismic evidence indicates the segment last ruptured about 1820, and caused subsidence of the lower Eel River valley. These subduction-zone segments constitute independent seismic sources for large earthquakes in the Humboldt Bay region. The main Cascadia subduction zone segment extends north from Humboldt Bay for about 1,000 kilometers. This zone last ruptured causing a great earthquake in 1700, and has the potential to generate great earthquakes in the future.
- Along the Cascadia subduction zone, the northwestern limit of the Mendocino triple junction region is interpreted to be where a transition from deformed to internally rigid Gorda oceanic



crust intersects the subduction zone. This northwestern limit to the triple junction region is considered to mark the southern extent of plate-boundary rupture during great earthquakes on the main Cascadia subduction zone.

- The structure of the main Cascadia subduction zone segment includes a prominent fold and thrust belt, roughly parallel to the leading edge of the North American plate, that includes the Little Salmon fault system. Faults within the Little Salmon fault system are interpreted to be steeply dipping (more than 40 degrees) and, together with the Table Bluff fault and Mad River fault zone, to accommodate a large part of the slip generated during great subduction earthquakes. Data from the Aleutian and Cascadia subduction zones indicate that intraplate deformation can take up much or all of the plate convergence, and that this deformation can extend landward to areas where the megathrust is as much as 17 kilometers deep.
- Offshore vertical displacements of the sea floor related to secondary faulting within the upper plate have been shown to be effective mechanisms for tsunami generation during the 1964 Alaska earthquake, and are suspected in other great tsunamigenic subduction-zone events. For Cascadia, a comparable mechanism, involving rupture on intraplate faults in the Little Salmon fault system, is considered to be responsible for generating the robust local tsunamis observed in the paleotsunami record.



Table 2-1

COMPARISON OF THE TIMING OF EVENTS ON THE MAIN SEGMENT OF THE CASCADIA SUBDUCTION ZONE WITH EVENTS ON THE EEL RIVER SEGMENT

Main Segment of the Cascadia Subduction Zone			Eel River Segment of the Cascadia Subduction Zone
Main Cascadia Subduction Zone (Atwater and Hemphill-Haley, 1997) (years BP)	West Trace, Little Salmon Fault, Salmon Creek Site (Clark and Carver, 1992) (years BP)	West Trace, Little Salmon Fault, Swiss Hall Site (Witter and others, 2002) (years BP) ¹	Eel River Syncline (Li, 1992; G. A. Carver, written communication, 2002) (years BP) ²
			~170 (1827 AD ± 28) ³
Event "Y," 300 (January 27, 1700)	~300	<460	
	~800		~830
Event "W," 1100		540-1230	
Event "U," 1300		1350 to 1560	~1290
Event "S," 1600	~1600	1530 to 1710	~1530
		1950 to 2300	~1930
Event "N," 2500			
Event "L," 2900			
Event "P," 3100			
Event "O," 3900			

Note: The Sixes River estuary, southern Oregon, studied by Kelsey and others (2002) is closer to Humboldt Bay than the southern Washington site studied by Atwater and Hemphill-Haley (1997). The Sixes River record for events within the past 2,000 years is less complete, however, and only 2 events (in years before A.D. > 1950, at 250 years and 1940 to 2130 years) are recognized (Kelsey and others, 2002, Table 7).

¹ Radiocarbon dates calibrated to calendar years (2-sigma, with an error multiplier of 0.1) using CALIB 4.2 (Stuiver and Reimer, 1993).

² Data regarding the carbon-14 ages are in PG&E files.

³ Age in calendar years using the tree-ring sequence method and high-precision radiocarbon dates calibrated to calendar years (2-sigma) using CALIB 3.0 (Stuiver and Reimer, 1993).

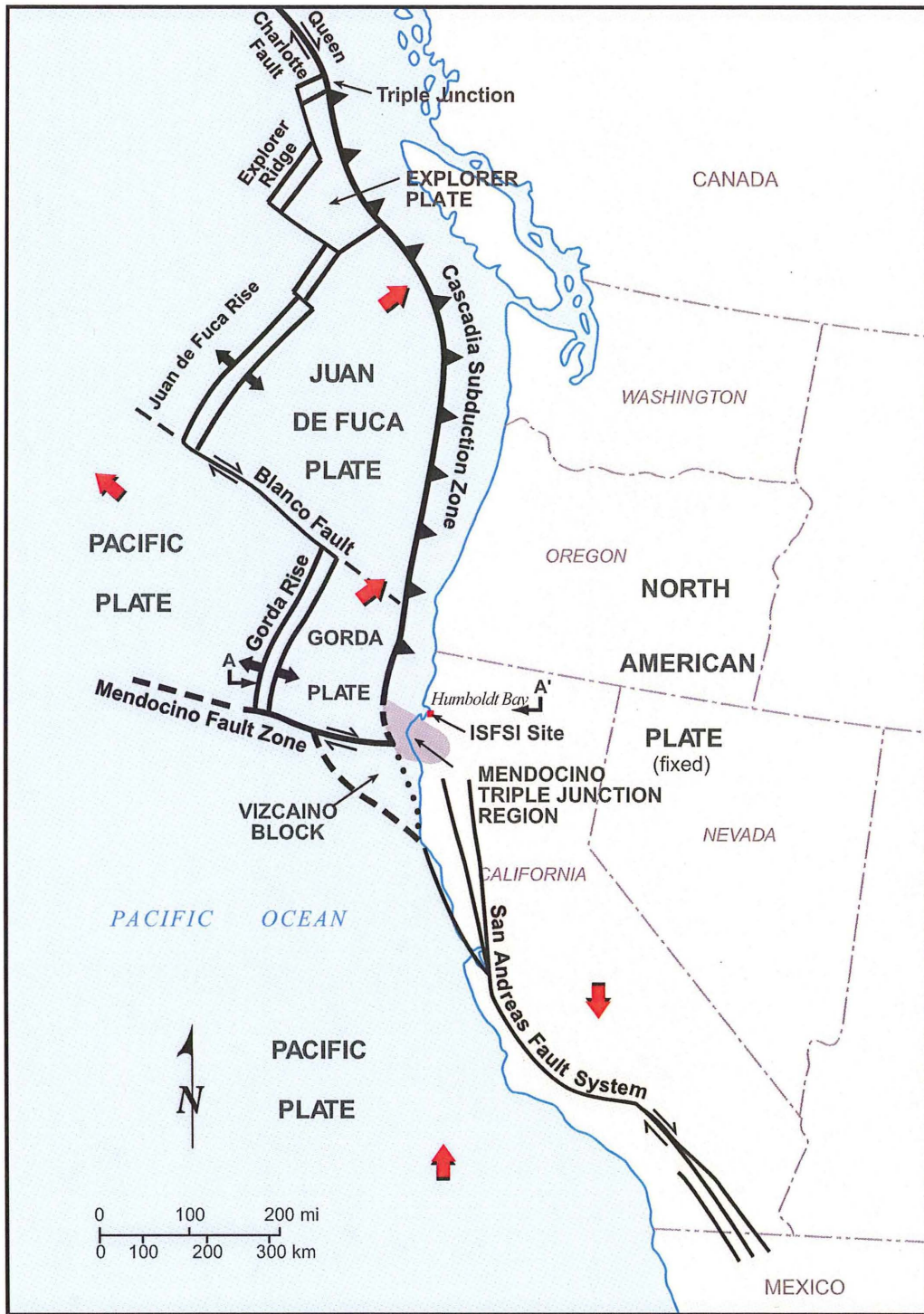


Figure 2-1 General plate tectonic setting of the western United States. Humboldt Bay and the proposed ISFSI site are on the western edge of the North American plate, at the north edge of the Mendocino triple junction region. Three plate-bounding fault zones, the San Andreas and Mendocino transform fault zones and the Cascadia subduction zone, intersect at the triple junction. Cross section A-A' is shown on Figure 2-7b.

S:\15100s\15117\15117.009\task_13105_0715_s2\102_0715_s2\fig_02-01.ai



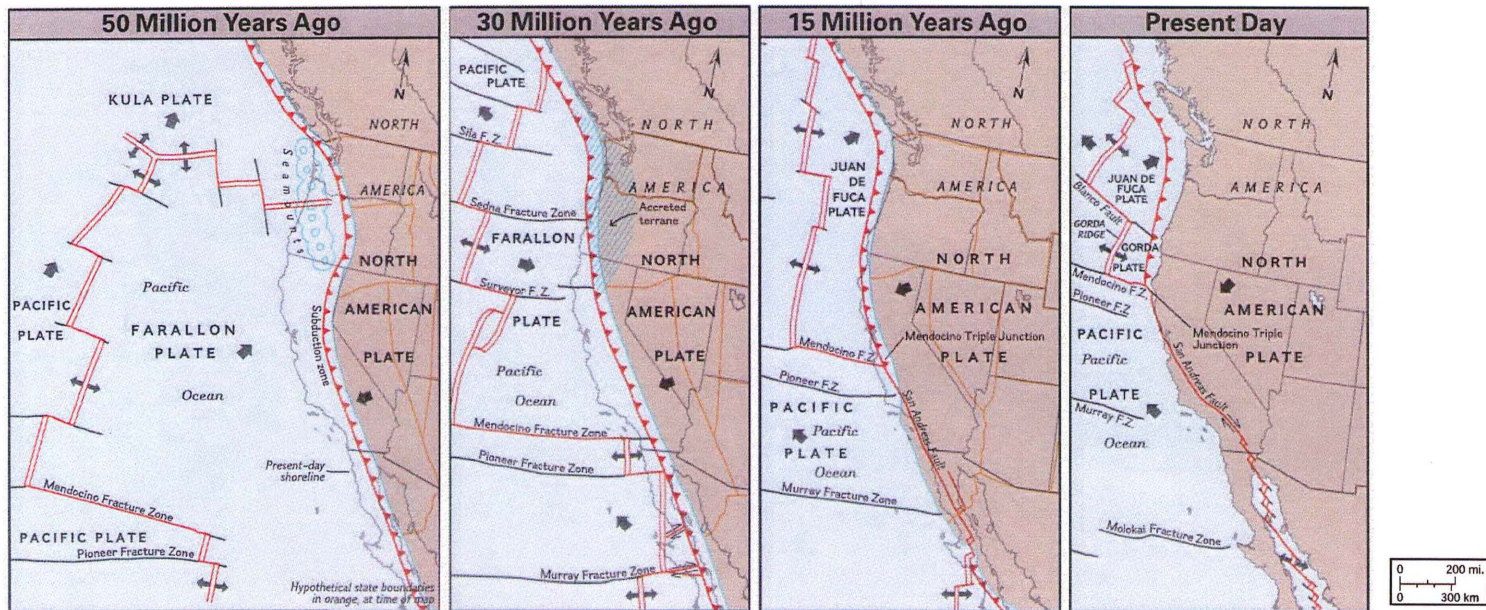


Figure 2-2 Tectonic evolution of the west coast of the United States during the past 50 million years (from National Geographic Society, 1995).

Figure 2-2

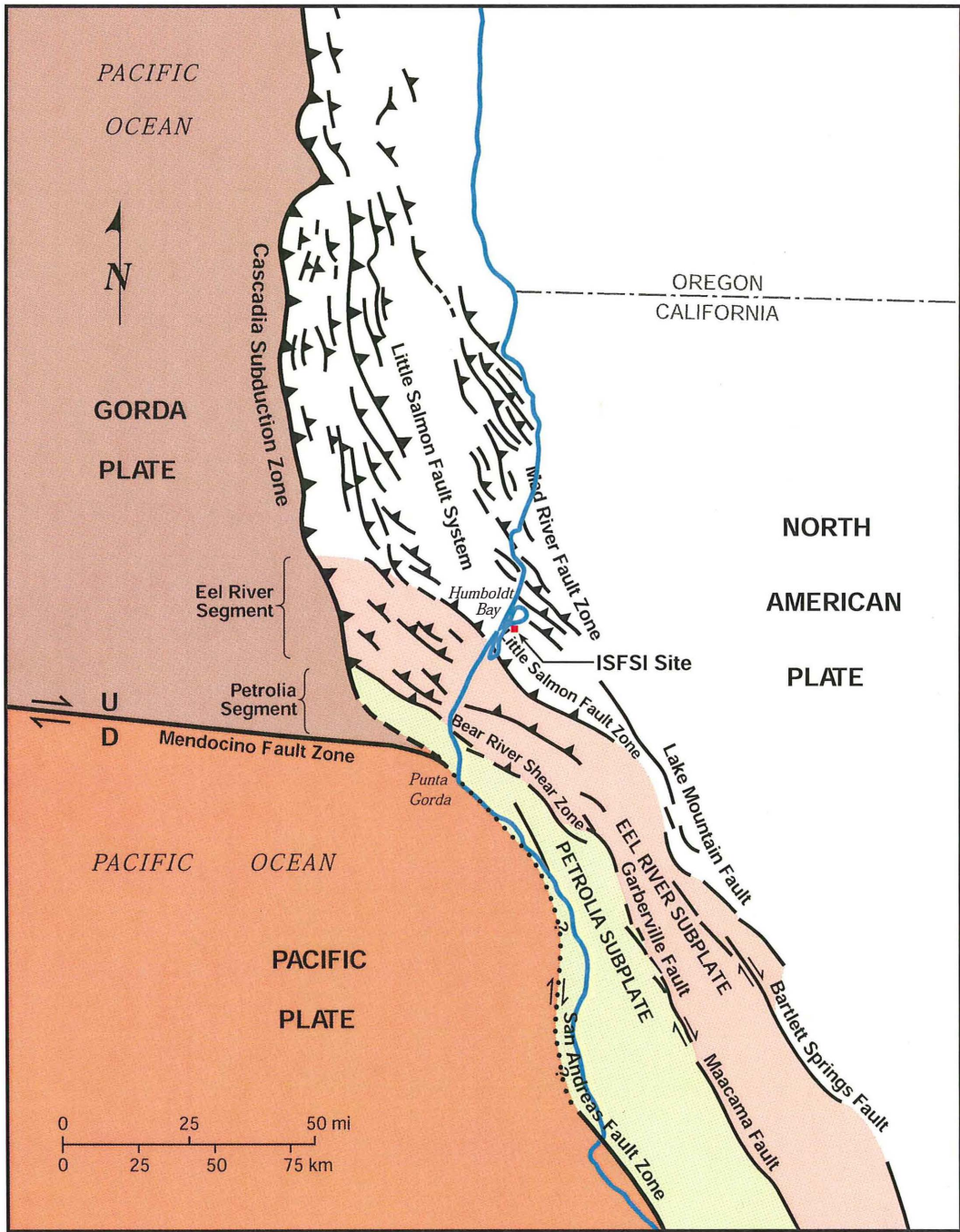


Figure 2-3 Map of subplates in the North American plate and major faults in northwestern California.

S:\5100s\5117\5117.009\task_13\02_0715_s2_fig_02-03.ai



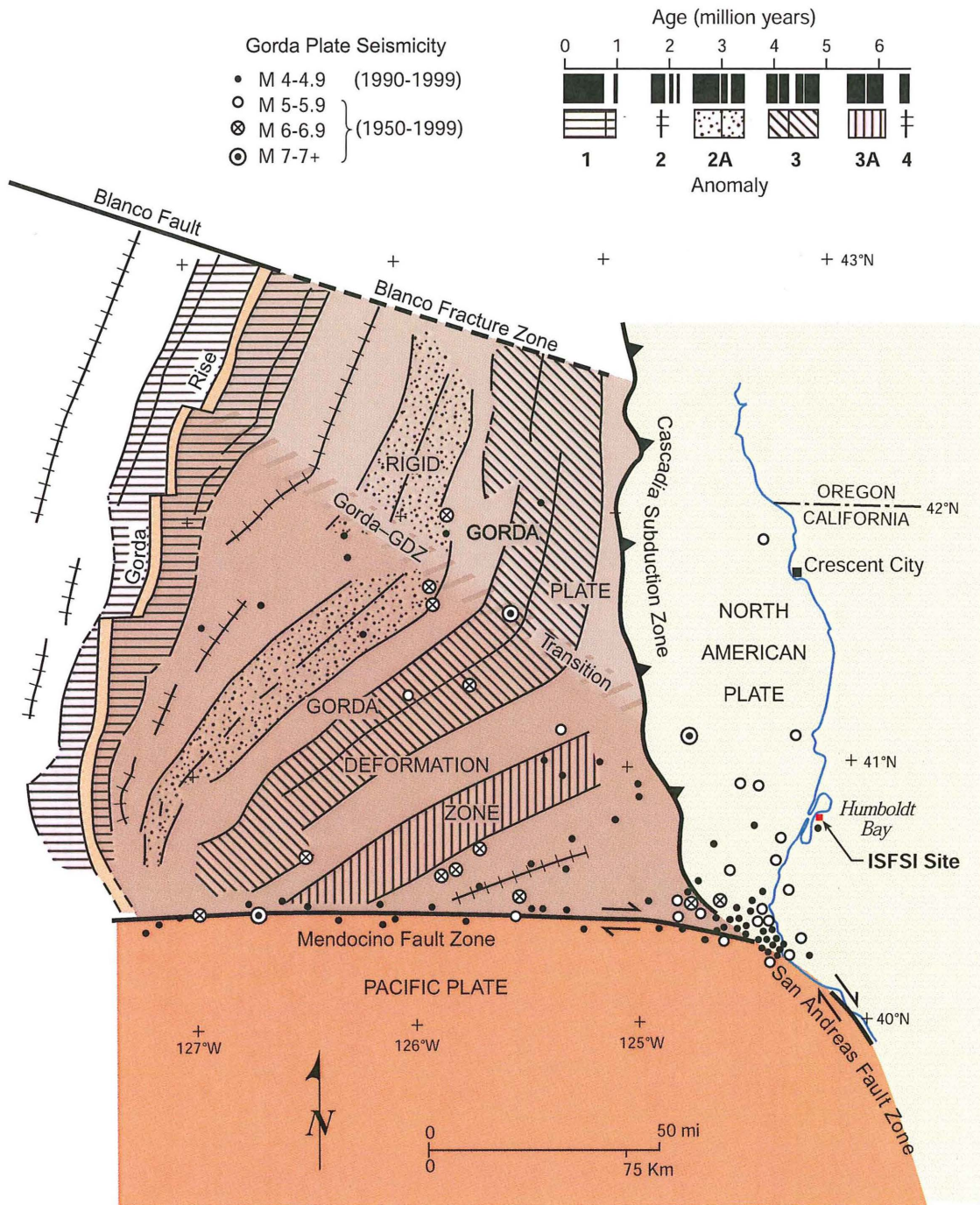


Figure 2-4 Tectonics of the Gorda plate (Modified from Wilson, 1989, Figure 3). The deforming and seismically active southern part of the plate and the internally rigid northern part are separated by a narrow transition that strikes northwest and intersects the subduction zone a short distance northwest of Humboldt Bay.

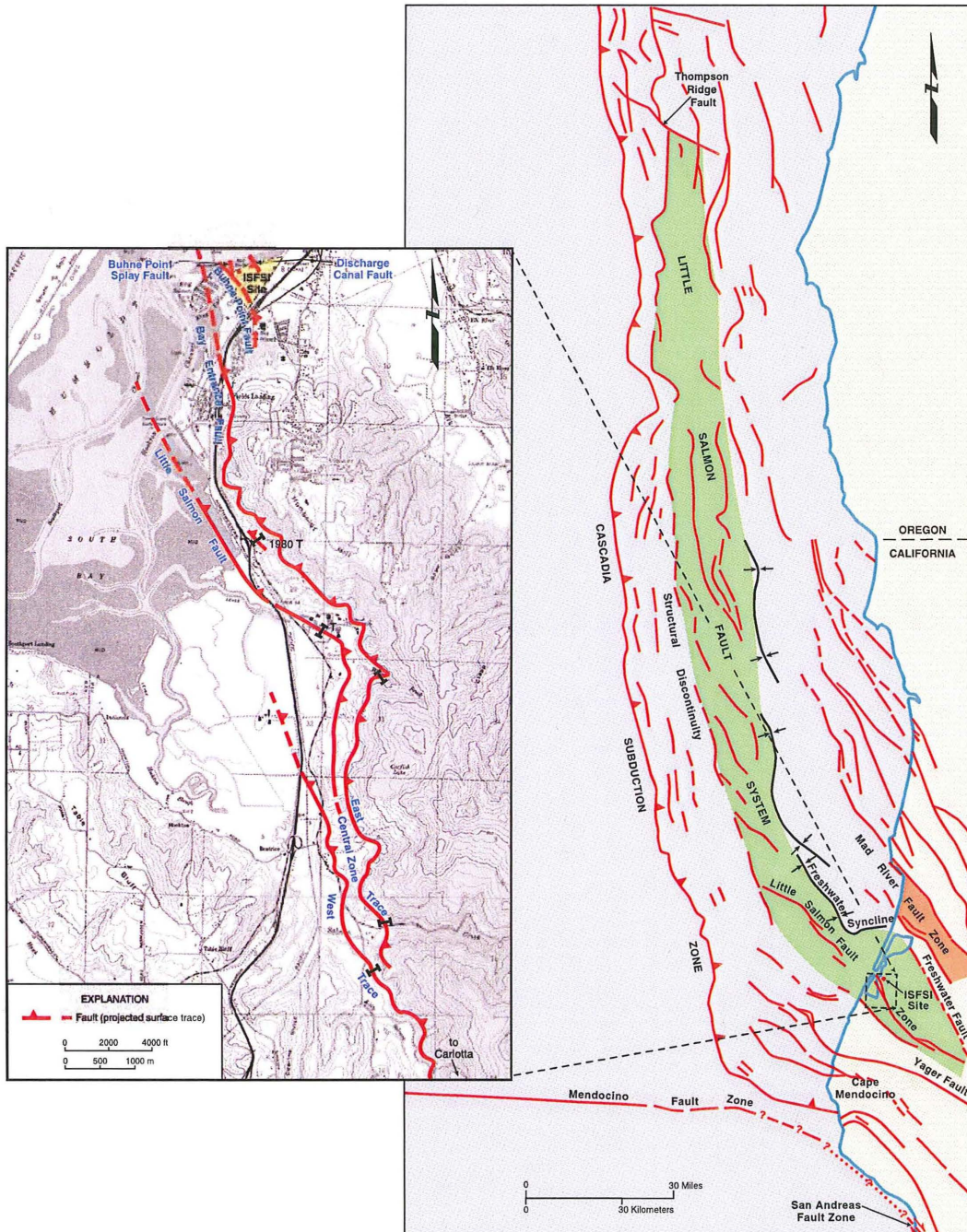


Figure 2-5 Schematic maps showing the components of the Little Salmon fault system. The Little Salmon fault zone is part of a system of active folds and reverse faults, the Little Salmon fault system, which extends for 330 kilometers from its intersection with the Freshwater fault northwestward to its intersection with the Thompson Ridge fault off the coast of southern Oregon. The Little Salmon fault zone, which is the closest capable fault to the Humboldt Bay ISFSI site, is 95 kilometers long (including the offshore traces as mapped by Clarke (1992) and the Yager fault). The Little Salmon fault zone contains multiple subparallel surface traces. Near the Humboldt Bay ISFSI site, the Little Salmon fault zone includes two primary traces, the Little Salmon fault and the Bay Entrance fault, and three subsidiary faults in the hanging wall, the Buhne Point fault, the Buhne Point splay fault, and the Discharge Canal fault.

S:\5103\5117\5117\009\task_13\02_0715_s2_fig_2-5.ai

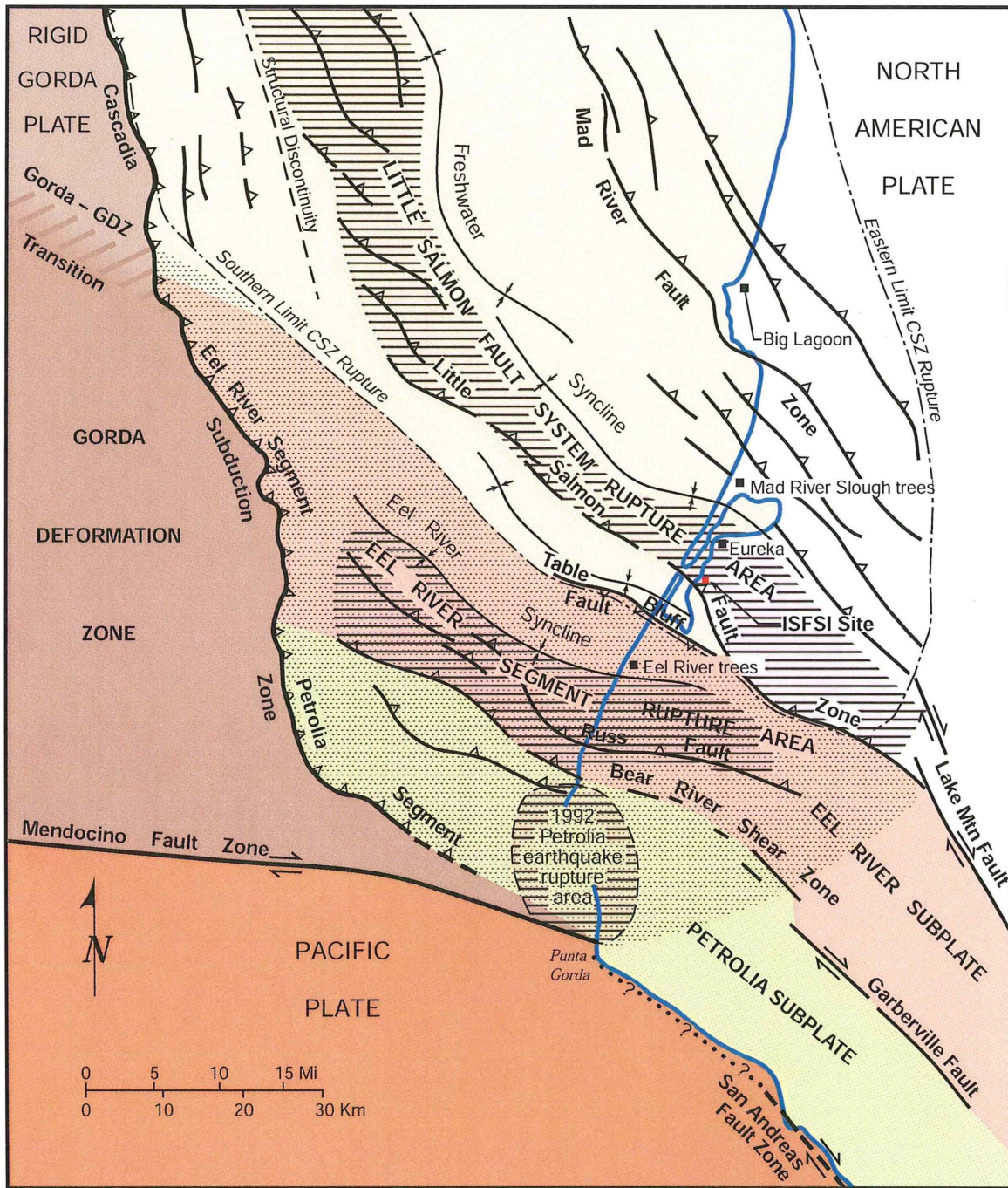


Figure 2-6 Major active faults and known or inferred earthquake rupture areas (line pattern) in the Mendocino triple junction region (stippled area). Paleoseismic data indicate the Little Salmon fault system ruptured during a great Cascadia subduction zone (CSZ) event, which may have ruptured as far as the southern limit of the CSZ, 300 years ago, and that the Eel River segment ruptured independently less than 200 years ago.

S:\5100s\5117\5117.009\task_13\02_0715_s2\fig_02-06.ai

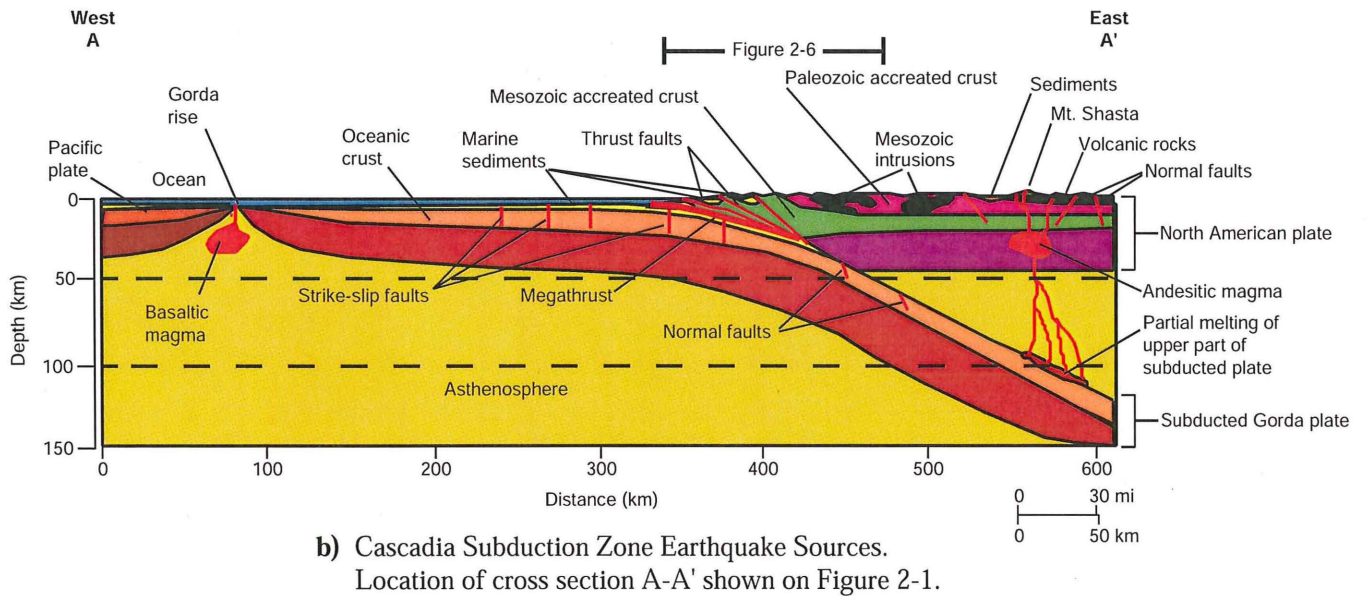
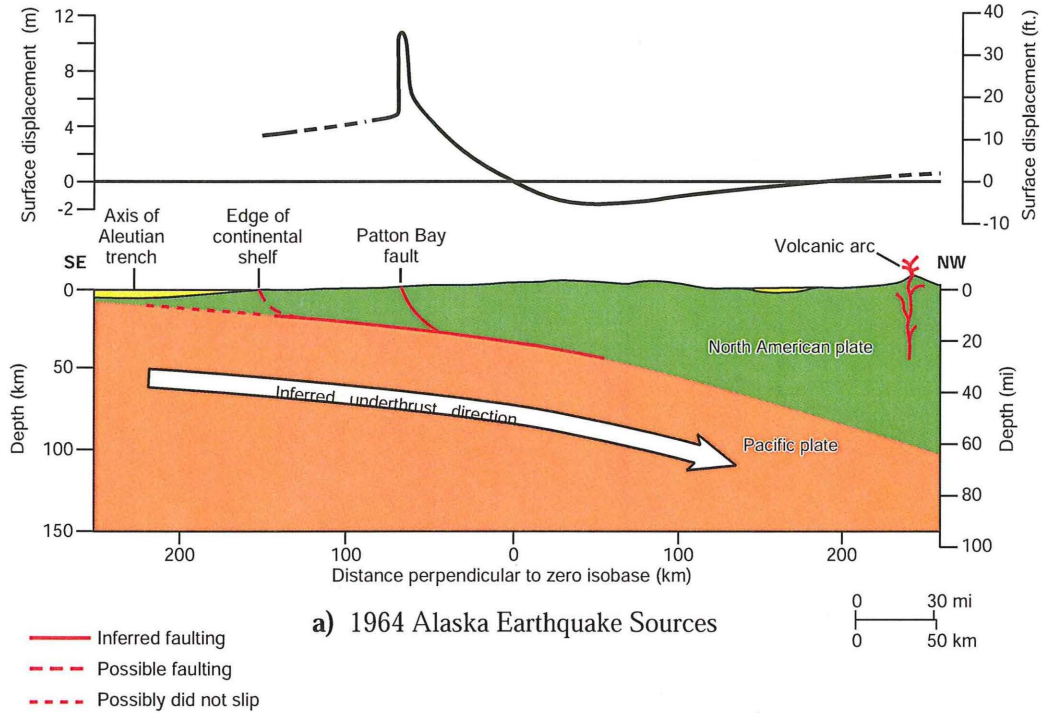


Figure 2-7 Schematic cross section showing the suggested mechanisms for the 1964 Alaska earthquake (Plafker, 1972), and postulated Cascadia subduction zone earthquake sources.

S:\15100s\15117\15117.009\task_13\02_0715_s2_fig_02-07.ai

Section 3.0

Regional Geology and Seismicity

3.1 INTRODUCTION

Because the seismic hazard at the Humboldt Bay ISFSI site is controlled, to a large extent, by nearby active faults, this discussion of the regional geologic setting and seismicity for the Humboldt Bay ISFSI site focuses primarily on the region within about 30 kilometers of the site. More distant sources were considered as part of the regional tectonic framework (Section 2.0), and are also considered in the seismic source characterization (Section 5.0). Regional seismicity data within 160 kilometers (100 miles) of the site also are considered in this section, with an emphasis on earthquakes that have occurred within 40 kilometers (25 miles) of the site. The details and analysis of the site geology are presented in Section 4.0, Site Geology.

3.2 REGIONAL GEOLOGY

Figures 3-1¹ and 3-2 are a generalized geologic map and cross section that show the major geologic terranes² and geologic structure of the Mendocino triple junction region. Figures 3-3 and 3-4 provide a more detailed geologic map and cross section that show the main structural features of the Humboldt Bay region. Table 3-1 contains a summary of the geologic history of the Humboldt Bay ISFSI site.

3.2.1 Regional Stratigraphy

The Humboldt Bay ISFSI site is in a broad depositional basin (the Eel River basin), which is underlain by a thick sequence of late Cenozoic³ marine sedimentary rocks of the Wildcat Group (QTw on Figure 3-1). A composite stratigraphic column of the onshore part of the Eel River

¹ Faults in the vicinity of Humboldt Bay are more accurately depicted on Figures 3-3 and 3-7.

² The term terrane refers to a rock or group of rocks and the area in which it outcrops.



basin is presented in Figure 3-5. The late Cenozoic deposits unconformably overlie basement rocks of the Late Jurassic to late Tertiary Franciscan Complex. Ogle (1953) divides the Wildcat Group into five formations (lithostratigraphic units) and defines a sixth, the Hookton Formation, which unconformably overlies the Wildcat Group. Woodward-Clyde Consultants (1980) conducted detailed stratigraphic and structural investigations of the site region, refining Ogles's map and clearly demonstrating the time-transgressive nature of the upper Tertiary and Quaternary formations. The following discussion is based primarily on their work (Woodward-Clyde Consultants, 1980, Appendix A), augmented by subsequent studies in the region.

Franciscan Complex (Pre-Wildcat Accreted Basement Rocks)

The Central Belt and Coastal Belt terranes of the Franciscan Complex form the basement rocks in the Humboldt Bay region. These terranes were accreted to the western margin of North America by plate convergence prior to development of the present Cascadia subduction zone.

The Late Jurassic and Cretaceous Central Belt Franciscan Complex, which crops out north and east of the Freshwater fault and the Coastal Belt thrust (Figures 3-1 and 3-3), consists of weakly to moderately metamorphosed sandy and silty turbidities, pillow basalt, thinly bedded chert, and interbedded shale. In many places the Central Belt rocks are intensely sheared, are tectonically mixed, and form a *mélange* in which more resistant basalt, sandstone, chert, and higher-grade metamorphic rocks including blueschist constitute tectonic blocks in a shaley matrix. The Central Belt Franciscan Complex, which was accreted to the northern California coastal region during the Late Jurassic to Cretaceous, makes up the pre-late Cenozoic basement along much of the northern California coast. These rocks (Figure 3-3) underlie the sedimentary rocks of the late Cenozoic Wildcat Group the north and northeast of Humboldt Bay, east of the Freshwater fault (Irwin, 1960).

The Coastal Belt Franciscan Complex is distinctly different from the Central Belt. Coastal Belt rocks consist mostly of lower to upper Tertiary marine sandstone (graywacke), siltstone, and shale that crop out to the southeast and south of Humboldt Bay (Evitt and Pierce, 1975). The Coastal Belt Franciscan Complex is subdivided into four terranes: (1) Coast Ranges terrane

³ The geologic time scale is presented in Table 1-1.

(sometimes referred to as the Coastal terrane); (2) King Range terrane; (3) False Cape terrane; and (4) Yager terrane (Figure 3-1) (McLaughlin and others, 1979). All of these, except the King Range terrane, occur within the Humboldt Bay region (Figure 3-3). These sedimentary rock sequences consist largely of turbidites that were accreted to the western margin of the Central Belt. The Coastal Belt terranes are unconformably overlain by the late Cenozoic sediments of the Wildcat Group.

The Yager terrane, which is the oldest unit within the Coastal Belt Franciscan Complex, includes sandy and silty turbidites of the early Tertiary Yager Formation. The Yager Formation is strongly folded and cut by numerous early and middle Tertiary faults. During the middle Tertiary, the Yager Formation was accreted to the western margin of North America and juxtaposed against rocks of the Central Belt *mélange* along the Freshwater fault and Coastal Belt thrust (Figures 3-1 and 3-3) (Clarke, 1992; Aalto and others, 1995). The Yager Formation underlies the Wildcat Group and younger sediments southeast of Humboldt Bay, from the vicinity of the Russ fault in the south to the Freshwater fault and Coastal Belt thrust on the north (Figure 3-3) in the lower Elk, Van Duzen, and Eel River drainages.

The youngest accreted basement rocks of the Coastal Belt Complex in the Humboldt Bay region make up the False Cape and the Coast Ranges terranes (McLaughlin and others, 2000). These units consist of highly sheared Miocene to early Pliocene sandstone, siltstone, and shale that reflect tectonic offscraping and shallow underplating of Farallon plate sediments in the proto-Cascadia subduction zone.

The Coast Ranges terrane, exposed south of the Russ fault and west of the Yager terrane, is a highly sheared *mélange* composed predominantly of sandstone, argillite, and minor conglomerate. The False Cape terrane is exposed along the coast south of the Russ fault between False Cape and Cape Mendocino (Aalto and others, 1995). The False Cape fault includes strongly deformed turbidite sediments locally sheared into *mélange* containing blocks of lower Wildcat Group sediments. Except for the active accretionary prism offshore, the False Cape and Coast Ranges terranes are the most recent sediments to be accreted on the edge of the North American plate, and are in part coeval with lower Wildcat Group sediments.



Wildcat Group and Falor Formation (Late Tertiary and Quaternary)

Franciscan basement rocks in the onshore Humboldt Bay region are unconformably overlain by a sequence of late Tertiary and Quaternary onlap deposits as much as 3,600 meters thick that were deposited on the upper plate of the modern Cascadia subduction zone. Their depositional history includes sedimentation in deep-trench and lower-slope basin environments during the Miocene, and progressive shoaling through the late Pliocene to shelf and marginal marine depositional settings during the early Pleistocene. Collectively, these sediments are named the Wildcat Group (Ogle, 1953) and are interpreted to have been deposited in a large, evolving forearc basin called the Eel River basin (Nilson and Clarke, 1987). Lower Wildcat Group sediments reflect deposition in a locally quiescent tectonic environment, as indicated by the lack of significant regional unconformities and relatively uniform lithofacies with parallel bedding that covered large areas.

In contrast, the lithologies of upper Wildcat Group sediments are laterally variable, reflecting depositional environments that ranged from deep marine on the west margin of the Eel River basin to fluvial on the east margin. Coarsening of sediments with increasing age toward the east indicates the westward shoaling of the basin. Macro- and microfossils, sedimentary structures, and other paleoenvironmental characteristics of the upper Wildcat Group sediments record northeast-to-southwest shallowing of the basin in response to the rapidly developed fold-and-thrust system associated with the evolution of the Cascadia subduction margin. The initiation of the contractional tectonics that followed deposition of the Rio Dell Formation drastically changed sedimentation patterns within the Eel River basin. Localized uplift due to anticlinal fold growth over active thrust faults divided the subsiding basin into several small depo-centers or subbasins. These subbasins, located in the synclinal regions of the fold-and-thrust belt, contain growth strata that record both basin subsidence and adjacent anticlinal uplift. This fold-and-thrust tectonics, coeval fore arc subsidence, and related patterns of sedimentation have continued through the Quaternary and dominate the geology of the region today.

In ascending order, Ogle's (1953) subdivision of the Wildcat Group consists of the Pullen, Eel River, Rio Dell, Scotia Bluffs, and Carlotta formations. In the lower Eel River Valley/Wildcat



Ridge area, the three lower formations consist predominantly of fine-grained sediments, whereas the two upper formations are made up of coarse-grained clastic sediments. In addition to these formations, Manning and Ogle (1950) delineate another formation in the Mad River Valley northeast of Humboldt Bay, the Falor Formation, which is now geographically separate from the Wildcat Group (Figure 3-3), but formed as the marginal marine and adjacent terrestrial facies of the upper Rio Dell sediments.

Pullen Formation - As described by Ogle (1953), the Pullen Formation consists mostly of diatomaceous siltstone and mudstone, with some ferruginous limestone nodules and a few thin glauconitic sandstone beds.

Eel River Formation - The Eel River Formation is composed of dark gray to black mudstone, siltstone, and interbedded sandstone. Most of the sandstone and some of the finer-grained sediments are reported to be glauconitic (Ogle, 1953).

Rio Dell Formation - The Rio Dell Formation consists of predominantly massive marine siltstone, lesser amounts of claystone, and fine- to very fine grained, poorly sorted sandstone. Water depths, inferred from microfossils at Centerville Beach (Ingle, 1976), ranged from about 1,800 meters near the base of the formation to about 90 meters at the top.

Scotia Bluffs Formation - The Scotia Bluffs Formation overlies and interfingers with the upper Rio Dell Formation in the Eel River area. The Scotia Bluffs Formation consists predominantly of massive fine- to medium-grained shallow marine sandstone and lesser amounts of pebbly conglomerate and siltstone that indicate deposition in a fluvial environment (Ogle, 1953). Marine fossils at its type locality in Scotia Bluffs indicate that at least part of the formation was deposited in water having depths of 30 meters or less (Faustman, 1964). The alternating marine and fluvial facies probably reflect glacio-eustatic sea-level-driven transgressions and regressions of the early to middle Pleistocene coastline.

Carlotta Formation - The Carlotta Formation overlies and interfingers with the Scotia Bluffs Formation. East of the Eel River and Fortuna, this formation consists of massive coarse-grained



conglomerate, poorly sorted sandstone, bedded and massive blue-gray siltstone, and blue-gray mudstone. The presence of coarse, poorly sorted conglomerate, the absence of marine fossils, and the presence of fossil redwood logs all suggest the Carlotta Formation was deposited in a predominantly continental environment. South of Ferndale, along Wildcat Ridge, the formation consists mostly of massive sandstone containing thin pebbly conglomerate. Coarse, massive conglomerate is limited to near the base of the formation.

Age and Correlation of Wildcat Group - The formations within the Wildcat Group are defined primarily based on lithology, and are time-transgressive. That is, the age of the stratigraphic units as defined by Ogle (1953) varies in different areas, particularly for the upper Wildcat units. Detailed geologic mapping by Woodward-Clyde Consultants (1980, Appendix A) shows that the base of the Scotia Bluffs and Carlotta formations step progressively higher in the stratigraphic section from east to west. The ages of the upper Wildcat formations in the vicinity of the Humboldt Bay ISFSI site are discussed further in Section 4.0.

Falor Formation - The Falor Formation in the upper Mad River Valley is more than 1 kilometer thick and consists of onshore and marginal marine facies in thrust-bounded slices across the Mad River fault zone (Manning and Ogle, 1950; Carver, 1987a). The basal part of the Falor deposits contains the Huckleberry Ridge tephra (Carver, 1987a), which is 1.8 to 2.0 million years old (Sarna-Wojcicki and others, 1991). Therefore, the basal Falor deposits are roughly correlative to the upper Rio Dell Formation at Centerville beach, which is dated by the 1.2- to 1.5-million-year-old Rio Dell ash (Sarna-Wojcicki and others, 1991).

Hookton Formation (Middle to Late Quaternary)

Based on exposures in the Table Bluff area, just south of Humboldt Bay, Ogle (1953) describes the Hookton Formation as yellow-orange gravel, sand, silt, and clay that unconformably overlie the Wildcat Group. Aware that the Hookton Formation is difficult to define as a regional stratigraphic unit, he stated, "No adequate type section can be given because of the extreme variability of these beds." Without a clear stratigraphic context, the Hookton Formation is difficult to distinguish from weathered sediments of the Carlotta and Scotia Bluffs formations. In the southeast part of the area, the Hookton Formation generally consists of silt, sand, and



coarse conglomerate. West and north of Tompkins Hill, it consists of fine-grained, well-sorted sand interbedded with pebbly conglomerate and thin silt and clay beds. The lithology of the Hookton Formation in the vicinity of the ISFSI site is described in more detail in Section 4.0.

Age and Correlation of Hookton Formation - It is difficult to distinguish between some sediments in the Hookton Formation and the upper part of the Wildcat Group at the outcrop or local scale. At the regional scale, strongly localized lateral and vertical variability of sediment type within the Hookton Formation reflects strong local tectonic influences on sedimentation. In contrast to the Wildcat Group, the Hookton and other post-Wildcat Group sediments and geomorphic surfaces, including marine terraces, show consistent east-to-west migration of the coastline and decreasing age of lithofacies toward the west. Paleomagnetic data, correlation of volcanic ashes, and radiometric dates also indicate that these upper deposits are progressively younger from east to west.

Woodward-Clyde Consultants (1980) recognized that the sediments that unconformably overlie the Wildcat Group near the Humboldt Bay Power Plant probably are not the same age as deposits mapped as Hookton Formation in other areas. Therefore, they restricted use of the term Hookton Formation to deposits that unconformably overlie the Wildcat Group in the Thompkins Hill/Table Bluff/Humboldt Hill area and in the subsurface in the Buhne Point area at the ISFSI site, excluding Holocene alluvium, marine terrace and bay deposits. This division is followed in this report.

Hookton deposits in this area contain dated and correlative volcanic ash layers that are useful in assessing the structural history of the area. These tephras, which have normal magnetic polarity, are interpreted to be younger than the transition between the Matuyama and Bruhnes magnetic polarity epochs (Woodward-Clyde Consultants, 1980), which occurred 780,000 years ago⁴

⁴Paleomagnetic data, radiometric dates, and correlation of volcanic ashes in the lower part of the unit indicate the base of the Hookton Formation is less than about 780,000 years and older than about 400,000 years old. The maximum age is based on the age of the Bruhnes/Matuyama boundary, which occurs either near the base of the Hookton Formation, or within the time span encompassed by the unconformity at the base of the Hookton Formation. The minimum age is based on K-Ar and fission track dates obtained on an ash bed, the Railroad Gulch Ash, in the lower part of the Hookton Formation. Based on these data, Woodward-Clyde Consultants (1980) estimated that deposition of the Hookton Formation in the Thompkins Hill area, 10 to 15 kilometers south of the site, began 600,000 ±100,000 years ago.



(Baksi and others, 1992). The base of the Hookton Formation is older than the Railroad Gulch ash. The Railroad Gulch ash correlates to the Rockland ash from the Lassen Peak area, California (Sarna-Wojcicki and others, 1985). Although the Rockland ash has been difficult to date and its age is still debated (Sarna-Wojcicki, 2000), it is at least 400,000 years old (Sarna-Wojcicki and others, 1985) and may be as old as 600,000 years (Lanphere and others, 2000). The age of the Hookton deposits beneath the ISFSI site is discussed in detail in Section 4.0.

Marine Terraces (Late Quaternary)

Although originally included as part of the Hookton Formation shown by Ogle (1953) and followed by Woodward-Clyde Consultants (1980), the sequence of uplifted marine terraces along the margins of hills and coastal bluffs in the Humboldt Bay region can be separated into distinct units. This sequence records late Pleistocene uplift and deformation associated with the growth of faults and folds in the upper plate of the Cascadia subduction zone (Carver and Burke, 1992). Marine terrace sequences in the Humboldt Bay region are associated with uplift and growth along the Table Bluff anticline and fault, the Humboldt Hill anticline and Little Salmon fault zone (Photo 3-1a), and the Eureka anticline (Figure 3-6). Intervening synclines, such as the South Bay and Freshwater synclines, are areas of active, episodic subsidence (Valentine and others, 1992).

The ages of marine terraces in the Humboldt Bay region and in other parts of northern California have been estimated by application of global sea level curves to flights of terraces, numerical dating, correlation of volcanic ash, and correlation based on relative soil profile development. The ages of the sequences of marine terraces north of the site near Trinidad and McKinleyville (Carver and Burke, 1992) and south of the site near Cape Mendocino (Merritts and others, 1991, 1992; Chadwick and others, 1992) have been estimated by correlation of the global sea level curve, following the practices applied elsewhere in the world (for example, Lajoie and others, 1991; Muhs and others, 1992; Hanson and others 1994). Carver and Burke (1992) stated, "Terrace age assignments are based on the best matches between: (1) altitude sequences of local terrace remnants, and (2) unique terrace altitude sets produced by applying uniform average uplift rates to known ages and altitude of formation of New Guinea terraces." In the Humboldt Bay region, soil profile development was used to correlate terraces in the Trinidad and



McKinleyville flights with terraces at Table Bluff (and elsewhere). Independent age dates, including limiting age estimates, also were used in developing age estimates for marine terraces.

The numerical dates from terraces in the Humboldt Bay area include thermoluminescence dates of silts (Berger and others, 1991; Berger, 1992) and correlation of the Loleta ash in a terrace deposit at the top of Table Bluff with the Bend Pumice tuff (Sarna-Wojcicki and others, 1991; Lanphere and others, 2000). These ages are consistent with those assigned to the terraces in the Humboldt Bay area (Figure 3-6); however, age assignments for the terraces at Humboldt Hill and in the Eureka area are more uncertain than are the ages for the terraces in the Table Bluff, McKinleyville and Trinidad areas. Correlations of the terrace sequences and the assigned ages of the local terraces are based primarily on the characteristics of their paleosols, rather than the soil chronosequences that have been developed for the dated terrace sequences at Trinidad, McKinleyville, and Cape Mendocino (Carver and Burke, 1992).

The marine terrace sequence developed in the region surrounding the ISFSI site has been well established by multiple lines of evidence. Nonetheless, alternative explanations for these features can be proposed. One alternative is that some of the topographically differentiated terraces, inferred to have distinct underlying platforms, could be combined because the underlying wave-cut platform is the same age. Another alternative is that some terraces are faulted, creating additional surfaces that have been interpreted as terraces of different ages. If faulting has produced vertically displaced terrace sections of the same age, however, these faults have not been recognized in the field. An alternative explanation for the high rates of uplift recorded by the lowest marine terrace (roughly 1 millimeter per year) adjacent to Eureka is that this uplift is driven by a local intraplate structure (e.g., a blind, active thrust, or reverse fault), as has been observed at other coastal sites in Northern California and southern Oregon (Polenz and Kelsey, 1999; Kelsey, 1990; McInelly and Kelsey, 1990). However, no specific evidence of such blind fault structures has been noted in previous mapping (e.g., Ogle, 1953; McLaughlin and others, 2000); nor has any evidence been mapped in the offshore that could trend onshore under the Eureka area (Clarke, 1990). Also, key stratigraphic contacts directly inland from Eureka are at nearly the same elevation throughout the region.



3.2.2 Regional Geologic Structure

The structural geology of the Humboldt Bay region is dominated by north-northwest-trending contractional structures formed during several phases of plate convergence that have affected the region since the Late Jurassic. Three classes of structures are evident at the regional scale:

1. faults, folds, and tectonic mélanges formed during multiple episodes of accretion of the Franciscan Complex basement rocks during the late Mesozoic and early Tertiary;
2. early and mid-Tertiary structures formed in the accreted continental margin prior to the plate tectonic organization of the modern Cascadia subduction zone; and
3. late Cenozoic structures (basin subsidence and localized anticlinal uplift) related to the tectonics of the modern Cascadia subduction zone

Figure 3-4 is a northeast-southwest geologic section across the Humboldt Bay region.

Franciscan Complex Basement Structures

The accretion of Franciscan Complex rocks in the Humboldt Bay region occurred during a long and complex deformational phase in the structural development of northwestern California that has included repeated episodes of tectonism (Jayko and Blake, 1987). As a result, the Franciscan rocks are strongly folded and faulted and locally are pervasively sheared. The various Franciscan Complex terranes are bounded by major faults that have large cumulative displacements.

The Central Belt contains the oldest Franciscan Complex rocks exposed in the Humboldt Bay region. Structures within the Central Belt include large-displacement faults that juxtapose different lithologic assemblages, and bodies of rock having different metamorphic grades. The Coastal Belt Franciscan Complex rocks are younger and have a lower grade of metamorphism. Locally, the Coastal Belt rocks are strongly folded and cut by many faults. The principal basement structures in the Humboldt Bay area are the Freshwater and Russ faults, which form the northeast and south tectonic boundaries of the Coastal Belt, respectively (Figure 3-3).



Freshwater fault - The Freshwater fault separates Franciscan rocks of the Central Belt on the east from the Coastal Belt on the west. The structural boundary between the Central Belt and the Coastal Belt continues south of the Humboldt Bay region in the northern and central California Coast Ranges (McLaughlin and others, 1994, 2000). Onshore, the Freshwater fault is a steep, easterly dipping, high-angle reverse fault that also may have accommodated large amounts of right slip. Offshore, the Freshwater fault is overlain by sediments deposited in the Eel River basin; most of the deformation on the Freshwater fault pre-dates deposition of the Wildcat Group (Ogle, 1953). The Freshwater fault is displaced by, and therefore predates, the Greenwood Heights fault in the Mad River fault zone (Figure 3-4).

Russ fault - The Russ fault extends for 33 kilometers from the coast east-southeast along the crest of Wildcat Ridge to the Eel River (Figures 3-1). The fault extends offshore another 24 kilometers to the northwest. The Russ fault forms the tectonic contact between the Yager terrane on the north and the Coast Ranges terrane on the south (Figures 3-1 and 3-3). Locally, the fault also lies along the contact between the Wildcat Group and basement of the Coast Ranges terrane. Based on bedrock mapping, McLaughlin and others (2000) interpret the Russ fault to be a steep, south-dipping major bedrock structure that extends to the top of the subducting Gorda Plate. As shown on their cross section (Figure 3-2), the fault is displaced down to the north, and appears to be associated with microseismicity.

At False Cape (Figure 3-1) the fault is exposed in the sea cliff, where it dips at a high angle to the north, and displaces two marine terraces vertically 22 meters and 36 meters (Carver and others, 1986a and 1986b). The apparent displacement is down to the south, which is opposite to the sense of the bedrock displacement. Based on the sea cliff exposure, the Russ fault is interpreted to be a north-dipping reverse fault that displaces lower Wildcat Group sediments and Coast Ranges terrane over rocks of the False Cape terrane, consistent with the interpretation of Aalto and others (1995). The inconsistency in the apparent vertical displacement may indicate a component of strike-slip motion (McCroory, 2000), or may reflect reactivation of the upper part of the fault during the current stress regime as a north-dipping reverse fault that bounds the southern margin of the Eel River syncline. Because of the uncertainties in the slip direction, the slip rate on the Russ fault is poorly constrained. Based on the displaced late Pleistocene marine



terraces, the rate of vertical separation across the fault is 0.2 millimeters per year (Carver and others, 1986b; McCrory, 2000).

Late Cenozoic Faults and Folds

Thrust faults and fault-related folds that make up the active Cascadia fold-and-thrust belt have strongly deformed lower Wildcat Group sediments, influenced the deposition of post-Rio Dell sediments, and affected the geomorphic development of the modern landscapes (Kelsey and Carver, 1988; Clarke, 1992). The interaction of subsidence and fold-thrust deformation has resulted in a clear tectonic distinction between the uplifting regions that overlie active thrust faults and fault-related anticlines, and subsiding basins that are coincident with the intervening synclinal regions.

The Quaternary anticlines in the Humboldt Bay region are interpreted to be active fault-related folds associated with thrusts in the Cascadia fold-and-thrust belt. These folds include the Table Bluff, Humboldt Hill, and Fickle Hill anticlines (Figures 3-4 and 3-6). These anticlines, which have as much as 1.5 kilometers of structural relief, record significant crustal contraction related to faulting. The anticlines are asymmetrical, having longer northeast limbs that dip between 20 and 40 degrees. The shorter southwest limbs dip steeply, and locally are overturned (Carver, 1987a; Kelsey and Carver, 1988).

Two major zones of thrust faults and related folding have been mapped in the Humboldt Bay region: the Mad River fault zone (Carver 1987a, Clarke and Carver, 1992), and the Little Salmon fault zone (Ogle, 1953; Woodward-Clyde Consultants, 1980; Carver 1987; Clarke and Carver, 1992) (Figures 3-3 and 3-4). At the regional scale, these thrust zones trend north and northwest, dip east and northeast, and displace Franciscan Complex basement and lower Wildcat Group rocks over the upper Wildcat Group and younger sediments (Figure 3-4).

The late Cenozoic thrusts in the Humboldt Bay region have generally shallow dips in the near surface. Measurements of the dips of thrust faults exposed in trenches, sea cliffs, road cuts, and other shallow exposures range from about 40 degrees to nearly horizontal, averaging about 25 degrees. Although most of the thrusts dip to the northeast, southwest dips also occur.



Changes in dip at depth on the thrusts in the Humboldt Bay region are indicated by exposures of the faults, by fault intersections in boreholes, and by the presence of large anticlines in the hanging walls of most of the major faults. The increase in dip at relatively shallow depths (<1 kilometer) on the thrusts is indicated by fault intersections in the deep wells at the Tompkins Hill gas field and from mapping of deeply eroded Wildcat sediments (Falor Formation) in the upper Mad River Valley (Carver, 1987a; Kelsey and Carver, 1988).

Mad River fault zone - At its closest point, the Mad River fault zone is approximately 23 kilometers north of the Humboldt Bay ISFSI site. The onshore part of the fault zone includes the Trinidad, Blue Lake, McKinleyville, Mad River, Fickle Hill, and Greenwood Heights faults (Figures 3-3 and 3-4). The surface traces of these faults are generally parallel, northwest-trending, and 2 to 5 kilometers apart. At the coast, the fault zone is about 20 kilometers wide. The offshore part of the Mad River fault zone trends north-northwest along the inner continental shelf as a 15- to 25-kilometer-wide belt of en echelon thrust faults and fault-generated folds (Figures 2-3, 2-5, and 3-3). The total length of the fault zone, including the offshore traces mapped by Clarke (1992), is about 80 kilometers. The thrust faults in the Mad River fault zone are interpreted to coalesce at depth, forming a southwest-vergent imbricate fan thrust system (Figure 3-4). The imbricate fan thrust system is inferred to root at depth into the Cascadia megathrust.

Individual faults within the Mad River fault zone juxtapose the basal contact of the Falor Formation (about 2 million years old) with the underlying Franciscan Complex in a series of northeast-tilted fault slices (Figure 3-4). Displacements on these faults range from about 1 to 3 kilometers. These displacements are based on measurement of the Franciscan/Falor contact and the stratigraphic thickness of faulted Falor Formation sediments across the Mad River fault zone in the upper Mad River Valley area.

Near the coast, the Mad River fault zone intersects a series of late Pleistocene shorelines represented by uplifted and faulted marine terraces (Woodward-Clyde Consultants, 1980; Carver and others, 1986b). Slip rates estimated for individual thrust faults in the Mad River fault zone,



based on dating of the terraces and the amount of uplift, are generally 1 to 2 millimeters per year. Across the zone, the cumulative rate indicated by the marine terrace deformation is about 5 to 9 millimeters per year (Carver, 1987a, 1987b; Kelsey and Carver, 1988; Burke and Carver, 1992; McCrory, 2000).

Little Salmon fault system and Little Salmon fault zone - The Little Salmon fault zone is part of a system of active folds and reverse faults that extends for 330 kilometers from its intersection with the Freshwater fault/Coastal Belt thrust near Bridgeville, California, northwestward to its intersection with the Thompson Ridge fault off the coast of southern Oregon (Figure 2-3). Offshore, this system is composed of north-northwest-trending en echelon anticlines and thrust faults. The fault system trends parallel to the deformation front associated with the leading edge of the Cascadia subduction zone. The southern and central part of the zone is bounded on the west by a well-defined structural discontinuity between northwest-trending structures within the Little Salmon fault system and the more north-south structures along the accretionary margin; on the east, it is bounded by large synclines (Figure 2-6). The northern boundaries of the system are not as well defined, but the system clearly does not extend beyond the west-northwest-trending Thompson Ridge fault, which truncates the more northerly trending structures of the Little Salmon fault system. The width of the fault system varies, but typically is about 20 kilometers. Near the site, the fault zone is about 25 kilometers wide, extending from the Table Bluff fault on the southwest, across the Little Salmon fault zone, to the axis of the Freshwater syncline (Figure 3-3).

The Little Salmon fault zone, which is the nearest capable fault to the site, has a total length of 95 kilometers, including the offshore traces as mapped by Clark (1992), and the Yager fault to the southeast (Figures 2-5 and 3-3). The fault zone was identified as a major late Cenozoic thrust first by Ogle (1953). The southeastern end of the Little Salmon fault zone is coincident with the end of the Little Salmon fault system (at its intersection with the Freshwater fault near the town of Bridgeville) (Kelsey and Carver, 1988). It trends northwest along the Van Duzen River Valley to Humboldt Bay (Ogle, 1953), then continues offshore from the coast obliquely across the continental shelf west and northwest of Eureka (Clarke, 1990, 1992). Detailed studies during the past 20 years along the margin of South Bay and Little Salmon Creek indicate the fault zone



consists of several imbricate branches that are well defined in the geomorphology (Figure 3-7). Along the southwestern flank of Humboldt Hill (about 6 kilometers south of the Humboldt Bay ISFSI site), the Little Salmon fault zone includes at least three southwest-vergent imbricate faults that have been active during the Holocene (Carver and Burke, 1988, 1989; Carver and others, 1988; Whitter and others, 2002). The westernmost trace, which lies along Little Salmon Creek (south of Salmon Creek), is the fault trace that has the largest Holocene displacement in this area, but the adjacent eastern trace has the greatest total displacement. Northwest of Salmon Creek, the western trace extends beneath and is hidden by modern sediments on the margin of Humboldt Bay west of Humboldt Hill. The middle trace (Little Salmon fault trace on Figure 3-7) traverses the western part of the College of the Redwoods campus (LACO Associates, 1999a, 1999b), and can be identified in borings southwest of the plant site. The east trace has been mapped from near Salmon Creek northwestward along the base of Humboldt Hill, traversing the eastern part of the College of the Redwoods campus. North of Humboldt Hill, the eastern trace, which passes southwest of Buhne Point and the ISFSI site, is called the Bay Entrance fault.

The Table Bluff fault is a 23-kilometer-long, west-northwest-trending imbricate thrust within the Little Salmon fault zone in the Little Salmon fault system (Figure 3-3). Although the Table Bluff fault is poorly exposed at the surface, Quaternary uplift and folding associated with it is apparent in the geomorphic expression and near-surface structure of the Table Bluff anticline. Interpretation of seismic profiles (ARCO seismic profiles, in PG&E files) and the outcropping structure of the Table Bluff anticline suggest that the fault forms a south-vergent thrust wedge beneath the anticline, with the upper several kilometers of the fault dipping to the south and southwest, and the deeper part of the fault dipping to the northeast (Figure 3-4). The deep geometry of the Table Bluff blind-thrust wedge is uncertain. The apparent merging or overlapping with the Little Salmon fault zone along strike suggests it probably splays off of the Little Salmon fault zone at depth. However, where the faults diverge and become widely separated, they are depicted as independent structures (Figure 3-4), and are assumed to extend down dip to the plate interface at the top of the Gorda Plate. Analogous “splay faults” which branch upward from the megathrust and cut through the upper plate have recently been imaged on the Nankai subduction zone, a shallow dipping subduction zone similar to Cascadia in southwest Japan (Park and others, 2002).



Near the coast, the vertical separation of the base of the Wildcat sediments across the Little Salmon fault zone and the Table Bluff fault (Little Salmon fault system) is more than 3,400 meters (Ogle, 1953; ARCO seismic profiles, in PG&E files), and the total dip-slip separation may be as much as 7 kilometers (Kelsey and Carver, 1988). The faulting of the Rio Dell Formation and other units of the Wildcat Group began about 700,000 years ago (during or soon after deposition of the Scotia Bluffs Formation about 800,000 years ago, and before the beginning of deposition of the Hookton Formation about 600,000 years ago) (Woodward-Clyde Consultants, 1980; Kelsey and Carver, 1988; Dupre and others, 1991). Depending on the fault dip, estimates of long-term slip rate range from 6 to 10 millimeters per year for the Little Salmon fault zone at Humboldt Bay, and from about 2 to 3 millimeters per year for the Table Bluff fault. Slip rates from trench studies for the east and west traces of the Little Salmon fault zone during the late Holocene on the east side of the South Bay produce similar estimates (Carver and Burke, 1988; Clarke and Carver, 1992). The total slip rate across the Table Bluff fault and the Little Salmon fault zone is between 8 and 13 millimeters per year (Carver, 1987a; Clarke and Carver, 1992; McCrory, 2000).

At the northern end of Humboldt Hill, the Little Salmon fault displaces the entire lower Hookton section, and places Rio Dell Formation over the Hookton sediments (Figure 3-8). The amount of vertical separation of the older units is progressively larger. In the vicinity of Humboldt Hill, the vertical displacement of the top of the Rio Dell Formation is 880 to 1,400 meters. The base of the Hookton Formation is displaced 319 to 564 meters, and the top of the unit F clay in the upper part of the lower Hookton Formation is displaced 210 to 247 meters. Using vertical displacement data from boring WCC-12 and a dip of 30 degrees, Woodward-Clyde Consultants (1980) calculated long-term average slip rates on the Little Salmon fault in the range of 1 to 3 millimeters per year. The vertical separation across the fault decreases north of Humboldt Hill, perhaps indicating that slip on the Little Salmon trace has transferred mostly to the Bay Entrance trace northwest of Humboldt Hill.

The style of deformation associated with late Quaternary slip on the Little Salmon fault zone at College of the Redwoods, about 5 kilometers south of the Humboldt Bay ISFSI site (Figure 3-7),



has been reconstructed based on geotechnical borings and trenches (LACO Associates, 1999b; Bickner and others, 2000). Trenches exposed 25- to 30-meter-wide zones of deformation containing multiple faults, fractures, and discrete fault-bend-fold axial surfaces in the hanging wall (Figures 3-9, 3-10, 3-11, 3-12). The structure varies along strike. Typical fault patterns consist of subparallel low- and high-angle faults having reverse and normal displacements. Southwest-dipping reverse faults are interpreted to be secondary backthrusts that increase in number and dip toward the main thrust tip, suggesting increasing proximity to the northeast-dipping master thrust (Bickner and others, 2000). Graben structures having about 1 meter of cumulative vertical separation also were mapped (Figure 3-10). The normal faults, which decrease in slip and terminate downward, record extension in the hanging wall as it rides over bends in the underlying thrust ramp. Folding of strata occurs across discrete axial surfaces that are interpreted to coincide with changes in dip of the underlying thrust ramp (for example, Figure 3-9). Fault-generated folding in the overriding thrust sheet results in differential displacement of the ground surface across active axial surfaces (Bickner and others, 2000). Because the Holocene sediments and soils had been removed by grading prior to construction of the campus buildings, the Holocene activity of the fault could not be assessed based on the trenches at College of the Redwoods.

Paleoseismic investigations along the Little Salmon fault zone by Carver and Burke (1986), Carver (1992), Carver and Aalto (1992), and Clarke and Carver (1992) constrain the size and the approximate timing of the most recent surface-faulting events. At the Little Salmon Creek exploration locality (Figure 3-7), at least three events during the past 1,700 years are interpreted from trench exposures across the western trace. By reconstructing the components of folding and faulting, the displacement per event was estimated to be between 3.6 and 4.5 meters. Displacements of 1 to 2 meters were identified along the eastern trace, which is a few hundred meters east of the western trace. Radiocarbon ages for the events on the western trace indicate that faulting occurred about 300, 800, and 1,600 years ago (Clarke and Carver, 1992). The ages of the displacements on the eastern trace could not be determined, but they probably were synchronous with events on the western trace. The results of the detailed paleoseismic studies demonstrate that the location, style, and pattern of deformation have been replicated during successive surface-faulting events on the Little Salmon fault zone.



A late Holocene history of earthquake-related deformation linked to displacement along the western trace of the Little Salmon fault has been reported by Witter and others (2002). At the Swiss Hall site (Figure 3-7; Photo 3-1a and b), a 1- to 1.5-meter-high moletrack scarp projects into Humboldt Bay and deforms late Holocene intertidal sediment. Complex folding of interbedded estuarine and tidal marsh deposits was identified in trenches and sediment cores excavated across the moletrack scarp, indicating that growth of the scarp was produced by coseismic folding. Stratigraphic and structural relations, radiocarbon age data, and diatom paleoecology provide evidence for three to four episodes of surface deformation related to earthquakes on the fault trace within the past 2,300 years. On the basis of radiocarbon age constraints, these earthquakes occurred sometime during the following intervals: event 4 between 2,300 and 1,840 years ago; event 3 between 1,710 and 1,530 years ago; event 2 between 1,230 and 540 years ago; and event 1 less than 460 years ago. At Hookton Slough, 1 to 2 kilometers west of the Swiss Hall site, buried tidal marsh soils provide evidence that episodes of sudden local sea-level rise occurred over extensive areas in southern Humboldt Bay. At least three and as many as five subsidence events are inferred based on stratigraphic analyses of cores near Hookton Slough. At least three of the subsidence events were accompanied by tsunamis that deposited sand on top of the buried marsh soils. The data suggest that submergence in the footwall of the Little Salmon fault occurred during upper-plate earthquakes. This study concludes that, where slip events on the Little Salmon fault were coincident with regional subsidence, the evidence supports an interpretation that the upper-plate faulting could have been triggered by coseismic rupture on the southern Cascadia plate interface.

Synclines - The regions between the major zones of fold-thrust deformation and uplift are characterized by broad, flat-floored Quaternary synclines that are active. These synclines, which include the Freshwater, South Bay, and Eel River synclines (Figure 3-3), are underlain by a thick section of Wildcat Group and younger sediments. The synclines, flanked by anticlinal uplifts and thrust generated uplifts, are isolated basins that formed in response to localized folding. A tectonic explanation for the synclines is not as apparent as for the anticlines. Elastic thinning of the backstop region of the crustal thrust faults and interseismic sedimentation probably



contribute to their growth. Isostatic adjustment from loading of the footwall by overthrusting of the upper plate is also a possible mechanism for growth of the synclines.

Holocene salt marsh sediments in the core of each syncline contain sequences of peat layers buried under intertidal mud. In the area of the broad Freshwater syncline, buried peat sequences are distributed throughout a 12-kilometer-wide zone. These sequences are interpreted as the stratigraphic record of coseismic subsidence during large thrust earthquakes along the plate interface (Clarke and Carver, 1992; Jacoby and others, 1995; Nelson and others, 1995). The similarity in radiocarbon ages of paleoseismic subsidence events in the Freshwater syncline along the Mad River Slough (Carver and others, 1992; Nelson and others, 1995) and adjacent to the Little Salmon fault on the south side of Humboldt Hill (Clarke and Carver, 1992) support the hypothesis that the two structures are kinematically and structurally related.

3.3 REGIONAL SEISMICITY

The region of the southernmost Cascadia subduction zone and the easternmost Mendocino fracture zone is one of the most seismically active areas in California. As per NUREG-1567 (2.4.6.2), this study considered seismicity in the area within 160 kilometers (100 miles) and within 40 kilometers (25 miles) of the ISFSI site. Also included is a discussion of earthquake strong-motion data recorded by the Humboldt Bay Power Plant strong-motion recording system, and effects observed at the plant.

3.3.1 Seismicity Catalog

The seismicity catalog used for this evaluation covers the period 1850 through April 2002, divided into historical data for the period 1850 through 1973, and more modern data for the period 1974 through April 2002. The historical data consist of magnitude 5 and larger events within 160 kilometers of the ISFSI site. The 1974 and later data are subdivided into magnitude 3 and larger earthquakes within the 160-kilometer radius, and magnitude 2 and larger within 40 kilometers of the site. Table 3-2 lists the sources from which location and magnitude data for the magnitude 5 and larger events were derived. The source of the 1974 and later data for magnitude 2.0 to 4.9 earthquakes is the U.S. Geological Survey (USGS, 2002a).



As shown in Table 3-2, the locations and magnitudes of magnitude 5 and larger events often were derived from several sources, including recent work by Bakun (2000) and Topozada and others (2000) for pre-1900 earthquakes. For pre-1900 earthquakes Topozada and others (1981) estimated intensity magnitudes calibrated to Richter local magnitudes. The intensity magnitudes reported by Bakun (2000) are estimated using the method from Bakun and Wentworth (1997) and are calibrated to moment magnitude as defined by Hanks and Kanamori (1979). The catalog used for this evaluation may not be complete at the magnitude 5 level, because it does not include events for which only maximum intensity is reported, and not magnitude. The lower limit of modified Mercalli intensity (MMI) is about VI for damaging earthquakes, which corresponds to about magnitude 5.5 (Dengler and others, 1992a). Generally, the earthquakes not included in the catalog have maximum intensities (MMI values) of V or VI. The various magnitude symbols (e.g., M_L , M_S , M) are defined in the notes at the end of Table 3-2. Special magnitude symbols, such as [ML] or \underline{M} , are also defined in there. These special symbols represent variations of magnitudes from specific sources.

Except for the 1700 Cascadia and 1906 San Francisco earthquakes, earthquake locations in Table 3-2 are plotted in Figures 3-13 and 3-14. When more than one location and/or magnitude is listed for an earthquake, the first listed is used in the figures. Figure 3-13 shows magnitude 5 and larger earthquakes from 1850 through 2000, and Figure 3-14 shows magnitude 3 and greater events from 1974 through April 2002, within the 160-kilometer radius. Preferred locations and magnitude values generally are taken from the most recently published evaluations. The oldest earthquake in the record dates from 1853, and the period 1853 through 1909 contains predominantly pre-instrument locations. 1910 was the start of the University of California, Berkeley, catalog (Bolt and Miller, 1975), which was the principal source of data for the period 1910 through 1973. 1974 marks the Pacific Gas and Electric Company's (PG&E's) installation of their first local network. Data from the PG&E network are now part of the seismicity database at the U. S. Geological Survey's Northern California Data Center.

Earthquakes in the historical record contain substantial uncertainties, which have also changed over time. Topozada and others (1981) estimated epicentral locations for pre-1900 earthquakes



in the area. Many locations were based solely on personal reports and local newspapers, and could be mislocated by 100 kilometers or more (Topozada and others, 1981; Dengler and others, 1992a). Between 1887 and 1932, earthquakes in the Humboldt region were located primarily using instruments at the University of California, Berkeley, campus (UCB) and at Mt. Hamilton (both installed in 1887) (Bolt and Miller, 1975), along with intensity observations. Dengler and others (1992a) suggest the location uncertainty for these events in this time range is about 100 kilometers.

The first seismographic station in the Humboldt region was installed in 1932 at Ferndale (Bolt and Miller, 1975; Dengler and others, 1992a). This station was transferred to the City of Ferndale in 1962; post-1962 data from this station has not been used by the UCB network (Lind Gee, personal communication, 2002). Following installation of stations at Arcata in 1948 and Fickle Hill (east of Eureka) in 1968, location uncertainties dropped to about 50 kilometers (Dengler and others, 1992a). Although the Arcata station is still in operation, the Fickle Hill station was removed in April 1994 (Lind Gee, personal communication, 2002). By 1994, however, as described below, the U. S. Geological Survey's local seismographic network provided enough coverage to constrain uncertainties to significantly less than 50 kilometers.

The first local seismographic network at the Humboldt Bay Power Plant was installed for PG&E in mid-1974 by TERA Corporation (Woodward-Clyde Consultants, 1980). The network, which operated for 12 years, consisted of 16 stations centered around the power plant (USGS, 2002b). UCB continued to operate two of the stations from 1986 to 1994 (USGS, 2002b). Between 1979 and 1982, the USGS installed a dozen more stations, partly in response to the offshore Trinidad earthquake of November 1980. Following the large earthquakes in August 1991, the USGS installed a few more stations, bringing the total to eighteen. The USGS stations continue to operate to the present.

Hypocentral uncertainty of onshore events, particularly for events of magnitude 3 and greater, is about 2 kilometers (D. Oppenheimer, personal communication, 2000). The uncertainties in offshore hypocentral locations are greater because these events occur outside the local seismic networks. The scatter of offshore hypocenters at depths greater than 30 kilometers on cross



section C-C' (Figure 3-15) is interpreted to indicate large uncertainties in depth location. Most offshore earthquakes in the region are assumed to be in the Gorda plate down to about 30 kilometers.

The threshold for magnitude detection is also an issue in earthquake records. The record of damaging ($M > 5.5$) earthquakes in the Humboldt region since 1850 likely is complete, because the area has been inhabited since that time, and more than one newspaper has been in continuous operation that would report such events (Dengler and other, 1992a). Figure 3-13 shows that magnitude 5 earthquakes are fairly evenly distributed across the offshore region to the 160-kilometer (100-mile) radius for the period of 1910 and later. The lack of offshore magnitude 5 events during the earlier period probably reflects limitations in the magnitude detection limit, rather than lack of offshore activity at the magnitude 5 level.

Events of magnitude 2 and greater within 40 kilometers (25 miles) of the ISFSI site are plotted on Figure 3-16. Most of the seismicity within the 40-kilometer radius likely is represented here. Estimates of the current thresholds for magnitude completion with distance from the coast are: magnitude 1.8 for onshore events; magnitude 2.3 for offshore events within about 30 kilometers of the coast; magnitude 3.0 out to about 75 kilometers; and magnitude 4.25 out to about 160 kilometers (D. Oppenheimer, personal communication, 2000). Consequently, some magnitude 3 to 4 earthquakes that occurred beyond about 75 kilometers may not be represented.

3.3.2 Magnitude 5 and Larger Earthquakes

The earthquake record for the past 150 years indicates that at least 120 earthquakes of magnitude 5 and larger occurred from 1850 through April 2002 within 160 kilometers of the Humboldt Bay ISFSI site (Figure 3-13; Table 3-2); 20 occurred within 40 kilometers of the site (Figure 3-16). Of magnitude 7 earthquakes, nine occurred between 1850 and 1994, three between 1873 and 1899, two in the early 1920s, and four between 1980 and 1994. The closest magnitude 7 earthquake to the ISFSI site is the 1923 event, about 30 kilometers to the southwest. The great ($M \sim 9$) 1700 Cascadia earthquake was reported prior to the local historical record, but was observed by the Japanese.



Bakun (2000) reanalyzed the locations of selected north coast earthquakes by considering that some moderate-sized events previously located on or near shore may actually be larger earthquakes located farther offshore. Several of the earthquakes he studied were in the Humboldt region, and are described below, including the magnitude 7 earthquake in 1873. This study generally relies on Bakun's (2000) revised locations and preferred magnitudes.

Described below are the magnitude 7 earthquakes and other selected events listed in Table 3-2, including the magnitude 9 Cascadia subduction zone earthquake of 1700 and the magnitude 7.8 San Francisco earthquake of 1906. For events after 1974, descriptions note whether the earthquakes triggered the Humboldt Bay Strong Motion Network (described in Section 3.3.4).

27 January 1700 - The occurrence of a great Cascadia subduction zone earthquake on this date has been documented using evidence of a major trans-Pacific tsunami that inundated the Northern California, Oregon, and Washington coastal regions and destroyed homes in Japan. Evidence of a tsunami along the western United States coastline includes tree ring information from submerged trees that were killed by salt water inundation along the main subduction zone, oral histories from local Native American tribes, and sudden subsidence of the Eel River syncline and Mad River Slough (see Section 2.4). Written records from Japan indicate the time of the earthquake was the evening of 27 January 1700, at 9:45 local time in the Pacific Northwest. Satake and others (1996; 2002) found that a long rupture length (magnitude ~9) would have been necessary to produce a tsunami that would produce damage in Japan.

23 October 1853 - Topozada and others (1981) locate this earthquake east of Humboldt Bay. Bakun (2000) estimates an intensity magnitude of 5.5, as did Topozada and others (2000). Bakun also believes this may represent a magnitude 6 to 7 earthquake located offshore. Stover and Coffman (1993) report that houses in Eureka "undulated like ships at sea," and people were thrown from their beds.

23 November 1873 - Topozada and others (1981) locate this earthquake onshore, north of Crescent City at the Oregon/California border. The earthquake was widely felt in Oregon and to Tacoma, Washington, as well as south to San Francisco and Sacramento (Topozada and others



(1981). Bakun (2000) prefers an onshore epicenter just north of the 160-kilometer radius, with a hypocenter either within the subduction zone, no deeper than about 15 kilometers, or within the shallower thrust faults of the North American plate. His location is based on MMI intensities of VIII reported near the coast. Topozada and others (1981) estimate an intensity magnitude of 6.7. Bakun (2000) estimates an intensity magnitude 7.3. Wong (2002) re-examines the event, estimating a focal depth of <25 to 30 kilometers within the Gorda Plate. He also believes there was possible strike-slip motion based on intensity patterns. The earthquake was felt as far south as San Francisco and north to Portland, Oregon; many chimneys were toppled in the region (Stover and Coffman, 1993).

9 May 1878 - Topozada and others (1981) report this earthquake as an intensity magnitude 5.8 event onshore near Shelter Cove. Based on a review of felt reports in the Point Arena area and comparisons to the twentieth century intensity patterns of other magnitude 7 earthquakes, Bakun (2000) believes this was a magnitude 7+ earthquake that occurred about 75 kilometers offshore along the Mendocino fault zone. This earthquake and the 1 September 1994 earthquake of magnitude 7 are the largest earthquakes associated with the Mendocino fault zone in the historical record. Damage included chimneys knocked down near Petrolia and landslides triggered along the coast in southern Humboldt County (Stover and Coffman, 1993).

16 April 1899 - Several locations and magnitudes have been proposed for this event. The difference in locations are largest concerning longitudinal coordinates (Table 3-2). Topozada and others (1981) list this as an intensity magnitude 5.7 off the Eureka coast. Ellsworth (1990) prefers a location 150 kilometers offshore, and a magnitude of 7.0. The largest MMI value for this event is VI (Topozada and others, 1981). Bakun (2000) believes this earthquake may be either a magnitude 5 to 6 event near the coast, or a magnitude 7 event farther offshore. Bakun (2000) does not believe the four reported intensities constrain the location. His distant location agrees with Ellsworth's (1990) location, as does his magnitude of 7. Stover and Coffman (1993) report that this earthquake was described "as one of the most severe shocks ever experienced," although it also caused only minor damage to a mill in Eureka.



18 April 1906 - The San Francisco earthquake of 1906 (moment magnitude 7.8) is included in this study because it ruptured from San Juan Bautista to near Cape Mendocino (Ellsworth, 1990), causing substantial damage in the Humboldt region. Topozada and Parke (1982) show Modified Mercalli Intensity values of VIII near Eureka, VI+ near Humboldt Bay, and IX near Petrolia and Ferndale. IX was the highest intensity based on damage (Stover and Coffman, 1993). Nearly every chimney in Ferndale collapsed following the earthquake, and liquefaction was observed in the Eel River Valley and near Humboldt Bay (Dengler and others, 1992b).

23 April 1906 - Meltzner and Wald (2002) consider this earthquake, which occurred 5 days after the 18 April 1906 main shock, to be an aftershock of the previous earthquake. The earthquake was felt widely throughout northern California and southern Oregon, with the strongest shaking along the Humboldt County coast (Meltzner and Wald, 2002). Stover and Coffman (1993) report that chimneys were toppled in Ferndale and clocks were stopped at Cape Mendocino, Eureka, and Trinidad Head. Topozada and others (2000) assign a magnitude of 6.4 to this event. Meltzner and Wald (2002) constrain the magnitude to between magnitude 6 ½ and 7. This study uses the Topozada and others (2000) location of 41°N, 124°W30, about 50 kilometers northwest of Eureka; Meltzner and Wald (2002) prefer a location centered farther west at about 40.8°N, 125.3°W.

January 31, 1922 - This earthquake is considered the largest historical north coast earthquake; felt reports extended from San Francisco to Eugene, Oregon (Dengler and others, 1995; Stover and Coffman, 1993). Recent catalogs report magnitudes of from 7.0 to 7.3 (Table 3-2). Smith and Knapp (1980) locate this earthquake about 45 kilometers offshore, west-northwest from Eureka, but the similarity of intensity patterns to those of the 1994 earthquake suggest it might have occurred farther offshore (Dengler and others, 1995).

January 22, 1923 - This earthquake caused major damage in the Cape Mendocino area (Dengler and others, 1995), including many houses damaged at Ferndale, Petrolia, and Upper Mattole; broken water lines; and a house shaken from its foundation in Pepperwood (Stover and Coffman, 1993). The UCB catalog reports a local magnitude 7.2 for the earthquake. Intensity VII and VIII values constrain the location to near the Cape Mendocino area, consistent with Smith and



Knapp's (1980) offshore location about 13 miles northwest of Cape Mendocino (Dengler and others, 1995). The intensity data, however, do not indicate whether the earthquake occurred along the Mendocino fault or slightly farther north, either within the southern part of the Gorda plate or along the Cascadia subduction zone, similar to the 1992 earthquake (discussed below). Using teleseismic data for the 7 June 1975 Ferndale earthquake (M_L 5.3) as a calibration event, Smith and Knapp (1980) relocate the 1923 event onshore, 20 kilometers east of Eureka. They acknowledge that their location is suspect, however, because errors in the P-wave arrival times were not compensated for in the relocation procedure.

20 August 1927 - This earthquake occurred offshore, about 50 kilometers northwest of Eureka. Although it was a moderate earthquake (M_L 5.0), it was felt sharply and caused fairly substantial local damage. Stover and Coffman (1993) report destroyed chimneys, broken windows and water pipes, and cracked walls in Eureka and Arcata and downed chimneys in Fortuna. They also report cracks in mud and moderate landsliding in Redwood Park (Eureka).

6 June 1932 - One person was killed and several more injured in Eureka (Stover and Coffman, 1993) as a result of this magnitude 6.4 earthquake (UCB, 2002), about 50 kilometers west-southwest of Eureka. There was substantial property damage in Eureka and Arcata, and nearly all of the chimneys in Fields Landing were destroyed (Stover and Coffman, 1993). Ground cracking and blowholes were observed on Cock Robin Island, at the mouth of the Eel River (Stover and Coffman, 1993).

21 December 1954 - This earthquake occurred on land, 40 kilometers east of Eureka (Ellsworth, 1990). Magnitude estimates include local magnitude 6.5 and Gutenberg Richter magnitude 6.6. One person was killed and several were injured; property damage was estimated at \$2.2 million (Stover and Coffman, 1993). It was felt widely, from Oregon to San Francisco, suggesting a shallow depth within the North American plate along the Mad River fault zone (Dengler and others, 1992a). The lack of documented surface rupture, however, makes the depth difficult to confirm (Dengler and others, 1992a). A local magnitude 4.7 aftershock occurred on 30 December 1954, causing minor damage, including further damage to Eureka's water supply pipeline (Stover and Coffman, 1993).



7 June 1975 - Called the Ferndale earthquake, this local magnitude 5.3 event occurred at a depth of 23 kilometers beneath Ferndale (CNSS, 2002), within the Gorda plate. Stover and Coffman (1993) report damage to chimneys in Fortuna and surrounding towns, including Ferndale; a water main broke at Rio Dell; and landslides were observed in the Fortuna-Rio Dell area. Aftershock activity was confined to the Gorda plate (Tera Corporation, 1975). The focal mechanism shows strike slip on north-northwest- and east-northeast-striking planes (Woodward-Clyde Consultants, 1980). Tera Corporation (1975) prefers a N70°E-striking, nearly vertical fault plane undergoing left-lateral motion. Pacific Gas and Electric Company (1975) assigns a focal mechanism of N75°E, dipping 72°SE. They also report minor damage at the Humboldt Bay Power Plant site; minor cracking in the blacktop of the plant entrance, a small crack in a newly poured concrete floor, and three small objects falling. The main shock triggered the Humboldt Bay Power Plant strong-motion network. The largest peak acceleration recorded was 0.3g on the free-field horizontal component, oriented east-west (Table 3-3; Section 3.3.4).

8 November 1980 - Called the Trinidad earthquake, this surface wave magnitude 7.2 earthquake occurred offshore, 50 kilometers northwest of the plant site within the Gorda Plate. No foreshocks were reported; however, two magnitude 5 aftershocks occurred to the southwest (Table 3-2), within the aftershock trend. Aftershock patterns show a northeasterly fault rupture (Tera Corporation, 1982) trending about N50°E (Stover and Coffman, 1993). Reported depths for this earthquake range from about 6 to 20 kilometers (see Table 3-2), exemplifying the hypocentral uncertainty for offshore regions. Tera Corporation (1982) and Eaton (1981) report a strike-slip focal mechanism with a preference for left slip on a N50°E-trending fault plane. There was substantial damage to structures, including a collapsed overpass across Highway 101 east of Fields Landing; two houses that were displaced from their foundations; and broken gas, water, and sewer lines (Stover and Coffman, 1993). The main shock triggered the Humboldt Bay Power Plant strong-motion network. Terra Technology Services (1980) reports a maximum free-field peak acceleration of 0.50g on the east-west horizontal component (Table 3-3, Section 3.3.4). However, they also report that these measurements are suspect because of instrument malfunctions prior to the earthquake.



16 August 1991 - This was the second of four large earthquakes that occurred within about a month along the coast of northern California and southern Oregon, and one of three that occurred within the Gorda plate. The short time between the four apparently independent events is unprecedented in the historical record for this area (McPherson and Dengler, 1992). The surface wave magnitude of this earthquake was 6.3; it was located about 95 kilometers offshore, west of Crescent City, and 120 kilometers west-southwest, within the Gorda plate. The event was preceded by a surface wave magnitude 6.9 earthquake on 12 July that occurred about 70 kilometers farther north (outside the study area) and 95 kilometers west-southwest from Gold Beach, Oregon, also within the Gorda plate (McPherson and Dengler, 1992). Although the earthquake was felt widely in northern California and southern Oregon, it did not trigger the Humboldt Bay Power Plant strong-motion network.

17 August 1991 (12:29 PM) - Called the Honeydew earthquake, this surface wave magnitude 6.2 event occurred 21 hours after the 16 August event described above. It was located on land, about 7 miles south of Petrolia and west of Honeydew, and 50 kilometers south of the Humboldt Bay Power Plant, at a depth of 12 kilometers (McPherson and Dengler, 1992). The earthquake caused minor damage in the towns of Petrolia and Honeydew. Some aftershocks were felt locally. It is the largest earthquake on land in the Mendocino triple junction region in this century (McPherson and Dengler, 1992). The proposed fault motion is thrust along a northeast-vergent fault plane, based on the focal mechanism and a zone of northwest-trending surface cracks up-dip from the hypocenter (Oppenheimer and Magee, 1991). The hypocenter is within the Petrolia subplate, a detached sliver of the North American plate (Section 2.2). The largest intensity values (MMI) of VIII were reported near Honeydew, also up-dip from the hypocenter; values of IV were reported in the Eureka area and near the plant site (McPherson and Dengler, 1992). The earthquake triggered the strong motion network at the Humboldt Bay Power Plant site. The largest peak acceleration recorded was 0.064g on the horizontal component (orientation not specified) of the free-field sensor (PG&E, 1991). This event is not included in Table 3-3 because peak ground motion was less than 10%g, which generally is below the damage threshold for structures.



17 August 1991 (3:17 PM) - This surface wave magnitude 7.1 earthquake was the third and largest of the Gorda plate earthquakes that occurred following the event of 12 July 1991. Occurring three hours after the 17 August event, it was located about 62 kilometers northwest of the plant site. The earthquake did not trigger the Humboldt Bay Power Plant strong-motion network.

25 and 26 April 1992 - This earthquake sequence, called the Petrolia sequence, included an onshore main shock of surface wave magnitude 7.1 on 25 April 1992 and two offshore aftershocks of surface wave magnitude 6.6 the following day. The 1992 main shock, at a depth of 10 kilometers, is considered evidence of fault rupture along the Gorda/North American plate interface (Oppenheimer and others, 1993); the aftershocks were Gorda intraplate earthquakes. Damage from these earthquakes was extensive. The region was declared a major disaster area by President Bush based on damage estimates of \$48 million to \$66 million (Oppenheimer and others, 1993). Although much of the damage was caused by the main shock, fires were triggered by the first large aftershock, nearly destroying a shopping center in Scotia (Oppenheimer and others, 1993). The focal mechanism for the main shock shows thrust motion along a N10°W-trending fault plane; mechanisms for both aftershocks show right slip along northwest-oriented planes (Oppenheimer and others, 1993). All three earthquakes triggered the Humboldt Bay Power Plant strong-motion network. Free-field horizontal peak accelerations of 0.22g, 0.25g, and 0.13g, respectively, were recorded (Table 3-3, Section 3.3.4). All were recorded on the east-west horizontal component; the maximum 0.22g (main shock) was recorded on both horizontal components.

1 September 1994 - This moment magnitude 7.0 (Bakun, 2000) earthquake was felt throughout a wide area from San Francisco to southwest Oregon (Dengler and others, 1995). Yet because the earthquake occurred about 150 kilometers offshore, it caused no reported damage. The location for this earthquake varies considerably, depending on which catalog is used. The catalog for this study incorporates the NEIC location using the Worldwide Network, per D. Oppenheimer (personal communication, 2000), as opposed to the USGS location that uses arrival times from only the local seismic network. This and the 1878 earthquakes are the largest historical earthquakes associated with the Mendocino fault zone. Focal mechanisms for the 1994



main shock and five of the largest aftershocks (none larger than magnitude 4.5) are strike slip, consistent with the strike of the Mendocino fault zone (Dengler and others, 1995). The combination of strike-slip focal mechanisms and east-northeast displacements measured at onshore stations indicates that the preferred motion is right slip along the fault zone (Dengler and others, 1995). These earthquakes did not trigger the Humboldt Bay Power Plant strong-motion network.

26 December 1994 - This moment magnitude 5.4 earthquake occurred 8 kilometers west of the Humboldt Bay ISFSI site. Although it was moderate in size, it was felt strongly at the plant site; the strong-motion system recorded horizontal peak accelerations of 0.55g (north-south component) (Table 3-3). Although no damage was reported at the site (Section 3.3.4), preliminary damage estimates in the Eureka area exceeded \$2.7 million (Dengler and others, 1995). This event occurred within the Gorda plate at 23 kilometers depth, caused by strike-slip motion along northwest- or northeast-oriented fault planes.

3.3.3 Association of Earthquakes with Tectonic and Geologic Structures

The magnitude 5 and larger historical data and the post-1973 data (Figures 3-13 and 3-14) show that most regional earthquake activity has been concentrated along the Mendocino fault zone and scattered to the north across the southern part of the Gorda plate in the Gorda deformation zone. A lower level of activity has occurred in the onshore North American plate. The Pacific plate west of the San Andreas fault zone and south of the Mendocino fault zone is relatively aseismic. Following is a summary of the association of earthquakes with the primary seismically active structures of the Humboldt Bay region: the Mendocino fault zone, the Gorda plate and Gorda deformation zone, the Petrolia subplate (location of the Petrolia earthquake sequence), and the North American plate.

Mendocino fault zone—The Mendocino fault zone is highly active, as reflected by the occurrence of magnitude 5 and greater earthquakes within about 20 kilometers of the fault zone since at least the late 1870s (Figure 3-14). Although there is uncertainty in locations of offshore events, the narrow, west-trending pattern of the earthquakes along the mapped fault trace (Figure



3-14) is consistent with the well-expressed topography and bathymetry of the Mendocino triple junction region (Section 2.3).

The 1878 and 1994 earthquakes are the largest associated with the Mendocino fault zone. Focal mechanisms for the 1994 main shock and five of the largest aftershocks show that fault motion is predominantly right slip (Dengler and others, 1995), consistent with previous focal mechanisms (Couch, 1980; Hill and others, 1990). The more accurately located magnitude 3 and larger events from the post-1973 data set (Figure 3-14) suggest that the diffuse historical earthquakes shown south of the Mendocino fault zone on Figure 3-13 may be somewhat mislocated, and probably occurred farther north within the fault zone.

Gorda plate and Gorda deformation zone – The offshore region of the Gorda plate is highly seismically active. Some of the larger Gorda plate earthquakes are the 1922, 1980, and three 1991 earthquakes described in Section 3.3.2. Smaller Gorda plate earthquakes were the 7 June 1975 Ferndale event (M_L 5.3), the 26 December 1994 event (M 5.4), and the 31 July 1987 event (M 5.2) (Figure 3-17). Bakun (2000) postulates that the 1873 earthquake, previously located by UCB onshore near the 42nd parallel, likely occurred slightly farther north (Figure 3-13) within the Gorda plate.

Most earthquakes within the Gorda plate are located in the Gorda deformation zone (GDZ) (Figures 2-3, 3-13, and 3-14). This trend is consistent with a change from a rigid to deforming Gorda plate southward across the GDZ. This pattern is evident in both larger ($M \geq 5$) and smaller ($M \geq 3$) earthquakes. Cross section C-C' (Figure 3-15) illustrates the Gorda slab plunging under the North American plate. The angle of subduction increases with depth to the east. The northeast cross section D-D' (Figure 3-15), across the southern part of the Mendocino triple junction region, shows a vertical pattern of events between about 18 and 30 kilometers horizontal distance, and then a steeply northeast-dipping pattern to about 30 kilometers depth. The change in dip at 15 kilometers is coincident with the interface between the Gorda and Pacific plates.



Cross section C-C' also shows that, at the magnitude 3 threshold, most activity has been within the Gorda plate. Magnitude 2 and larger earthquakes (Figure 3-17) within 40 kilometers of the site also indicate that most of the events are within the Gorda plate and near the Mendocino triple junction region. Earthquake activity within both the Gorda and North American plates dies out to the north, as seen on cross section E-E' (Figure 3-17).

The 1980 Trinidad earthquake and prolific aftershock sequence provided evidence of shearing in the southern part of the GDZ. Most of the focal mechanisms west of the Mendocino triple junction and north of the Mendocino fault zone indicate left slip along northeast trends (McPherson, 1992a).

North American plate - The North American plate (including the Petrolia and Eel River subplates) has been characterized by occasional moderate earthquakes that occur onshore, to the east and northeast, within the study area. Examples are the 1954 (M_{G-R} 6.6) earthquake near Mad River, and the 1991 Honeydew earthquake (M_S 6.2). Based primarily on felt reports, Dengler and others (1992) conclude that the 1954 earthquake likely was associated with the Mad River fault zone. The 1991 Honeydew earthquake occurred along a northeast-vergent thrust fault within the Petrolia subplate. North American plate focal mechanisms from McPherson (1992a) show primarily reverse and strike slip along northwest trends.

Post-1973 microseismic activity within the North American plate, within a 40-kilometer radius of the site, shows isolated events and diffuse clusters along the coast near the Little Salmon fault zone, the Eel River syncline, and the Russ fault (Figure 3-16). Similar to seismicity patterns for the subducted Gorda plate, earthquake activity within the North American plate dies out to the north and east, as seen on cross section E-E' (Figure 3-17). Except for the activity near the Russ fault, seismicity patterns do not appear to be associated with specific faults. Cross section E-E' shows that most of the activity near the Eel River syncline occurs in the Gorda plate; activity near the Little Salmon fault zone occurs in the Gorda and North American plates. The small clusters between about 5 and 10 kilometers depth may be associated with the Table Bluff fault zone.

The shallow (2- to 6-kilometer-deep) activity beneath the surface trace of the Russ fault (cross section E-E' on Figure 3-17) is consistent with McLaughlin and others' (2000) cross section (Figure 3-2) that is oriented parallel to and southeast of E-E'. The events shown in McLaughlin and others' (2000) cross section suggest a steep southerly dip of the Russ fault, which is opposite from the interpretation of a northerly dip shown on Figure 3-17. McLaughlin and others' (2000) locations were obtained from a detailed velocity analysis filtered to show the most precise locations (M. Magee, personal communication, 2000).

Petrolia subplate - The 1992 M_S 7.1 Petrolia earthquake helped define the Petrolia subplate. With the exception of the 1700 Cascadia event, this is the only event in the catalog that is interpreted to be an interplate earthquake, occurring at the interface between the Gorda and North American plates. The low-angle thrust motion is consistent with subduction along the interface of the Gorda and North American plates (Petrolia subplate), at the southernmost end of the Cascadia subduction zone.

The dense concentration of events near Cape Mendocino includes aftershocks from the 1992 Petrolia earthquake, some of which are shown in Figure 3-17. The spatial gap in activity beneath the 1992 aftershocks, between about 12 and 16 kilometers depth, as seen in both cross sections, is coincident with the plate interface region, as interpreted from Figure 3-1 and Geomatrix (1994). Oppenheimer and others (1993) suggest the gap may be a ductile aseismic zone.

3.3.4 Earthquake Ground Motions Recorded at Humboldt Bay Power Plant

Pacific Gas and Electric Company (PG&E) has operated a strong-motion recording network at the Humboldt Bay power plant continuously since September 1971 (Bechtel Power Corporation, 1975). The network has gone through several upgrades in the past 30+ years. The first instruments consisted of a Teledyne MTS-100 strong-motion recording system and three FB-103 triaxial force-balance accelerometers, one in the refueling building at elevation +12 feet (4 meters), one in the Reactor Caisson at elevation -66 feet (-20 meters), and one in the storage building at +12 feet (4 meters) (PG&E, 1975). These instruments were replaced in 1977 with sensors and recorders from Terra Technology. This new network also consisted of three three-component forced-balance accelerometer sensors and a central recording system, in this case a



DCA-300-P9. This system used the same Unit 3 locations for the sensors, except that the sensor in the outside storage building was moved to a better free-field site in the north yard. The DCA-300-P9 recorded on cassette tapes, similar to the Teledyne/Terrametrics system. In 1991 the system was upgraded to use DOS-based Ramdeck software to communicate with the recorder and to download and analyze data more efficiently. In 1997 the recorder was upgraded again to a GNC-R recorder (Terra Technology). The communication software for this latest upgrade is DOS-based but can be used with Windows OS.

A stand-alone three-component accelerometer (model SSA-2 by Kinometrics) also has been in operation at the plant site since 1991. It was located in the administration building until 2001; it now resides in the main building communications room. To provide for continuous coverage, this recorder is used primarily as an alternate recorder when the central recording system is down for maintenance or replacement. For example, the records from the 26 December 1994 earthquake (Table 3-3) were recorded only on the SSA-2 instrument because the Terra Technology system was down for maintenance at the time of the earthquake.

Since 1975, the strong-motion instruments at the Humboldt Bay Power Plant have recorded six earthquakes having peak horizontal accelerations greater than 0.10g. These were the 1975 Ferndale (M_L 5.3) earthquake, the 1980 Trinidad (M_S 7.2) earthquake, the 1992 Petrolia main shock (M_S 7.1) and two aftershocks (both M_S 6.6), and the 1994 (M_L 5.4) earthquake. Table 3-3 lists these events, their recorded free-field ground motions, the effects observed at the plant, and the tectonic source of each event. The events are labeled on Figure 3-13 using numbers that correspond to those in the table.

The largest peak horizontal acceleration recorded by PG&E's network (0.55g) was from the 26 December 1994 earthquake, 8 kilometers from the plant. The event was felt strongly at the plant (Table 3-3). The second-largest reported acceleration was 0.50g on the east-west horizontal component from the November 1980 Trinidad earthquake, located 50 kilometers northwest of the plant. However, Terra Technology Services (1980) reports that an instrument malfunction occurred prior to the earthquake. A blown fuse on the battery charger produced insufficient battery power to obtain a good record of the event. Despite their efforts to recover the data, they



report that the amplitudes of the waveforms may be incorrect, which means that the recorded peak accelerations may also be incorrect.

The 1975 Ferndale earthquake, located 22 kilometers southeast of the plant, produced a peak horizontal acceleration of 0.30g. Both this and the 1994 events were located at about 23 kilometers depth (Figure 3-17). The 1992 earthquakes, located between 55 and 70 kilometers from the plant, produced peak accelerations of 0.13g to 0.25g.

No structural damage was reported at the Humboldt Bay Power Plant from any of the events described above. After the 1992 main shock, however, new hairline cracks were observed in the walls of the refueling building. Other effects were water sloshing in the spent fuel pool following the 1975 and 1992 (main shock) earthquakes, tools falling from racks after the 1980 event, and fuses falling from the startup transformer during the 1994 earthquake.

3.4 SUMMARY OF REGIONAL GEOLOGY AND SEISMICITY

Regional Stratigraphy

- The Humboldt Bay ISFSI site is in a broad depositional basin, the Eel River basin, that is underlain by a thick sequence of late Cenozoic marine sedimentary rocks. The late Cenozoic deposits unconformably overlie basement rocks of the Cretaceous to late Tertiary Franciscan Complex that were accreted to the western margin of North America by plate convergence prior to the development of the present Cascadia subduction zone about 20 million years ago.
- The thick (as much as 3,600 meters) sequence of late Tertiary and Quaternary deposits, which are referred to collectively as the Wildcat Group, was deposited on the upper plate of the modern Cascadia subduction zone. The lower Wildcat Group sediments reflect deposition in a locally quiescent tectonic environment. In contrast, the upper Wildcat Group sediments are laterally variable, recording northeast-to-southwest shortening of the basin by a rapidly developed system of folds and thrust faults. Contractual tectonics initiated about 700,000 years ago, following deposition of the Rio Dell Formation, when localized uplift due



to anticlinal folding over active thrust faults divided the subsiding Eel River basin into several small subbasins.

- The late Pleistocene Hookton Formation and other post-Wildcat Group sediments and geomorphic surfaces, including uplifted marine terraces, record continued uplift of the hills and subsidence of the basins associated with the growth of faults and folds in the upper plate of the Cascadia subduction zone.

Regional Geologic Structure

- The Humboldt Bay region is dominated by north-northwest-trending contractional structures formed during several phases of plate convergence that have affected the region since the Late Jurassic. Three ages of structures are evident at the regional scale.
 1. Faults, folds, and tectonic mélanges formed during multiple episodes of accretion of the Franciscan Complex basement rocks during the late Mesozoic and early Tertiary.
 2. Early and mid Tertiary structures formed in the accreted continental margin prior to the development of the present plate tectonic structure of the Cascadia subduction zone.
 3. Late Cenozoic structures (basin subsidence and localized anticlinal uplift) have been created by the tectonics of the modern Cascadia subduction zone.
- The interaction of subsidence and fold-thrust deformation during the past approximately 700,000 years has resulted in a clear tectonic distinction between the uplifting areas that overlie active thrust faults and fault-related anticlines (for example, the Table Bluff, Humboldt Hill, and Fickle Hill anticlines), and subsiding local basins that are coincident with intervening synclines.
- Two major zones of thrust faults and related folding have been mapped in the Humboldt Bay region: the Mad River fault zone, and the Little Salmon fault system.
- The Mad River fault zone is an approximately 80-kilometer-long, 15- to 25-kilometer-wide belt of en echelon thrust faults and fault-generated folds that trend north-northwest and dip predominantly northeast. The onshore part of the fault zone includes the Trinidad, Blue Lake, McKinleyville, Mad River, Fickle Hill, and Greenwood Heights faults. Late Quaternary slip rates on individual faults within the zone, based on dating of uplifted marine



terraces, are generally 1 to 2 millimeters per year. The cumulative slip rate across the zone is about 5 to 9 millimeters per year.

- The Little Salmon fault *system* is a 15- to 25-kilometer-wide belt of en echelon anticlines and active thrust faults that extends for 330 kilometers parallel to the deformation front associated with the leading edge of the Cascadia subduction zone. Onshore, near the site, the Little Salmon fault system includes the Table Bluff fault and the Little Salmon fault zone. The slip rate for the Little Salmon fault zone is estimated to be between 6 and 10 millimeters per year, and 2 to 3 millimeters per year for the Table Bluff fault.
- The Little Salmon fault *zone* is the nearest capable fault to the site. Including the Yager fault to the southeast and offshore traces to the northwest, it has a total length of 95 kilometers. The fault zone consists of multiple imbricate traces that are well defined in the geomorphology, deforming Holocene geomorphic surfaces and sediments. Near the Humboldt Bay ISFSI site, the fault zone consists of two main faults (the Little Salmon fault and the Bay Entrance fault), and two subsidiary faults (the Buhne Point and Discharge Canal faults). Paleoseismic investigations along the fault zone southeast of the site (at the Little Salmon Creek exploration locality) indicate that at least three surface-faulting events occurred along the western trace of the fault zone during the past 1,700 years. Radiocarbon dates indicate that these events occurred about 1,600, 800, and 300 years ago. The results of the detailed paleoseismic studies demonstrate that the location, style, and pattern of deformation have been replicated during successive surface-faulting events on the Little Salmon fault zone.
- The Table Bluff fault is a 23-kilometer-long thrust in the Little Salmon fault system. Seismic profiles and surface mapping indicate the fault consists of a south-vergent thrust wedge beneath the actively deforming Table Bluff anticline.

Regional Seismicity

- The Humboldt region (within 160 kilometers [100 miles] of the ISFSI site) is an area of high seismic activity in which 121 earthquakes of magnitude 5 and greater have been recorded during the past 150 years, including nine magnitude 7 events. Most of these earthquakes



have occurred in the offshore region within and along the southern margin of the Gorda plate on the Mendocino fault zone.

- In general, the regional pattern of modern magnitude 3 and larger earthquakes shows the Gorda plate subducting beneath the North American plate, and the Mendocino fault zone as a distinct boundary between the rigid Pacific plate and the deforming Gorda plate.
- Moderate to large earthquakes have been recorded within or on the shared boundaries of all three primary tectonic structures within 160 kilometers of the ISFSI site. The April 1992 Petrolia earthquake occurred on the interface of the Gorda and North American plates (Petrolia subplate) on the Petrolia segment of the Cascadia subduction zone, and the January 1700 event appears to have ruptured the main segment of the Cascadia subduction zone. Gorda plate earthquakes include the 1975, 1980, and 1991 offshore events; the December 1994 main shocks; and two 1992 aftershocks. The 1991 Honeydew earthquake occurred within the Petrolia subplate, a detached sliver of the North American plate. The September 1994 earthquake, and likely the 1878 earthquake, occurred on the Mendocino fault zone.
- Seismic activity in both the Gorda and North American plates decreases significantly north of the Mendocino triple junction region and east of the offshore Gorda plate. Within the triple junction region, the Gorda plate is more seismically active than is the North American plate.
- The Pacific plate south of the Mendocino fault zone and west of the San Andreas fault zone has few earthquakes.
- Except possibly for microearthquakes beneath the Russ fault, seismic activity cannot be associated confidently with specific faults within 40 kilometers (25 miles) of the ISFSI site.
- Two moderate Gorda plate earthquakes within 20 kilometers of the ISFSI site produced relatively large ground motions at the Humboldt Bay Power Plant. The M_L 5.3 event of November 1975 produced peak horizontal accelerations of 0.30g, and the M_L 5.4 event of December 1994 produced peak accelerations of 0.55g.



TABLE 3-1
GEOLOGIC HISTORY OF THE HUMBOLDT BAY ISFSI SITE
 Pacific Gas and Electric Company
 Humboldt Bay ISFSI

Timing	Event	Evidence	Interpretation
Holocene	Continued activity in the fold-and-thrust belt in the upper plate of the Cascadia subduction zone. Timing of upper-plate earthquakes apparently coincides with great earthquakes on the Cascadia subduction zone.	Buried Holocene marsh soils	Holocene estuarine deposits deposited in upper-plate synclines record evidence for sudden subsidence during earthquakes on adjacent crustal structures. Timing of subsidence coincides with events on the Cascadia subduction zone. These upper-plate synclines include the Eel River, South Bay, and Freshwater synclines.
Late Pleistocene-Holocene	Continued late Pleistocene and Holocene activity in the fold-and-thrust belt in the upper plate of the Cascadia subduction zone	Geomorphic surfaces	Marine and fluvial terraces provide evidence for activity of upper-plate thrust faults, because they show uplift and growth of anticlines in the hanging walls of thrust faults.
Late Pleistocene-Holocene	Local fluvial deposition	Hookton Formation and related units	Coeval deposition and development of the fold-and-thrust system creates localized depocenters over synclines (the Eel River, South Bay, and Freshwater synclines) and localized erosion over anticlines.
Ca. 700 ka	Initiation of upper-plate deformation in a series of northwest-trending folds and northeast-dipping thrust faults. Uplift of Klamath Mountains, likely related to approach of Mendocino triple junction.	---- Unconformity ----	Timing of unconformity is controlled by its position above the Scotia Bluffs Formation (800 ka) and below the Hookton Formation (600 ka). Extensive erosion on upper plate of Little Salmon fault, removing the majority of the Wildcat group.
Late Pleistocene	Fluvial and estuarine deposition near sea level records glacio-	Wildcat Group, fluvial portion;	Redwood logs in the Carlotta Formation indicate it is terrestrial or very near shore. Fluvial deposits are intercalated with marine.



TABLE 3-1
GEOLOGIC HISTORY OF THE HUMBOLDT BAY ISFSI SITE

Pacific Gas and Electric Company

Humboldt Bay ISFSI

	eustatic sea level changes.	Carlotta Formation	This intercalation probably represents glacio-eustatic sea level cycles. The Carlotta Formation is derived primarily from local sources, the Eastern and Central Belt Franciscan Complex, indicating onset of uplift of the nearby Klamath Mountains.
Late Miocene to Pleistocene	Deposition and rapid submergence ca. 9 ma, then shoaling, basin filling, and gradual shallowing.	Wildcat Group, marine portion, including: Pullen, Eel River, Rio Dell, and Scotia Bluffs formations	Trace fossils and lithology at the base of the Pullen Formation indicate this unit is fluvial to littoral. Rapid submergence of the area to depths of 2 to 3 km is then recorded by the clayey deposits of the upper Pullen, Eel River, and Rio Dell formations. These deposits record gradual shoaling and basin-filling. Trace fossils in the Scotia Bluffs Formation indicate deposition in ~30 m of water. The abrupt submergence ca. 9 ma may relate to greater than normal plate convergence, or to the passing of a structure in the subducted plate that divided relatively young, warm, buoyant lithosphere from relatively old, cold, dense lithosphere. Along the Eel River at Scotia, an angular unconformity separates the tightly folded Yager turbidites from the tilted but relatively undeformed Wildcat Group.



TABLE 3-2
MAGNITUDE 5 AND LARGER EARTHQUAKES WITHIN 160 KILOMETERS (100 MILES)
OF THE HB-ISFSI SITE, 1850 THROUGH APRIL 2002

Pacific Gas and Electric Company
Humboldt Bay ISFSI

Date	Origin Time (GMT)	Latitude (deg. min.)	Longitude (deg. min.)	*Depth (km)	Location References	§Magnitude	Magnitude References
01/27/1700	~05:00	Cascadia	Subduction	Zone	Satake and others, 1996	~9	Satake and others, 1996
10/23/1853	11:00	40 48?	-124 12?	0	Bakun, 2000; Topozada and others, 1981; Topozada and others, 2000	[MI] 5.5; (M _L) 5.7; <u>M</u> 5.5	Bakun, 2000; Dengler and others, 1992a; Topozada and others, 2000
11/13/1860	00:00	40 48?	-124 12?	0	Bakun, 2000; Topozada and others, 1981; Topozada and others, 2000	[MI] 6.1; (M _L) 5.7; <u>M</u> 5.5	Bakun, 2000; Dengler and others, 1992; Topozada and others, 2000
10/01/1865	17:15	40 48?	-124 6?	0	Bakun, 2000	[MI] 6.2	Bakun, 2000
		40 48	-124 12	0	Topozada and others, 1981; Topozada and others, 2000	(MI) 5.4; <u>M</u> 5.5	Topozada and others, 1981; Topozada and others, 2000
03/02/1871	21:05	40 18?	-124 30?	0	Bakun, 2000	[MI] 6.3	Bakun, 2000
		40 24	-124 12	0, 12.3	Ellsworth, 1990; Geomatrix, 1995; Topozada and others, 2000	M 6; {MI} 6.2; <u>M</u> 6.3	Ellsworth, 1990; Geomatrix, 1995; Topozada and others, 2000
11/23/1873	05:00	42 12?	-124 12?	0	Bakun, 2000	[MI] 7.3	Bakun, 2000



TABLE 3-2
MAGNITUDE 5 AND LARGER EARTHQUAKES WITHIN 160 KILOMETERS (100 MILES)
OF THE HB-ISFSI SITE, 1850 THROUGH APRIL 2002

Pacific Gas and Electric Company
Humboldt Bay ISFSI

Date	Origin Time (GMT)	Latitude (deg. min.)	Longitude (deg. min.)	*Depth (km)	Location References	[§] Magnitude	Magnitude References
		42	-124	0	Toppozada and others, 1981	(MI) 6.7; <i>M</i> 6 3/4	Toppozada and others, 1981, Ellsworth, 1990
		42	-124 12	0	Toppozada and others, 2000	<u>M</u> 6.9	Toppozada and others, 2000
		42 48	-124 30	0	Geomatrix, 1995	{MI} 6.7	Geomatrix, 1995
09/30/1875	12:30	40 42	-124	0	Bakun, 2000; Toppozada and others, 2000	[MI] 5.9; <u>MI</u> 5.9	Bakun, 2000; Toppozada and others, 2000
		40 06.0	-124	0	Toppozada and others, 1981; Geomatrix, 1995	(MI) 5.5; {M} 5.8	Toppozada and others, 1981; Geomatrix, 1995
05/09/1878	04:25	40 24?	-125 12?	0	Bakun, 2000; Toppozada and others, 2000	[MI] 7.0; <u>M</u> 7.0	Bakun, 2000; Toppozada and others, 2000
		40 6	-124	0	Toppozada and others, 1981	(MI) 5.8; <i>M</i> 6	Toppozada and others, 1981; Ellsworth, 1990
01/28/1884	07:30	41 6	-123 18	0	Bakun, 2000; Toppozada and others, 2000	[MI] 4.9; <u>M</u> 6.1	Bakun, 2000; Toppozada and others, 2000 (Event plotted in Figures 3-14 to 3-17)



TABLE 3-2
MAGNITUDE 5 AND LARGER EARTHQUAKES WITHIN 160 KILOMETERS (100 MILES)
OF THE HB-ISFSI SITE, 1850 THROUGH APRIL 2002

Pacific Gas and Electric Company
Humboldt Bay ISFSI

Date	Origin Time (GMT)	Latitude (deg. min.)	Longitude (deg. min.)	*Depth (km)	Location References	[§] Magnitude	Magnitude References
		41 6	-123 36	0	Toppozada and others, 1981	(MI) 5.7	as average MI 5.5) Toppozada and others, 1981
07/26/1890	09:40	40 18?	-124 30?	0	Bakun, 2000	[MI] 6.3	Bakun, 2000
		40 30	-124 12	0	Ellsworth, 1990; Toppozada and others, 2000	<i>M</i> 6 ¼; <u>M</u> 6.3	Ellsworth, 1990; Toppozada and others, 2000
		40 30	-124 30	8.4	Geomatrix, 1995	{MI} 5.9	Geomatrix, 1995
09/30/1894	17:36	40 18	-123 42	0	Bakun, 2000	[MI] 6.5; <i>M</i> 6	Bakun, 2000; Ellsworth, 1990
		40 18	-124 30	0	Toppozada and others, 1981; Toppozada and others, 2000	(MI) 5.9; <u>M</u> 6.5	Toppozada and others, 1981; Toppozada and others, 2000
04/15/1898	07:07	39 18?	-123 54?	0	Bakun, 2000	[MI] 6.8	Bakun, 2000
		39 12	-123 48	0	Toppozada and others, 1981; Toppozada and others, 2000; Geomatrix, 1995	(MI) 6.4; <u>M</u> 6.7	Toppozada and others, 1981; Toppozada and others, 2000
04/16/1899	13:40	41?	-126?	0	Ellsworth, 1990	[MI] 7.0; <i>M</i> 7	Bakun, 2000, Ellsworth, 1990



TABLE 3-2
MAGNITUDE 5 AND LARGER EARTHQUAKES WITHIN 160 KILOMETERS (100 MILES)
OF THE HB-ISFSI SITE, 1850 THROUGH APRIL 2002

Pacific Gas and Electric Company
Humboldt Bay ISFSI

Date	Origin Time (GMT)	Latitude (deg. min.)	Longitude (deg. min.)	*Depth (km)	Location References	[§] Magnitude	Magnitude References
		40 30	-125 30	0	Geomatrix, 1995 Toppozada and others, 1981	{MI} 6.7	Geomatrix, 1995
		41	-124.4	0		(MI) 5.7	Toppozada and others, 1981
04/18/1906	13:12	37 42	-124 30	0	Ellsworth, 1990	M 7.8; <i>M</i> 8 1/4	Meltzner and Wald, 2002; Ellsworth, 1990
04/23/1906	21:10	41	-124 30	0	Toppozada and others, 2000	<u>M</u> 6.4	Toppozada and others, 2000
		40 52.8	-125 21	0	Meltzner and Wald, 2002	M 6.7	Meltzner and Wald, 2002
08/11/1907	12:19	40 30	-125 30	0	Toppozada and others, 2000	<u>M</u> 6.4	Toppozada and others, 2000
08/18/1908	10:59	40 48	-124	0	Toppozada and others, 2000, Toppozada and others, 1978	<u>M</u> 5.8; MI 5.0	Toppozada and others, 2000, Toppozada and others 1978
05/18/1909	01:19	41	-124 0	0	Toppozada and others, 1978	MI ≤ 5.5	T. Toppozada, pers. comm., 2002
		40 34.8	-124 10.2	12.9	Geomatrix, 1995	<i>M_L</i> 6.1	Geomatrix, 1995
10/29/1909	06:45	40 18?	-124 12?	0	Bakun, 2000	<i>M_S</i> 5.8	Bakun, 2000



TABLE 3-2
MAGNITUDE 5 AND LARGER EARTHQUAKES WITHIN 160 KILOMETERS (100 MILES)
OF THE HB-ISFSI SITE, 1850 THROUGH APRIL 2002

Pacific Gas and Electric Company
Humboldt Bay ISFSI

Date	Origin Time (GMT)	Latitude (deg. min.)	Longitude (deg. min.)	*Depth (km)	Location References	[§] Magnitude	Magnitude References
		40 30	-124 12	14.0, 0	Geomatrix, 1995, Ellsworth, 1990 & Topozada and others, 2000	M _L 6.0; M 5.8; <u>M</u> 6.0	Geomatrix, 1995; Ellsworth, 1990; Topozada and others, 2000
03/19/1910	00:11	40 49.8	-124 10.2	17.7, 0	Geomatrix, 1995; Bolt and Miller, 1975	M _L 6.0	Geomatrix, 1995; Bolt and Miller, 1975
		40?	-125?	0	Ellsworth, 1990; Topozada and others, 2000	M 6.0; <u>M</u> 6.0	Ellsworth, 1990; Topozada and others, 2000
12/31/1915	12:20	41	-126	0	CNSS, 2002	M _L 6.5; M 6.5	UCB, 2002; Ellsworth, 1990
07/15/1918	00:23	41	-125	0	Geomatrix, 1995; CNSS, 2002; Topozada and others, 2000	M _L 6.5; M 6.5; <u>M</u> 6.5	Geomatrix, 1995 & UCB, 2002; Ellsworth, 1990; Topozada and others, 2000
09/15/1919	14:07	40 48	-124 12	0	Topozada and others, 1978	M _I ≤ 5.5	T. Topozada, pers. comm., 2002
		40 49.8	-124 10.2	17.7	Geomatrix, 1995	M _L 5.5	Geomatrix, 1995
01/26/1922	09:31	41	-126	0	CNSS, 2002; Ellsworth, 1990	M _L 6.0, M 6.0	CNSS, 2002; Ellsworth, 1990
01/31/1922	13:17	41 0.0	-125 30	0	CNSS, 2002; Ellsworth, 1990; Topozada and others, 2000	M _{G-R} 7.3; M 7.3; <u>M</u> 7.3; M _L 7.3	Bakun, 2000; Ellsworth, 1990; & Topozada and others, 2000; UCB, 2002



TABLE 3-2
MAGNITUDE 5 AND LARGER EARTHQUAKES WITHIN 160 KILOMETERS (100 MILES)
OF THE HB-ISFSI SITE, 1850 THROUGH APRIL 2002

Pacific Gas and Electric Company
Humboldt Bay ISFSI

Date	Origin Time (GMT)	Latitude (deg. min.)	Longitude (deg. min.)	*Depth (km)	Location References	[§] Magnitude	Magnitude References
		40 52.2	-125 21	0	Geomatrix, 1995; Smith and Knapp, 1980	M _L 7.0; M _L 7.3	Geomatrix, 1995; Smith and Knapp, 1980
01/22/1923	09:04	40 30	-124 30	0	CNSS, 2002; Ellsworth, 1990	M _{G-R} 7.2; M 7.2, M _L 7.2	Bakun, 2000; Ellsworth, 1990; UCB, 2002
		40 24	-124 54	0	Topozada and others, 2000	<u>M</u> 7.2	Topozada and others, 2000
		40 48	-124 3		Smith and Knapp, 1980	M _L 7.2	Smith and Knapp, 1980
04/29/1923	02:31	41	-125	0	CNSS, 2002	M _L 5.0	CNSS, 2002
06/04/1925	12:02	41 30	-125	0	CNSS, 2002; Ellsworth, 1990; Topozada and others, 2000	M _L 6.0; M 6; <u>M</u> 6.0	UCB, 2002; Ellsworth, 1990; Topozada and others, 2000
12/10/1926	08:38	40 45	-126	0	CNSS, 2002; Geomatrix, 1995; Ellsworth, 1990	M _L 6.0; M 6.0	UCB, 2002; Geomatrix, 1995; Ellsworth, 1990
08/20/1927	20:05	41	-124 36	0, 4.8	Bolt and Miller, 1975; Geomatrix, 1995	M _L 5.0	Bolt and Miller, 1975; Geomatrix, 1995



TABLE 3-2
MAGNITUDE 5 AND LARGER EARTHQUAKES WITHIN 160 KILOMETERS (100 MILES)
OF THE HB-ISFSI SITE, 1850 THROUGH APRIL 2002

Pacific Gas and Electric Company
Humboldt Bay ISFSI

Date	Origin Time (GMT)	Latitude (deg. min.)	Longitude (deg. min.)	*Depth (km)	Location References	§Magnitude	Magnitude References
09/23/1930	02:58	40 57	-124 12	0	Toppozada and others, 2000	<u>M</u> 5.5	Toppozada and others, 2000
		40 49.8	-124 10.2	17.7	Geomatrix, 1995	M _L 5.0	Geomatrix, 1995
12/11/1930	09:00	40 24	-124 48	0	Toppozada and others, 2000	<u>M</u> 5.5	Toppozada and others, 2000
		40 4.8	-124 30	0	Bolt and Miller, 1975	[M _L] 5.0	Toppozada and others, 1978
03/10/1931	03:28	40	-125	0	Toppozada and others, 2000	<u>M</u> 5.6	Toppozada and others, 2000
08/23/1931	18:01	40 12	-125 36	0	CNSS, 2002; Geomatrix, 1995	M _L 5.3	CNSS, 2002; Geomatrix, 1995
09/09/1931	13:40	40 48	-125	0	CNSS, 2002; Geomatrix, 1995; Toppozada and others, 2000	M _L 5.8	CNSS, 2000; Geomatrix, 1995; Toppozada and others, 2000
06/06/1932	08:44	40 45	-124 30	0, 11.2	CNSS, 2002; Ellsworth, 1990; Geomatrix, 1995	M _{G-R} 6.4; M _L 6.4; <i>M</i> 6.4	Bakun, 2000; UCB, 2000; Geomatrix, 1995; Ellsworth, 1990
		40 48	-124 18	0	Toppozada and others, 2000	<u>M</u> 6.4	Toppozada and others, 2000
07/06/1934	22:49	41 15	-125 45	0	Ellsworth, 1990; Toppozada and others, 2000	M _{G-R} 6.5; <i>M</i> 6.5; <u>M</u> 6.5	Bakun, 2000; Ellsworth, 1990 & Toppozada and others, 2000

